

LIMBS, GENITALS, AND GENE REGULATORY NETWORKS: IDENTIFYING CONSERVED
TARGETS OF TBX5 IN EMBRYONIC FORELIMBS AND GENITALIA

by

AARON-JAY P. ALCALA

(Under the Direction of Douglas B. Menke)

ABSTRACT

Although the morphology of the amniote limb and phallus differ dramatically, these appendage types express a similar suite of transcription factors and signaling molecules during development. This observation led to the hypothesis that the amniote phallus may have evolved, in part, through co-option of components of an ancient appendage gene regulatory network. Consistent with this, previous work from our lab has shown that many enhancers active in developing limbs are also active in the genital tubercle (GT). However, it remains unknown whether transcription factors expressed in the limbs and phallus interact with the same enhancers to regulate similar suites of target genes. In this dissertation, I address this question by investigating the regulatory targets of the TBX5 transcription factor. TBX5 plays a critical role in the growth and development of the vertebrate forelimb and is also known to be expressed in the developing genitalia of several amniote species. Using TBX5 ChIP-seq in mouse embryonic forelimbs and GTs, I have identified thousands of binding sites in each of these appendage types. Approximately 32% of forelimb peaks are shared with the GT

and are significantly enriched near genes involved in limb development. Thus, despite the high overlap of active enhancers in embryonic limbs and genitalia, there are differences in the set of TBX5-bound *cis*-regulatory targets in these tissues. To investigate the degree to which TBX5 binding events are conserved in amniote appendages, I also performed parallel TBX5 ChIP-seq experiments in embryonic appendages of *Anolis* lizards, turtles, and alligators. Furthermore, I conditionally knocked out the *Tbx5* gene during the early development of mouse forelimbs and genitalia and used RNA-seq to uncover genes that exhibit TBX5-dependent expression. Using an integrative ChIP-seq and RNA-seq approach, I have identified putative direct target genes regulated by TBX5 in embryonic appendages. Overall, the large genomic and transcriptomic datasets I have generated: 1) enhance our understanding of how TBX5 governs appendage development and 2) serve as valuable resources to form testable hypotheses of the mechanisms underlying the growth of these structures.

INDEX WORDS: TBX5, Limb development, Genital Tubercle, Amniote Phallus, Enhancers, Chromatin Immunoprecipitation sequencing (ChIP-seq), RNA sequencing (RNA-seq), Evo-devo, Gene regulatory networks

LIMBS, GENITALS, AND GENE REGULATORY NETWORKS: IDENTIFYING CONSERVED
TARGETS OF TBX5 IN EMBRYONIC FORELIMBS AND GENITALIA

by

AARON-JAY P. ALCALA

B.S., Georgia State University, 2014

M.S., Georgia State University, 2016

A Dissertation Submitted to the Graduate Faculty of The University of Georgia in Partial

Fulfillment of the Requirements for the Degree

DOCTOR OF PHILOSOPHY

ATHENS, GEORGIA

2023

© 2023

Aaron-Jay P. Alcala

All Rights Reserved

LIMBS, GENITALS, AND GENE REGULATORY NETWORKS: IDENTIFYING CONSERVED
TARGETS OF TBX5 IN EMBRYONIC FORELIMBS AND GENITALIA

by

AARON-JAY P. ALCALA

Major Professor:	Douglas B. Menke
Committee:	Jonathan T. Eggenschwiler
	James D. Lauderdale
	Robert J. Schmitz
	Michael A. White

Electronic Version Approved:

Ron Walcott
Vice Provost for Graduate Education and Dean of the Graduate School
The University of Georgia
May 2023

DEDICATION

First, this dissertation is dedicated to the memory of my former mentor, Dr. Bill Walthall, who passed away during the course of my PhD research. Bill was an exceptional educator and dedicated mentor. Thank you for igniting my passion in genetics and developmental biology. I will always remember the question you first proposed to me, which led me to pursue research in this field:

“How does a *finite* amount of genetic material generate a seemingly *infinite* amount of biological complexity?”

I further dedicate this work to my parents, Luz and Willy Alcala, who have fully supported and encouraged me throughout my journey. Your sacrifices have ensured I could thrive in this country and build a better future for myself and my family.

Finally, I must express deep gratitude to my wife, Adani, for her endless love, patience, and support. You have been the light on my darkest days in grad school and encouraged me to never give up. I appreciate you constantly reminding me that “I need to graduate” (haha). I could not have accomplished any of this without you.

ACKNOWLEDGEMENTS

It truly takes a village to complete a PhD. I am sincerely thankful for all the people below, who helped me overcome the emotional turmoil a PhD causes.

First, I must express my heartfelt gratitude to my family and friends for their unwavering love and support. Thank you for reminding me that my PhD does not define me. I also want to thank my Pickleball friends, who welcomed me into the sport in the last year and gave me a fun place to take care of my physical and mental health.

Thanks to my advisor Doug Menke for his support, patience, and dedication to making me an independent scientist. Your passion for evo-devo is infectious and has kept me motivated to complete my PhD despite all the research challenges I have had to face. Your glass-half-full mentality has shown me that optimism can make all the difference when facing adversity. I am also grateful for the help of my committee members, Jim Lauderdale, Bob Schmitz, Mike White, and Jonathan Eggenschwiler, who wanted nothing more than my success as a researcher.

I am grateful for my labmates Sukhada Samudra and Ashley Rasys, who not only provided great mentorship for me as a scientist, but also became great friends. Thank you to Dr. Sungdae Park, who has supported me from day one of my PhD research and has patiently answered all my “stupid” questions. Special thanks to my other lab members, past and present, for their support: Sergio, Shirley, Shana, Christina, Megan, Rida, Anna, Amber, and Ben. I must also thank our “army” of undergrad and high school

researchers in the lab who helped care for our lizard colony and made the lab a fun and lively place to be. Lastly, thank you to my fellow grad students in the department who not only gave me advice on my research but also encouraged me to overcome adversity.

I express gratitude to Catherine Brown, a brilliant, diligent, and cheerful undergrad researcher that helped me with several aspects of my projects and contributed heavily to our research of genital development. I am glad you are doing amazing things, and hope you remember me when you become a prominent scientist so you can offer me a job in the future.

Thank you to the research staff of the UGA Biomedical Microscopy Core, Georgia Genomics and Bioinformatics Core, Georgia Electron Microscopy, Georgia Advanced Computing Resource Center, and Animal Facilities, including Muthugapatti Kandasamy, Benjamin Cronheim, Mary Ard, and John Shields. Your patience and assistance made the production of the incredible genomic and microscopic datasets for this dissertation possible. Special thanks to Gary, who would visit and chat with me on late evenings when I was the only one left in the lab. Your optimism energized me when I thought there was nothing left in my tank. Your words of wisdom helped me recognize that the sacrifices I was making were meaningful and worthwhile.

Finally, I must thank my science communicator friends and mentors: Stephanie Castillo, Alejandra Ruiz León, Alex Dainis, Magot Popecki, Rob Nelson, and Haley Nelson. You have taught me how to communicate science with intention and empathy. Thanks for inspiring me and showing me how to pave your own career path in the field of sci-comm.

TABLE OF CONTENTS

	Page
ACKNOWLEDGEMENTS	v
LIST OF TABLES	ix
LIST OF FIGURES	x
CHAPTER	1
1 INTRODUCTION AND LITERATURE REVIEW	1
Mechanisms Underlying Limb Development and Evolution	1
Role of <i>Tbx5</i> in Governing Limb Growth and Patterning	9
<i>Tbx5</i> in Organ Development and Human Disorders	12
Processes of Genital Development and Evolution	14
The Revolution of High-throughput Sequencing Technologies	16
2 TBX5 DIRECTLY TARGETS CONSERVED COMPONENTS OF THE FORELIMB GENE REGULATORY NETWORK	21
Abstract	22
Introduction	23
Results	25
Discussion	34

Methods	39
Figures and Tables.....	43
3 TBX5 REGULATES APPENDAGE GENES TO CONTROL PATTERNING OF THE DEVELOPING EXTERNAL GENITALIA.....	72
Abstract	73
Introduction.....	74
Results	76
Discussion	84
Methods	88
Figures and Tables.....	93
4 CONCLUSIONS AND FUTURE DIRECTIONS	127
REFERENCES.....	133

LIST OF TABLES

	Page
Table S2.1. Normalized counts of <i>Tbx5</i> exons in control and cKO forelimbs	60
Table S2.2. Sample of differentially expressed genes in embryonic forelimbs of <i>Tbx5</i> cKO mice.....	61
Table S2.3. Sample of peaks from TBX5 CHIP-seq in forelimbs	62
Table S2.4. Coordinates of TBX5 binding at validated limb enhancers	67
Table S2.5. Putative direct targets of TBX5 in embryonic forelimbs	68
Table S2.6. List of limb genes regulated by TBX5	70
Table S3.1. Normalized counts of <i>Tbx5</i> exons in control and cKO genital tubercles	120
Table S3.2. Differentially expressed genes in embryonic genitalia of <i>Tbx5</i> cKO mice ...	121
Table S3.3. Sample of peaks from TBX5 CHIP-seq in external genitalia	123
Table S3.4. Coordinates of TBX5 binding at validated appendage enhancers	125
Table S3.5. List of validated genital enhancers bound by TBX5 in the mouse genital tubercle	126

LIST OF FIGURES

	Page
Figure 2.1. <i>Tbx5</i> cKO mice display a variety of forelimb disorders.....	43
Figure 2.2. Differentially expressed genes (DEGs) in forelimbs of <i>Tbx5</i> conditional knockout (cKO) mice at E10.5.....	45
Figure 2.3. Genome-wide enrichment of TBX5 binding in mouse embryonic forelimbs .	47
Figure 2.4. Genome-wide occupancy of TBX5 binding events in reptile embryonic forelimbs	49
Figure 2.5. Deeply conserved TBX5 binding events in embryonic forelimbs of amniotes	50
Figure 2.6. TBX5 directly regulates limb genes by binding VISTA-validated enhancers...	52
Figure 2.7. Proposed role of <i>Tbx5</i> in the gene regulatory network underlying forelimb development.....	53
Figure S2.1. <i>Tbx5</i> mutants display omphalocele	54
Figure S2.2. RNA-seq data quality assessment by sample clustering.....	55
Figure S2.3. TBX5 binds many of the same regions as HOX13	56
Figure S2.4. Additional examples of TBX5 binding at validated limb enhancers	58
Figure S2.5. <i>Tbx5</i> regulates several components of the Hedgehog signaling pathway ...	59

Figure 3.1. ISL1 directly regulates a conserved enhancer of <i>Tbx5</i> in the embryonic phallus.....	94
Figure 3.2. GTE1 displays enhancer activity in the mouse genital tubercle.....	95
Figure 3.3. Conditional ablation of <i>Tbx5</i> leads to reduced size of preputial swellings and urethral hypoplasia.....	97
Figure 3.4. Differentially expressed genes (DEGs) in GTs of <i>Tbx5</i> conditional knockout (cKO) mice at E12.5.....	99
Figure 3.5. Genome-wide enrichment of TBX5 binding in the mouse GT.....	101
Figure 3.6. Genome-wide enrichment of TBX5 binding in the embryonic mouse forelimb, genital tubercle, heart, and lung.....	103
Figure 3.7. Genome-wide occupancy of TBX5 binding events in brown anole embryonic hemiphalluses.....	105
Figure 3.8. Deeply conserved TBX5 binding events in the embryonic phallus of amniotes.....	106
Figure 3.9. TBX5 binds validated appendage enhancers in the forelimb and genital tubercle.....	108
Figure S3.1. Introduction of a <i>Tbx4</i> null allele in the <i>Tbx5</i> mutant background does not lead to a more severe phenotype in the GT.....	109
Figure S3.2. RNA-seq data quality assessment by sample clustering (GT).....	110

Figure S3.3. qPCR validation of differentially expressed genes identified in RNA-seq analysis.....	111
Figure S3.4. Genome-wide enrichment of TBX5, centered on forelimb peaks.....	113
Figure S3.5. Genome-wide enrichment of TBX5, centered on genital peaks.....	115
Figure S3.6. Genome-wide enrichment of TBX5, centered on heart peaks.....	117
Figure S3.7. Genome-wide enrichment of TBX5, centered on lung peaks.....	119

CHAPTER 1

INTRODUCTION AND LITERATURE REVIEW

Mechanisms Underlying Limb Development and Evolution

Locomotion, feeding, breeding, and other behaviors are enabled by paired fins/limbs that evolved in vertebrates. The vertebrate limb has become a fundamental model system to study developmental biology and gene regulation. Because limbs grow on the exterior of the embryo, they are easy to observe and manipulate surgically and pharmacologically. Furthermore, modification of gene expression using conditional knockout or transient transgenesis allows disruption of limb organogenesis without causing embryonic lethality. These characteristics have made the limb a leading model to interrogate the precise gene regulatory networks and signaling pathways required to properly pattern complex organs. The incredible diversity observed in forelimb and hindlimb morphology across species also makes the limb an outstanding tool to investigate the role of gene regulation in evolutionary developmental biology.

Three distinct limb segments form in limbed tetrapods: the stylopod (humerus/femur), zeugopod (ulna/radius; tibia/fibula), and autopod (wrist/fingers; ankle/toes). Forelimbs (FLs) and hindlimbs (HLs) initially emerge from the lateral plate mesoderm of the embryo as buds composed of mesenchymal cells covered by an ectodermal layer. The lateral plate mesoderm gives rise to the muscular and skeletal elements of the limb (Sun et al., 2002). Limb development consists of four major events:

induction, initiation, outgrowth, and morphogenesis. During limb formation, widely conserved signaling pathways - fibroblast growth factor (FGF), Sonic hedgehog (SHH), and Wnt signaling - are known to regulate and pattern the proximal-distal (PD), anterior-posterior (AP), and dorsal-ventral (DV) axes of the limbs, respectively.

For instance, the PD axis is governed by the apical ectodermal ridge (AER), which is the main source of FGF ligands, while the AP axis is patterned by SHH, a morphogen produced in the zone of polarizing activity (ZPA) (Riddle et al., 1993; Saunders, 1948). In the dorsal ectoderm, WNT7A regulates the development of the DV axis of the limb (Brian A. Parr & McMahon, 1995). In the mouse, limb formation occurs throughout several embryonic stages (Wanek et al., 1989). Limb induction along the cranial-caudal axis of the body occurs at approximately embryonic day 9 (E9.0) and by E9.0-E9.5 limb initiation has occurred. At later stages, outgrowth occurs during E10.0-E11.5 and morphogenesis continues in coordination after E11.5 to pattern the limb along three dimensions (Logan, 2003; Petit et al., 2017). Patterning across developmental axes is orchestrated by genes under the control of *cis*-regulatory elements such as promoters, enhancers, and silencers.

Sonic hedgehog (Shh), an ortholog of the *Hedgehog* gene in *Drosophila*, encodes a morphogen expressed in the zone of polarizing activity at the posterior margin of the limb. SHH has been shown to regulate cell proliferation in the limb by mediating cell cycle regulators such as D cyclins (Towers et al., 2008). Classical experiments have found that when cells expressing *Shh* were grafted to the anterior portion of the chick wing bud, digits were duplicated in a symmetrical manner (Riddle et al., 1993). In other

words, a total of six digits grew with a pattern of digits 3-2-1-1-2-3 from anterior to posterior. SHH also controls limb bud width by activating proliferation of the mesenchyme and by regulating the anteroposterior length of the AER (Smith & Wolpert, 1981; C. Tickle et al., 1975). Recent work has challenged the idea that SHH is a direct morphogen, and instead functions as an initiator of this process. When digit 4 and 5 progenitors were exposed to a transient pulse (2-3 hours) of SHH, the limb bud underwent nearly normal digit specification, showing that SHH response acts in a short range (J. Zhu et al., 2022). After this initiation period, Shh signaling is important as a long-range signal to promote cell survival during outgrowth but is no longer necessary for digit specification (J. Zhu et al., 2022).

The limb-specific expression of *Shh* is controlled by the zone of polarizing activity regulatory sequence (ZRS), a *cis*-regulatory element located almost 1 megabase upstream of the *Shh* promoter (Lettice et al., 2002). Ablation of the complete ZRS region in embryonic mice leads to the loss of *Shh* expression in limb buds and severe limb truncations (Sagai et al., 2005). ZRS enhancer activity is deeply conserved in vertebrates but has progressively lost its function in snakes (Kvon et al., 2016; Leal & Cohn, 2016). Replacing the ZRS sequence in mice with the python ZRS sequence, which has a deletion in an ETS1 transcription factor binding site, leads to “serpentized” mice that have nearly completely truncated limbs (Kvon et al., 2016). Intriguingly, while snakes have mutations in the ZRS enhancer, this regulatory element lacks relevant mutations in limbless lizards (Roscito et al., 2022). Overall, these findings suggest that while sequence changes in enhancers may contribute, in part, to morphological evolution of the limb,

there are likely several different mechanisms underlying the evolution of limblessness in reptiles.

Fibroblast growth factors in the apical ectodermal ridge activate *Shh* expression in the ZPA of the limb (Jin et al., 2018; Laufer et al., 1994; Niswander et al., 1994). In *Fgf10*-ablated mice, the limb bud initiates formation but abruptly terminates outgrowth, resulting in limb truncation and hypoplasia of the scapulae and pelvis (Min et al., 1998; Sekine et al., 1999). Knockout of *Fgfr2b*, the receptor for FGF10, leads to similar limb phenotypes in mice (De Moerlooze et al., 2000). FGF10 in the mesenchyme triggers *Fgf8* expression in the ectoderm, which then forms a positive feedback loop with *Fgf10* and promotes outgrowth of the limb away from the main body axis (Ohuchi et al., 1997; Sekine et al., 1999). *Fgf10* has been proposed to induce an epithelial-mesenchymal transition (EMT) in the epithelial somatopleure, enabling formation of limb progenitors that form different segments of the limb (Gros & Tabin, 2014).

WNT7A, a key regulator of dorsal-ventral patterning in the limb, also functions to regulate the expression of *Shh* (Geetha-Loganathan et al., 2008; Brian A. Parr & McMahon, 1995). *Wnt7a* is expressed in the dorsal ectoderm and induces *Lmx1b* in the mesenchyme of the dorsal limb to specify dorsal mesodermal cell fates of the zeugopod and autopod (Chen et al., 1998; Brian A. Parr & McMahon, 1995; Riddle et al., 1995). Ectopic expression of *Lmx1b* in the ventral mesenchyme leads to symmetrical double-dorsal limbs. Knockout of *Wnt7a* in mice leads to ventralized paws with sole pads on both surfaces and dorsal-to-ventral transformations of cell fate in the mesoderm. Canonical Wnt signaling is also necessary to maintain the apical ectodermal ridge.

Ablation of β -catenin - an intracellular signal transducer protein downstream of Wnt signaling- leads to initial formation of the AER, but the structure disappears and is not maintained (Barrow et al., 2003). During limb bud outgrowth, *Wnt5a* is expressed in the distal mesenchyme under the AER (Brian A. Parr & McMahon, 1995). *Wnt5a*-deficient mice exhibit decreased proliferation in the progress zone below the AER, shortening of the proximal skeleton, and absence of digits (Yamaguchi et al., 1999).

Several TGF- β -encoding proteins belong to the BMP group of paracrine signals that are crucial to limb morphogenesis (Pignatti et al., 2014). BMP7, BMP2, and BMP4 exhibit spatiotemporally restricted expression patterns in the limb mesenchyme and ectoderm and play many roles during initiation, outgrowth, and patterning of cartilage and skeletal elements. Constitutive loss of *Bmp7* expression in mice leads to anterior polydactyly (G. Luo et al., 1995), while conditional knockout of *Bmp2* and *Bmp4* in the ectoderm using an *Msx2*-Cre mouse line leads to dorsalization of the limb, upregulation of AER-expressed *Fgf4* and *Fgf8* genes, and elevated proliferation (Maatouk et al., 2009). Furthermore, *Bmp2/Bmp4* conditional mutants exhibited reduced interdigit apoptosis polydactyly, interdigital webbing, and bifurcation of digits. Interestingly, retention of interdigital webbing in the bat forelimb is associated with unique expression patterns of the BMP inhibitor *Gremlin* as well as *Fgf8* that is not observed in mouse limbs (Weatherbee et al., 2006). Duck hindlimbs, which are also webbed, express *Gremlin* in a manner that is not observed in chicken hindlimbs (Merino et al., 1999). These findings suggest that the modulation of BMP and FGF signals may be involved in the evolutionary gain of webbed limbs.

Positioning of the forelimb and hindlimb along the anteroposterior axis of the embryo is governed by *Hox* genes (Pineault & Wellik, 2014). Cross-species comparative studies provided the first pieces of evidence that *Hox* gene expression domains correlate with positioning of limbs (Burke et al., 1995; M. J. Cohn et al., 1997; Minguillon et al., 2012; Nishimoto et al., 2014). A more recent report overexpressed *Hoxb4* and repressed *Hoxc9* in the interlimb and found that *Tbx5* expression extended into the interlimb region and led to displacement of the final forelimb position (Moreau et al., 2018). This was the first functional evidence that shifting both the forelimb field (*Hoxb4* expression) and interlimb field (*Hox9* expression) is sufficient to directly regulate forelimb position. These researchers also found that the dynamics of *Hoxb* gene activation during gastrulation correlate with the differing forelimb positioning observed in three bird species that exhibit natural variations in limb positioning - the zebra finch, chicken, and ostrich.

In addition to the role of *Hox* genes in limb positioning, the posterior *Hox* paralogs (*Hox9-Hox13*) control limb skeleton patterning along the PD axis. Loss of *Hox10* paralogs leads to severe mispatterning of the zeugopod (Wellik & Capecchi, 2003), loss of *Hox11* paralogs causes nearly complete elimination of the radius/ulna (stylopod) in the forelimb (Boulet & Capecchi, 2004; Davis et al., 1995), and loss of *Hox13* paralogs results in a total loss of autopod elements (Fromental-Ramain et al., 1996). *Hoxd12* also functions to properly pattern the autopod (Knezevic et al., 1997). The *Hox5* and *Hox9* paralogous groups are necessary to regulate the AP axis in the forelimb (B. Xu et al.,

2013; B. Xu & Wellik, 2011). Eliminating function for all *HoxA* and *HoxD* genes in the limb leads to skeletal elements that are severely truncated (Kmita et al., 2005).

Several genes encode transcription factors that play critical roles in determining whether cells will produce forelimbs or hindlimbs. These include *Isl1*, *Pitx1*, and *Tbx4* in the hindlimb and *Tbx5* in the forelimb. *Isl1* is essential for the initiation of the hindlimb bud and regulates the expression of *Tbx4*, but not *Pitx1*, in the lateral plate mesoderm (Kawakami et al., 2011; Minchey, 2022). *Isl1* conditional knockout mice display disordered nuclear localization of β -catenin (Kawakami et al., 2011), suggesting an upstream role in the Wnt signaling pathway. *Pitx1* is critical in determining hindlimb-specific morphology and directly binds to hindlimb-specific enhancer A (HLEA) and HLEB to activate the expression of *Tbx4* in the hindlimb bud (Infante et al., 2013; Lanctôt et al., 1999; Menke et al., 2008). PITX1 ChIP-seq experiments in the *Anolis* lizard hindlimb shows that this transcription factor also binds HLEB in lizards (Wang et al., 2018). Deletion of HLEB in mouse leads to reduced *Tbx4* expression during early hindlimb outgrowth (E9.5-E10.5) (Infante et al., 2015). *Tbx5* is necessary to initiate forelimb budding (Agarwal et al., 2003; Bruneau et al., 2001; Rallis et al., 2003).

Tbx5 and *Tbx4* are paralogous genes expressed in the prospective forelimb and hindlimb, respectively. During limb bud initiation, transcription factors encoded by both of these genes activate *Fgf10* in the limb mesenchyme (Agarwal et al., 2003; Naiche & Papaioannou, 2003). FGF10 signaling activates *Fgf8* in the overlying ectoderm and establishes a positive feedback loop, which is necessary and sufficient for limb outgrowth (Ohuchi et al., 1997). The limb-type restricted patterns of *Tbx5* and *Tbx4*

expression suggest that these genes could have roles in determining the morphological differences between forelimbs and hindlimbs, respectively. In the chick, ectopic expression of *Tbx5* in the hindlimb leads to the development of a wing-like hindlimb, and ectopic expression of *Tbx4* expression in the forelimb leads to the formation of a leg-like forelimb (Rodriguez-Esteban et al., 1999; J. K. Takeuchi et al., 1999).

Furthermore, several pigeon and chicken breeds that have feathered feet show abnormally high levels of *Tbx5* expression in embryonic hindlimbs (Domyan & Shapiro, 2017). However, several gene deletion-gene replacement studies in mouse have challenged this model and suggest that *Tbx5* and *Tbx4* have common roles in limb initiation and outgrowth, but do not establish limb-type morphologies (Minguillon et al., 2005, 2009). In summary, these studies suggest that *Tbx5* may have different roles in distantly related species.

Modifications in *Tbx5* and *Tbx4* expression are hypothesized to have contributed to the gain of paired appendages during vertebrate evolution. Lancelets (also known as amphioxii) are fish-like, invertebrate chordates that lack limbs and possess a single ancestral *Tbx4/5* gene (Delsuc et al., 2006; Ruvinsky et al., 2000). Expression of the amphioxus *Tbx4/5* gene in the mouse limb field is sufficient to rescue forelimb formation in conditional *Tbx5* mutants (Minguillon et al., 2009). Transgenic experiments show that the amphioxus genome lacks regulatory elements necessary to drive *Tbx4/5* gene expression in the lateral plate mesoderm, the domain in which *Tbx5* and *Tbx4* are necessary to promote limb formation. Together, these results suggest that changes in *Tbx5* and *Tbx4* expression are required to acquire paired appendages.

A reduction in digit size and/or digit count is observed in several groups of mammals including the odd-toed ungulates (e.g., horses, rhinoceroses, tapirs) and even-toed ungulates (e.g., cattle, pigs, camels, sheep, deer). The bovine autopod differs from the typical pentadactyl pattern of other mammals (such as mice and humans) as it only develops two elongated digit primordia. During the earliest stages of limb formation, cow and mouse limbs show similar expression domains of *Shh* but the expression of *Gli1*, a transcription factor downstream of Shh signaling, extends into the posterior mesenchyme (Lopez-Rios et al., 2014). Furthermore, expression of *Ptch1*, a SHH receptor, is restricted to the ectoderm in cattle and pigs, whereas in mice *Ptch1* expands into the posterior mesenchyme (Cooper et al., 2014). This alteration in expression is suggested to have evolved due to sequence changes in a *Ptch1* limb cis-regulatory module, LRM (Lopez-Rios et al., 2014). Other mechanisms for digit reduction have been suggested in other mammals such as jerboas, camels, and horses, which undergo expanded apoptosis to sculpt the tissue surrounding remaining toes (Cooper et al., 2014).

Role of *Tbx5* in Governing Limb Growth and Patterning

The *Tbx5* gene encodes a T-box transcription factor that plays a vital role in the growth and development of the forelimb in vertebrates including zebrafish (Ahn et al., 2002), salamanders (M. Suzuki et al., 2018), chickens (Rodriguez-Esteban et al., 1999), mice (Agarwal et al., 2003), and humans (Basson et al., 1997). Constitutive knockout of *Tbx5* in mice leads to a total absence of forelimb buds, as well as a misshapen linear heart tube (Agarwal et al., 2003; Bruneau et al., 1999). Conditional knockout of *Tbx5* in

the presumptive limb mesenchyme with *Prx1-Cre* causes mice to develop with a complete absence of forelimbs and skeletal elements of the pectoral girdle, including the scapula and clavicle (Rallis et al., 2003). *In situ* hybridization assays in these *Tbx5* conditional mutant mice show reduced forelimb region expression of *Fgf8* and *Shh*, markers of the AER and ZPA, respectively, indicating a crucial role of *Tbx5* in establishing these signaling centers. Expression analyses of the hindlimb markers *Tbx4* and *Pitx1* show that both of these genes are restricted to the hindlimb in *Tbx5* mutants, suggesting that *Tbx5* does not function to repress these genes in the forelimb.

Functional studies in mice and zebrafish have demonstrated that TBX5 activates *Fgf10* in the mesenchyme during limb bud initiation (Agarwal et al., 2003; Ng et al., 2002; Nishimoto et al., 2015). TBX5 can bind to regions of the *Fgf10* promoter to activate its expression (Agarwal et al., 2003). FGF10 then activates *Fgf8* in the ectoderm to form a positive regulatory loop important for proximal-distal outgrowth of the limb (Ohuchi et al., 1997; Sekine et al., 1999; X. Xu et al., 1998). While *Tbx5* feedback is required to activate *Fgf10* expression and subsequent forelimb bud initiation, it is only necessary in a narrow period during the earliest stage of limb growth. A time course conditional ablation of *Tbx5* in mice shows that limb bud formation is mainly impacted if *Tbx5* is deleted before E10.5 (Hasson et al., 2007). Beyond this stage, *Tbx5* ablation has minor effects on forelimb outgrowth and skeletal patterning and continued expression of *Fgf10* expression. *Tbx5* is also necessary for soft tissue patterning of the forelimb muscles and tendons (Hasson et al., 2010). In this study, the researchers used a

tamoxifen-inducible *Prx1-Cre* line to ablate *Tbx5* in limb mesenchymal cells and analyzed candidate muscle patterning genes that showed altered expression patterns.

A combination of Wnt/ β -catenin, retinoic acid (RA), and Hox signals regulates expression of *Tbx5* in the presumptive limb field (Sheeba & Logan, 2017). A forelimb-specific *cis*-regulatory element regulating *Tbx5* was found to contain binding sites for HOX transcription factors (Minguillon et al., 2012; Nishimoto et al., 2014). The 3' Hox paralog groups (Hox4 and Hox5) expressed in rostral regions of the LPM activate *Tbx5* in the presumptive forelimb region (Nishimoto et al., 2014). In the caudal regions of the LPM, the 5' Hox genes (Hoxc8/9/10) set a boundary for *Tbx5* and repress its expression in the hindlimb-forming region. Disruption of RA signaling leads to depletion of *Tbx5* expression and RA-responsive elements at the *Tbx5* locus are required for its activity (Nishimoto et al., 2015). Experiments in zebrafish have shown that Wnt2b activates *tbx5* during pectoral fin induction (Ng et al., 2002).

Based on the forelimb-restricted expression pattern of *Tbx5* examined across vertebrates, *Tbx5* has been hypothesized to specify limb-type identity. Misexpression of *Tbx5* in chicken hindlimb buds leads to a partial transformation of the leg into a wing, and ectopic hindlimb expression of *Tbx5* is found in breeds of pigeon and chicken with feathery feet (Domyan et al., 2016; Rodriguez-Esteban et al., 1999; J. K. Takeuchi et al., 1999). *Tbx5* expression is delayed in embryonic forelimbs of the emu relative to chick, suggesting that changes in *Tbx5* expression may have contributed to the evolution of reduced wing size in emus (Bickley & Logan, 2014). Furthermore, expression of *Tbx5* in the opossum, a marsupial born with precociously developed forelimbs, happens much

earlier in the presumptive forelimb field compared to in the mouse (Keyte & Smith, 2010). Thus, alterations in *Tbx5* expression have been proposed to contribute to the evolution of forelimb morphology.

Tbx5 in Organ Development and Human Disorders

Haploinsufficiency of *TBX5* in human patients causes Holt-Oram syndrome (HOS), a clinical disorder characterized by upper limb aberrations and malformations of the cardiac septa and cardiac conduction system (Basson et al., 1997; Q. Y. Li et al., 1997). Upper limb disorders include defects of the hand and fingers or bones in both the lower and upper arm (Newbury-Ecob et al., 1996). Conditional deletion of *Tbx5* in various mouse models have recapitulated the range of forelimb defects examined in HOS (Rallis et al., 2003; Sulaiman et al., 2016; H. Xu et al., 2019). A study using a *Tbx5* conditional mutant mouse model generated with *Gli1-CreER* found that *Tbx5* inhibits several components of the Shh signaling pathway (H. Xu et al., 2019). *TBX5* transcriptionally activates *Ptch1*, a known repressor of Shh signaling, by binding regulatory elements at the *Ptch1* locus.

Tbx5 null mice die early during development (between E9.5-E10.5) due to severe heart disorders and improper pulmonary development (Bruneau et al., 2001; De Bono et al., 2018; Hoffmann et al., 2014; Steimle et al., 2018; Xie et al., 2012). During early heart development, *TBX5* predominantly functions as a transcriptional activator of genes involved in cardiomyocyte maturation and septum morphogenesis (Steimle & Moskowitz, 2017). Disrupting *Tbx5* function in mice leads to an absence or reduction of

the anterior region of the atrial septum (Bruneau et al., 2001). Overexpression of *Tbx5* in both the left and right sides of the early ventricular septum leads to deformed ventricular chambers and the absence of ventricular septum (Koshiba-Takeuchi et al., 2009; Liberatore et al., 2000; J. K. Takeuchi et al., 2003).

During later cardiac growth, TBX5 is necessary for cardiac conduction system patterning and mature cardiomyocyte function maintenance. *Tbx5* has been shown to govern heart morphology by specifying the cardiac conduction system in the embryo and maintaining the identity of the conduction system in the adult (Arnolds et al., 2012; Moskowitz et al., 2007, 2004). One study showed that *Tbx5* and *Nkx2-5* interact and are necessary and sufficient to activate *Id2*, which is necessary for proper development of the conduction system (Moskowitz et al., 2007). While TBX5 has been previously reported to primarily function as a transcriptional activator (Ouimette et al., 2010; Zaragoza et al., 2004), one study found that TBX5 can interact with components of the nucleosome remodeling and histone deacetylase complex to suppress target gene expression in the heart (Waldron et al., 2016).

The mesodermal components of the heart and lung share a common developmental origin (Herriges & Morrisey, 2014; Peng et al., 2013). In addition to its role in heart development, *Tbx5* has also been shown to regulate lung morphogenesis, both alone and in coordination with *Tbx4* (Arora et al., 2012). Conditional deletion of *Tbx5* using a *Tbx4-CreER* mouse line causes abnormal lung branching, while deleting both *Tbx5* and *Tbx4* leads to downregulated WNT2 and BMP4 signaling (Arora et al., 2012). One study found that *Tbx5* is necessary for lung initiation in both the mouse and

frog, but not for the swim bladder in zebrafish (Steimle et al., 2018). The researchers also found that TBX5 directly activates *Wnt2* and *Wnt2b* in cardiopulmonary progenitors of the posterior secondary heart field. Wnt signaling is required to promote Shh signaling required for atrial septation.

Processes of Genital Development and Evolution

The external genitalia are sex organs that comprise of the penis, clitoris, scrotum, and labia. Striking similarities are observed between developing limbs and external genitalia, which differ greatly in both form and function. Interestingly, these appendage types undergo parallel phases of development: induction of a growth field along the axis of the embryo, initiation of budding, and coordination of outgrowth and patterning along three dimensions. Furthermore, these appendages use similar suites of genes and signaling molecules during embryogenesis (Martin J. Cohn, 2011; Infante et al., 2018). Prior work from our lab has found that many enhancers active in developing limbs are also active in the genital tubercle (GT) (Infante et al., 2015). However, it remains undetermined whether transcription factors expressed in the limbs and phallus interact with the same enhancers to regulate similar sets of target genes.

In amniotes (mammals, birds and reptiles), paired genital swellings emerge from the body wall adjacent to the embryonic cloaca (Gredler, 2016; Gredler et al., 2014; Perriton et al., 2002). In mammals, birds, and several reptiles such as turtles and alligators, these swellings fuse to form an ambisexual genital tubercle (GT), the precursor to the penis and clitoris (Gredler et al., 2014; K. Suzuki et al., 2002). In

squamates (lizards and snakes), the paired buds remain separated and mature into hemipenes in males or hemiciltres in females (Gredler et al., 2015; Leal & Cohn, 2015). Differentiation of the mesenchyme and urethra is organized during proximodistal outgrowth to produce sexual dimorphic characteristics of the genitalia. Although the morphology of external genitalia is incredibly diverse across amniotes and between sexes (Gerald R. Cunha et al., 2019, 2014; Weiss et al., 2012), similarities in early development suggest that the phallus evolved from a common ancestor over 310 million years ago (Gredler, 2016; Sanger et al., 2015). Using micro-Computed Tomography (μ CT) and lineage tracing experiments in three amniote clades, researchers found that the embryonic origin of external genitalia has changed during evolution, likely due to a shift in cloacal position (Tschopp et al., 2014). The genitalia grow directly from the hindlimb buds in squamates, whereas the mouse genital tubercle arises from ventral and tail bud mesenchyme (Tschopp et al., 2014).

In the mouse, the paired genital swellings are first detected at 10.5, merge to form a GT by E11.5, and undergo dramatic morphological changes during sexual differentiation at E15.5 and beyond. Androgen and estrogen receptors in the mesenchyme control male- and female-specific signaling pathways (Govers et al., 2019; Yang et al., 2010; Zheng et al., 2015). *Bmp4* is expressed before GT outgrowth (at E9.5) and is required for initiation of the GT by promoting *Wnt5a*, *Hoxd13*, and *p63* (Kajioka et al., 2019). *Shh* knockout mice exhibit GT agenesis and depleted *Fgf8* expression, suggesting the requirement of Shh signaling for GT initiation and outgrowth and formation of the distal urethral epithelium (Haraguchi et al., 2001). A study from our lab

has shown that deletion of HLEB, a hindlimb-genital enhancer of *Tbx4*, leads to pelvic and urogenital disorders in adult mice (Infante et al., 2015). *Isl1*, a gene that encodes a LIM-homeodomain transcription factor, is necessary for the development of urogenital organs and functions to regulate mesenchymal expansion in the GT via regulation of *Bmp4*, *Wnt5a*, and *Fgf10* (Ching et al., 2018; R. Zhang et al., 2017). Work from our lab has also shown that ISL1 directly activates *Tbx5* in the GT (Minchey, 2022).

In addition to the embryonic forelimbs, heart, and lungs, *Tbx5* expression has been observed in the mouse genital tubercle (Chapman et al., 1996; Douglas et al., 2012). Intriguingly, *Tbx5* is found at a later stage of GT development (E18.5) in the urethral plate epithelium of males but not females (Douglas et al., 2012). Expression of *Tbx5* has also been reported in the chick genital papilla (Gibson-Brown et al., 1998) and in anole lizard and snake hemiphalluses (Tschopp et al., 2014). A recent whole-genome sequencing association study has implicated *TBX5* as a susceptibility gene for posterior urethral valves (PUV) (Chan et al., 2022). PUV is a urogenital tract disorder characterized by membranes forming in the male posterior urethra, preventing outflow of urine. While *Tbx5* has a deeply conserved expression pattern in the amniote phallus, it remains unknown what role *Tbx5* plays during external genital development.

The Revolution of High-throughput Sequencing Technologies

Recent advances in genomics and transcriptomics are enabling the high-throughput exploration of genes and regulatory elements involved in appendage development with unprecedented resolution (Tschopp & Tabin, 2017). Chromatin immunoprecipitation followed by high-throughput sequencing is a technique used to

identify the transcription factors, cofactors, and histone marks genome-wide that are involved in organogenesis (Collas, 2010). One study mapped predicted limb, forebrain, and midbrain enhancers in mice embryos (Visel et al., 2009) using ChIP-seq against p300, an acetyltransferase and transcriptional coactivator (Eckner et al., 1994). Using transgenic mouse assays, they validated 86 of these sequences bound by p300 (Visel et al., 2009).

Another report explored chromatin state signatures associated with tissue-specific enhancer activity and gene expression in limb tissues. Cotney and colleagues identified 28,377 putative enhancers by genome-wide profiling of several histone marks known as H3K27ac and H3K27me3 (Cotney et al., 2012). Using high-throughput RNA sequencing (RNA-seq), they characterized transcriptomes of E10.5 mouse forelimb and hindlimb buds and found that relative enrichments of H3K27ac and H3K27me3 at promoter regions correlate with gene expression (Cotney et al., 2012). Overall, they find that active developmental enhancers tend to be marked by enrichment of H3K27ac, hypersensitivity to sonication, and depletion of H3K27me3. Further ChIP-seq experiments have revealed thousands of limb enhancers in other species such as bats (Eckalbar et al., 2016), monkeys (Cotney et al., 2013), and humans (Cotney et al., 2013). Over 3,300 human and mouse enhancer candidates identified using ChIP-seq in limbs and other tissues have been experimentally validated in transgenic mice and are reported in the VISTA Enhancer Browser (Visel et al., 2007). Prior work from our lab used ChIP-seq against H3K27ac to show that many enhancers active in developing forelimbs and hindlimbs are also active in the genital tubercle (Infante et al., 2015).

In addition to ChIP-seq, other massively parallel sequencing techniques have been used to explore putative enhancers. DNase I hypersensitive sites sequencing (DNase-seq) is a technique that utilizes DNase I to digest regions of DNA that are nucleosome depleted and likely bound by a transcription factor (Crawford et al., 2006; Song & Crawford, 2010). Several DNase-seq experiments published in the Mouse ENCODE project (Yue et al., 2014) were integrated with several chromatin mark datasets to train a machine learning framework used to predict active enhancers in developing limbs (Monti et al., 2017). A more modern technique to investigate chromatin accessibility is the Assay for Transposase-Accessible Chromatin with high-throughput sequencing (ATAC-seq), which is becoming more prominent in the field due the lower number of cells required for each experiment and the relative simplicity of its protocol (Buenrostro et al., 2015).

One study used ATAC-seq to investigate chromatin remodeling in mouse forelimb buds and found that the majority of accessible regions (>70%) overlaps with an active histone mark (Jhanwar et al., 2021). In this report, the researchers also performed ATAC-seq in a total of three stages (E9.75, E10.5, E11.5) of forelimb development and reveal the temporal dynamics of chromatin accessibility. Integrating the accessibility datasets with transcriptomic data in limbs showed that there was a temporal correlation between differentially accessible chromatin regions and differentially expressed genes. Parallel ATAC-seq and RNA-seq assays were performed in chicken wing buds and identified species-specific regulatory heterochrony. A recent study used ATAC-seq in the mouse E10.5 cloacal region and E13.5 and E17.5 genital tubercle to characterize

chromatin dynamics in the developing genitalia (Amândio et al., 2019). In summary, these chromatin accessibility datasets are useful resources to find predicted transcription factor binding sites across the genome.

RNA-seq is a powerful technique for transcriptome-wide profiling of differential gene expression (Emrich et al., 2007; Lister et al., 2008). Comparing the expression profiles of morphologically staged-matched E10.5 forelimbs and E11.0 hindlimbs using RNA-seq found that very few genes are limb-type specific in mice (Nemec et al., 2017). Consistent with prior studies, *Tbx5* is forelimb-restricted, while *Isl1*, *Tbx4*, *Pitx1*, and several 5' *HoxC* genes mark the hindlimb. Another study used RNA-seq to compare transcriptomes of mouse, opossum, bat, and pig forelimbs and hindlimbs (Maier et al., 2017). In conclusion, this study found that gene expression patterns show more variation among species at later stages of limb development, while results within species are more variable. RNA-seq has also been used to compare transcriptomes of developing limbs and genitalia from mouse and anole embryos (Tschopp et al., 2014). In this report, the researchers found that the lizard hemiphallus transcriptome clusters well with the hindlimb one. In contrast, the mouse genital tubercle transcriptome is more distinct from the limb molecular architecture. These gene expression analyses support their findings that genitalia grow directly from budding hindlimbs in squamates, while the mouse genital tubercle arises from ventral and tail bud mesenchyme (Tschopp et al., 2014).

Ultimately, the transcriptomic and genomic datasets produced in appendages serve as valuable resources to study gene regulation. Capitalizing on published datasets

can generate hypotheses of the mechanisms governing appendage development and help narrow down candidates to experimentally validate.

CHAPTER 2

TBX5 DIRECTLY TARGETS CONSERVED COMPONENTS OF THE FORELIMB GENE

REGULATORY NETWORK ¹

¹ Alcala A.J., et al., to be submitted to *bioRxiv*.

Abstract

Tbx5 encodes an evolutionary conserved transcription factor essential in directing forelimb growth and development. While it is known that TBX5 activates *Fgf10* during forelimb bud initiation, other regulatory targets of TBX5 have remained largely unexplored. We have used an integrative ChIP-seq and RNA-seq approach to reveal the *cis*-regulatory elements and target genes directly regulated by TBX5 in embryonic mouse forelimbs. Furthermore, we compare TBX5 binding events in the developing forelimbs of mice, Anolis lizards, turtles, and alligators to identify ancient TBX5 regulatory targets. In each of these amniote species, we find that TBX5 occupies genomic regions strongly enriched near genes involved in limb development. Many of the TBX5 binding sites we identify overlap with functionally validated enhancers that are active in the limbs. Global gene expression analyses in embryonic forelimbs of *Tbx5* conditional knockout mice uncover hundreds of genes that exhibit TBX5-dependent expression. We intersected our list of misregulated genes with genes that have nearby TBX5 binding sites to identify 671 putative targets of TBX5. Seventy-four of these are associated with ancient TBX5 binding events shared between the mouse and reptile species we analyzed. Overall, our results suggest that *Tbx5* directly regulates key components of the Hedgehog, Wnt, and BMP signaling pathways during early patterning of the forelimb.

Introduction

The *Tbx5* gene encodes a T-box transcription factor that plays a crucial role in growth and development of the vertebrate forelimb (Agarwal et al., 2003). Constitutive knockout of *Tbx5* in mice results in a complete absence of forelimb buds, as well as a deformed linear heart tube (Agarwal et al., 2003; Bruneau et al., 1999).

Haploinsufficiency of *TBX5* in human patients leads to Holt-Oram syndrome (HOS), a clinical diagnosis characterized by upper limb malformations and defects of the cardiac septa and cardiac conduction system (Basson et al., 1997; Q. Y. Li et al., 1997). Disorders of the upper limb include defects of the hand and digits or bones in both the lower and upper arm (Newbury-Ecob et al., 1996). Conditional ablation of *Tbx5* in several mouse models have recapitulated the range of forelimb disorders observed in HOS (Rallis et al., 2003; Sulaiman et al., 2016; H. Xu et al., 2019).

Based on the forelimb-restricted expression pattern of *Tbx5* observed across vertebrates, *Tbx5* has been proposed to specify limb-type identity. Misexpression of *Tbx5* in chick hindlimbs results in a partial transformation of the leg into a wing-like limb, and ectopic expression of *Tbx5* is observed in breeds of pigeon and chicken with feathery feet (Domyan et al., 2016; Rodriguez-Esteban et al., 1999; J. K. Takeuchi et al., 1999). In the emu, expression of *Tbx5* is delayed in embryonic forelimbs relative to chick, leading to the hypothesis that alterations in *Tbx5* expression might have contributed to the evolution of reduced wing size in emus (Bickley & Logan, 2014). Furthermore, *Tbx5* expression in the opossum, a marsupial born with precociously developed forelimbs, occurs much earlier in the presumptive forelimb field compared to

mouse (Keyte & Smith, 2010). Thus, *Tbx5* is not only essential for the initiation of forelimb growth, but changes in *Tbx5* expression have also contributed to the evolution of forelimb morphology.

Functional studies in zebrafish and mice have shown that *Tbx5* triggers *Fgf10* in the mesenchyme during limb bud initiation (Agarwal et al., 2003; Ng et al., 2002; Nishimoto et al., 2015). TBX5 can interact with regions of the *Fgf10* promoter to activate its expression (Agarwal et al., 2003). FGF10 then interacts with *Fgf8* in the ectoderm to form a positive regulatory loop crucial for proximal-distal outgrowth of the limb (Ohuchi et al., 1997; Sekine et al., 1999; X. Xu et al., 1998). FGFs in the apical ectodermal ridge (AER) promotes the SHH morphogen in the zone of polarizing activity (ZPA), which specifies the anterior-posterior axis of the limb (Laufer et al., 1994; Niswander et al., 1994). Analyses of a mouse model with conditionally-ablated *Tbx5* in forelimbs show that Hedgehog signaling is regulated by the direct transcriptional regulation of *Ptch1* by TBX5. While prior work has shown that the TBX5 transcription factor can bind thousands of putative *cis*-regulatory elements in embryonic mouse forelimbs (Nemec et al., 2017), little is known about how these interactions regulate gene expression in the limb.

In this study, we use a comparative ChIP-seq approach to reveal ancient TBX5 binding events in embryonic forelimbs of mice, *Anolis* lizards, turtles, and alligators. We find that deeply conserved TBX5 binding sites are enriched near genes implicated in limb morphogenesis and near components of the Hedgehog, Wnt, and BMP signaling pathways. Many of these regions occupied by TBX5 overlap functionally validated enhancers. By associating TBX5 binding events with genes that exhibit TBX5-dependent

expression, we uncover putative direct targets of TBX5. Overall, our results shed light on how *Tbx5* regulates key components of the limb gene regulatory network.

Results

Tbx5 cKO mice show a variety of forelimb disorders and misregulation of limb patterning genes

To investigate downstream targets of *Tbx5* in limb development, we inactivated the gene in forelimb buds by generating mice carrying the *Tbx5* conditional allele, *Tbx5*^{flox/flox} (Bruneau et al., 2001), and a transgene expressing *Cre* recombinase in the limb mesoderm, *HoxB6-Cre* (Lowe et al., 2000). *Tbx5* cKO (*Tbx5*^{flox/flox}; *HoxB6-Cre*) mice displayed a variety of limb disorders, including oligodactyly, polydactyly, and severe truncation of forelimbs (Fig. 2.1). *Tbx5* conditional mutant mice die perinatally, but the cause of mortality was not identified. Analysis of gross anatomy showed omphalocele, the protrusion of abdominal organs outside of the body (Fig. S2.1).

To identify genes with TBX5-dependent expression, we compared global gene expression patterns between embryonic forelimbs of wild-type and *Tbx5* cKO mice at E10.5. We used a total of six control replicates and five mutant replicates for RNA-seq. An additional *Tbx5* cKO replicate was excluded because it displayed higher normalized counts at exon 3 of *Tbx5*, and the replicate did not cluster similarly with other mutant replicates (Table S2.1, Fig. S2.2). Overall, we found 1,772 differentially expressed genes (DEGs); 766 are downregulated, while 1,006 are upregulated (Fig. 2.2A, Table S2.2). However, only 195 of these 1,772 DEGs exhibit a fold change greater than two.

Previous studies have shown that fibroblast growth factor 10 (*Fgf10*) expression is reduced in forelimb buds of both constitutive and conditional *Tbx5* knockout mice, and *Fgf10* is a direct regulatory target of TBX5 (Agarwal et al., 2003; Rallis et al., 2003). Consistent with these findings, our RNA-seq data demonstrate that *Fgf10* expression is reduced in *Tbx5* mutant forelimbs (Fig. 2.2B). Although we find underexpression of the limb ectoderm marker *Fgf4*, we do not observe a statistically significant difference in *Fgf8* expression (Table S2.2). In addition to FGF signaling, *Tbx5* is also implicated to regulate several components of the Hedgehog signaling pathway (Rallis et al., 2003; H. Xu et al., 2019). A further look into our list of differentially expressed genes identifies downregulation of several Hedgehog components including *Shh*, *Gli1*, and *Ptch1* (Fig. S2.5).

To determine whether specific gene categories or molecular pathways are enriched among genes that are differentially expressed in *Tbx5* mutants, we used the gene-set enrichment tool ShinyGO (Ge et al., 2020). Top ranked clusters among downregulated genes relate to appendage development, limb morphogenesis, and Hedgehog signaling (Fig. 2.2C). Upregulated genes are enriched for terms related to connective tissue and skeletal system development (Fig. 2.2D, top). Furthermore, the upregulated set is enriched for genes involved in the Hedgehog, Wnt, and TGF- β signaling pathways (Fig. 2.2D, bottom).

For these gene set enrichment analyses (GSEA), we used all protein coding genes in the genome. This could confound interpretation of enriched gene sets since thousands of genes do not have detectable expression in limbs and thus have no chance

of being categorized as differentially expressed genes (Timmons et al., 2015; Wijesooriya et al., 2022). To overcome this bias, we also performed GSEA using all genes that have an average normalized count (baseMean) greater than five. We find that enriched terms from the GO Biological Process and KEGG Pathway databases do not differ substantially when using this average normalized count threshold in analyses of both the downregulated and upregulated gene sets (data not shown).

Conserved TBX5 binding events are enriched near limb genes across amniotes

To identify genomic targets occupied by TBX5 in mouse limbs, we performed TBX5 ChIP-seq on chromatin from E10.5 forelimb buds. Analysis of our TBX5 ChIP-seq replicates in E10.5 forelimbs identified 13,580 highly reproducible peaks (Table S2.3), a number comparable to the 10,273 TBX5 peaks published in a former study (Nemec et al., 2017). While only 42% (5,708/ 13,580) of our TBX5 peaks overlap with this previously published dataset, Nemec and colleagues (2017) only used one replicate in their analysis. The disparity of peak co-occupancy between these two datasets may also be due to differences in the sensitivity and specificity of antibodies used (Kidder et al., 2011).

We compared our TBX5 ChIP-seq data with a previously published H3K27ac ChIP-seq dataset performed in mouse embryonic forelimbs (Infante et al., 2015). We find that many regions flanking TBX5 binding sites are marked by bimodal H3K27ac peaks (Fig. 2.3A), a pattern that indicates enhancers in an active state (Creyghton et al., 2010). A majority of TBX5 binding sites occur far from transcriptional start sites of their

associated genes, suggesting that TBX5 primarily binds at distal enhancers, rather than at promoter regions (Fig. 2.3B). Gene set enrichment analysis shows that TBX5 occupies genomic regions near genes with human orthologs implicated in limb disorders (Fig. 2.3D, left). These peaks are also enriched near genes involved in the Hedgehog, Wnt, BMP, and FGF signaling pathways (Fig. 2.3D, right).

De novo motif analysis shows that the second top enriched DNA sequence is the known T-box binding motif, AGGTGHBA (Conlon et al., 2001; Wilson & Conlon, 2002) (Fig. 2.3C). Interestingly, the top enriched motif is a composite T-box-Hox site, consistent with the top motif found in previously published TBX5 ChIP-seq data (Nemec et al., 2017). Another past study has shown that Hox and T-Box factors co-occupy many of the same binding sites in embryonic limbs and can interact to regulate transcription (Jain et al., 2018). Furthermore, HOXA11 ChIP-seq data identified the T-box consensus DNA sequence enriched in *de novo* motif analysis (Desanlis et al., 2020). We intersected our TBX5 peaks with published HOX13 peaks (Sheth et al., 2016) and find 40% (5,470/13,580) overlap (Fig. S2.3), further supporting the idea that TBX5 and HOX proteins co-bind many of the same regions across the genome in embryonic forelimbs.

While many of these TBX5-bound regions occupy well-conserved non-coding sequences, conservation of DNA sequence does not sufficiently determine that TBX5 binds orthologous elements conserved in other species. To identify deeply conserved TBX5 binding events, we used the same antibody to perform TBX5 ChIP-seq on forelimbs from four additional amniote species: brown anole, green anole, turtle (*T. scripta*), and alligator (*A. mississippiensis*). Mammals and reptiles last shared a common ancestor

approximately 310 million years ago (Evans, 2009; Pyron, 2010). Therefore, TBX5-binding events that are shared between mice and these reptiles likely represent ancient binding interactions shared in diverse species of limbed amniotes.

Our CHIP-seq experiments identified thousands of TBX5 binding events in each reptilian species observed (Fig. 2.4). In all species, we find enrichment of both the Tbox-Hox composite and known TBX5 binding motif. We used a multi-species alignment and `halLiftover` (Hickey et al., 2013) to map CHIP-seq peak coordinates from reptile genomes to the mouse genome (Table S2.3). In brown anole, green anole, turtle, and alligator forelimbs, TBX5 binding events with conserved sequences in the mouse genome are near genes with human orthologs linked to limb disorders (Fig. 2.4). Like in mice, most of these TBX5-bound regions tend to occur far from the transcriptional start sites of their associated genes. We intersected our mouse TBX5 binding sites with orthologous peak coordinates of the four reptile species analyzed and found 329 TBX5-bound regions deeply conserved in all five species. These 329 loci represent the subset of putative *cis*-regulatory elements that are sequence conserved between amniotes and are bound by TBX5 in embryonic forelimbs of these species.

TBX5 occupies genomic loci that are enriched near misregulated limb genes

While RNA-seq has identified hundreds of predicted target genes of TBX5 in developing forelimbs, many of these are likely to be indirect downstream effects of *Tbx5* ablation. We used the Genomic Regions Enrichment of Annotations Tool (GREAT) (McLean et al., 2010; Tanigawa et al., 2022) to associate TBX5 peaks with genes they are

likely to regulate. This allows us to intersect our differential expression data with our ChIP-seq datasets to reveal putative direct targets of TBX5. Integrating our mouse ChIP-seq and RNA-seq datasets identified 671 direct target genes (Table S2.5). Forty-four of these are associated with embryonic limb development or morphogenesis (Table S2.6). Interestingly, performing GSEA on the 1,101 indirect target genes identified from RNA-seq resulted in no significant enriched terms, while GSEA on the direct target gene set found enrichment in terms associated with limb development and the Hedgehog, Wnt, and TGF- β signaling pathways (data not shown).

Of the 671 direct targets, 315 genes are upregulated in *Tbx5* mutants, while 356 genes are downregulated. Although TBX5 has previously been reported to function as a transcriptional activator (Ouimette et al., 2010; Zaragoza et al., 2004), another study found that TBX5 can interact with components of the nucleosome remodeling and histone deacetylase (NuRD) complex to repress target gene expression in the heart (Waldron et al., 2016). These findings suggest that TBX5 may act as either an activator or repressor in certain contexts.

Intersecting our mouse RNA-seq data with genes associated with deeply conserved binding events of TBX5 identified 74 direct target genes (32 downregulated, 43 upregulated) (Fig. 2.5A, Table S2.5). These ancient targets are enriched for genes involved in limb patterning and morphogenesis (Fig. 2.5B, Table S2.6). Among the downregulated set includes *Hoxd10* and *Hoxd11*, which play major roles in patterning the limb stylopod and zeugopod, respectively (Davis et al., 1995; Wellik & Capecchi, 2003). Key autopod development genes *Hoxd12* and *Hoxd13* (Fromental-Ramain et al.,

1996; Knezevic et al., 1997) are also downregulated ancient regulatory targets of TBX5. An upregulated direct target includes the membrane glycoprotein gene *Gas1*, a known mediator of the *Fgf10/Fgf8* regulatory loop during limb development (Liu et al., 2002).

TBX5 directly influences forelimb development through binding at validated limb enhancers

While our CHIP-seq data identified many genomic intervals bound by TBX5 in forelimbs, we capitalized on published datasets to narrow down our list of direct targets of *Tbx5*. First, we compared our TBX5-occupied sites with hundreds of experimentally validated, limb-specific enhancers aggregated in the VISTA Enhancer Browser (Visel et al., 2007). We observe 58.8% of VISTA-tested enhancers active in the limb (211/359) are also bound by TBX5 (Fig. 2.6A). In contrast, only 12.2% of loci that do not have activity in the limb (354/2,910) overlap mouse forelimb TBX5 binding sites. Because enhancer-promoter interactions can sometimes be separated by hundreds of kilobases, we next reviewed published Capture-C data from mouse embryonic forelimbs (Andrey et al., 2017) to identify regulatory associations that might be missed using predictive tools such as GREAT. Chromosome Conformation Capture-based technologies such as Capture-C can reveal interactions between regulatory elements and their associated promoters (Downes et al., 2022; Hughes et al., 2014).

One of the predicted regulatory targets of TBX5 is *Wnt5a*, which is expressed in the distal mesenchyme under the apical ectoderm ridge (AER) (B. A. Parr et al., 1993) and required for morphogenesis of limb elements (Kumawat & Gosens, 2016). *Wnt5a*-

deficient mice show decreased proliferation of the progress zone below the AER, truncation of the proximal skeleton, and absence of digits (Yamaguchi et al., 1999). We find that *Wnt5a* is downregulated in *Tbx5* cKO embryos and is associated with a conserved TBX5 binding site that is over 460 kb downstream of the gene. This region overlaps with hs1430, a highly limb-specific enhancer that forms a long-range interaction with the *Wnt5a* promoter (Fig. 2.6B).

Fibroblast growth factor 10 (*Fgf10*) is expressed in the prospective limb mesoderm, and *Fgf10* mutants display nearly complete truncation of the embryonic forelimbs and hindlimbs (Ohuchi et al., 1997; Sekine et al., 1999). Furthermore, previous work has shown that *Tbx5* triggers *Fgf10* during limb bud initiation (Agarwal et al., 2003; Ng et al., 2002; Nishimoto et al., 2015). Consistent with these studies, we observe reduced *Fgf10* expression in *Tbx5* mutants and TBX5 binding at validated limb enhancers neighboring the *Fgf10* locus (hs516, mm917) (Fig. S2.4). We find conserved TBX5 occupancy at the *Fgf10* promoter, a previously described region that TBX5 can bind to directly activate *Fgf10* expression (Agarwal et al., 2003; Ng et al., 2002). Ancient TBX5 binding is also found near the *Gas1* locus at the validated limb enhancer hs1461. *Gas1*, which is downregulated in *Tbx5* mutants, encodes a membrane glycoprotein that positively regulates *Fgf10* expression (Liu et al., 2002).

Ephrin receptor genes are involved in cell migration, axon guidance, and early embryonic patterning (Drescher, 1997). We observe that *Tbx5* directly regulates several Eph receptors, including *Epha4*, *Epha7*, *Epha8*, and *Ephb1*. In addition to the motor neurons innervating the forelimb and the hindlimb, *Epha4* is strongly expressed in the

mesenchyme of the dorsal limb bud towards which dorsal axons project (Helmbacher et al., 2000; Ohta et al., 1996). *Epha4* mutant mice display peroneal muscular atrophy due to disordered pathfinding of motor axons in the limb (Helmbacher et al., 2000). We observed a conserved TBX5 binding event within the limb-specific enhancer, hs1507 (Fig. S2.4). This peak overlaps a domain in contact with the *Epha4* promoter.

The anterior-posterior axis of the limb is organized by the zone of polarizing activity (ZPA), a key signaling center controlled by the Sonic hedgehog (SHH) morphogen (Riddle et al., 1993; Saunders, 1968). Our RNA-seq dataset reveals misregulation of several Hedgehog signaling pathway components in *Tbx5*-depleted forelimbs (Fig. S2.5). These include *Gli1* and *Gli2*, transcription factors which act primarily as transcriptional activators in the presence of Shh signaling (Cheryll Tickle & Towers, 2017). Another Hh signaling gene, *Megf8*, is upregulated in *Tbx5* mutants and has been previously identified as a membrane protein implicated in Carpenter syndrome, a human disorder characterized by polysyndactyly of the hands and feet (Twiggy et al., 2012). We also observe misregulation of the *Ptch1* and *Ptch2* transmembrane receptors, which regulate *Smoothened* (*Smo*) in the Hedgehog signaling pathway (Ingham et al., 2000; Zhulyn et al., 2015).

Conditional inactivation of *Ptch1* in mouse limb mesenchyme leads to oligodactylous forelimbs (Butterfield et al., 2009). *Ptch1* has also been implicated to play a role in the evolution of digit loss in pig and cow limbs (Cooper et al., 2014; Lopez-Rios et al., 2014). In all five species analyzed using ChIP-seq, we find conserved TBX5 binding at the limb *cis*-regulatory module (LRM), a previously described enhancer of *Ptch1*

(Lopez-Rios et al., 2014). We also see ancient binding of TBX5 at mm1687 (Fig. S2.4), a previously identified *cis*-regulatory element of *Hand2* in the limb (Monti et al., 2017). *Hand2*, which is underexpressed in *Tbx5*-ablated forelimbs, has been shown to control *Shh* expression in the ZPA (Galli et al., 2010; Osterwalder et al., 2014).

A further examination of our ChIP-seq datasets identifies *Hoxa13* and *Twist1* as conserved targets of TBX5 (Fig. 2.6B), genes crucial for autopod development. Deletion of *Hoxa13* leads to the absence of the most anterior digit and disrupted chondrogenesis in the carpal and tarsal elements (Fromental-Ramain et al., 1996; Sheth et al., 2012). Conditional loss of *Twist1* in the mesoderm leads to polydactyly, supernumerary carpal bones, and malformations of zeugopod and stylopod elements (Loebel et al., 2012). *Hoxa13* directly activates *Shh* by binding at the ZPA Regulatory Sequence (ZRS) (Johnson et al., 2014; Leal & Cohn, 2016), while *Twist1* inhibits *Shh* in the mesenchyme of the anterior limb bud (Z. Zhang et al., 2010). We find that ancient TBX5 binding sites associated with *Hoxa13* and *Twist1* overlap human enhancers active in limbs (hs1430, hs2306, and hs2307) (Fig. 2.6B). The two TBX5 peaks observed at hs2306 indicate the possibility that this noncoding element may actually consist of separate enhancers with discrete activity (reviewed in Halfon, 2019). Overall, our combined ChIP-seq and RNA-seq analyses suggest that *Tbx5* coordinates digit patterning by both direct and indirect regulation of Hedgehog signaling components.

Discussion

Over twenty years of functional studies have demonstrated the crucial role of *Tbx5* in orchestrating forelimb outgrowth and morphology across vertebrates (Agarwal et al., 2003; Ahn et al., 2002; Rallis et al., 2003; Jun K. Takeuchi et al., 2003). However, the direct regulatory targets of TBX5 have remained largely unexplored. While previous work has identified thousands of putative TBX5 binding sites in embryonic mouse forelimbs (Nemec et al., 2017), it remained unclear which of these interactions directly influence gene expression during limb growth. We have used an integrative ChIP-seq and RNA-seq approach to identify the direct regulatory targets of TBX5. Our study provides unprecedented insight into the role *Tbx5* plays in the gene regulatory network underlying forelimb development (Fig. 2.7).

Haploinsufficiency of *TBX5* in human patients leads to Holt-Oram syndrome (HOS), which is characterized by disorders of the heart, clavicle, and upper limbs (Basson et al., 1997; Q. Y. Li et al., 1997). Forelimb malformations are fully penetrant and exhibit a spectrum of defects of the hand and digits or bones in both the lower and upper arm (Newbury-Ecob et al., 1996). Consistent with phenotypes reported in a previously generated *Tbx5* haploinsufficient mouse model (H. Xu et al., 2019), our conditional mutant mice recapitulate dactyly and arm disorders observed in HOS patients (Fig. 2.1). The severity of the forelimb disorder in *Tbx5^{flox/flox}; HoxB6-Cre* mice ranged from oligodactyly to nearly complete limb truncation, which may be due to either differences in the timing of *Tbx5* knockout or variation in the fraction of cells that are *Tbx5*- ablated between mutant embryos. The normalized read count of exon 3 varies in *Tbx5* cKO

embryonic forelimbs (Table S2.1), suggesting that the varying efficiency of *Tbx5* deletion may also explain the spectrum of forelimb disorders observed in mutants.

While *Prrx1-Cre*-mediated ablation of *Tbx5* completely prevents the growth of a forelimb bud (Rallis et al., 2003), our *Tbx5* cKO mice maintain forelimb initiation. The presence of a forelimb bud in *Tbx5^{flox/flox}; HoxB6-Cre* embryos enabled us to collect tissue for a transcriptome-wide investigation of differential gene expression. Our RNA-seq analysis of early forelimb development uncovered that many genes pivotal for limb growth and patterning are misregulated in *Tbx5* cKO embryos (Table S2.2 and Table S2.6). In alignment with previous studies, we see downregulation of *Fgf10* in *Tbx5* mutants. Interestingly, we do not observe a statistically significant difference in *Fgf8* expression. Because *HoxB6-Cre* mice appear to express *Cre* recombinase only in the posterior mesoderm of the forelimb bud (Lowe et al., 2000), it is possible that incomplete ablation of *Tbx5* throughout the mesenchyme is permitting some activity of the *Fgf10/Fgf8* feedback loop. This may explain why forelimb outgrowth is still observed in certain *Tbx5^{flox/flox}; HoxB6-Cre* mutants.

FGFs in the apical ectodermal ridge (AER) promote *Shh* expression in the zone of polarizing activity (ZPA) of the limb (Laufer et al., 1994; Niswander et al., 1994). A SHH-FGF positive feedback loop facilitates distal progression and patterning of the limb bud (Delgado & Torres, 2017). Accordingly, we identified misregulation of many components of the Hedgehog pathway (Fig. 2.7, Fig. S2.5). Although we observe a significant decrease of *Shh* expression in the *Tbx5* mutant, we do not see TBX5 binding near the *Shh* locus or at the ZRS enhancer. However, we find three mouse TBX5 peaks over 290

kb upstream of *Shh* that are near a domain contacting the *Shh* promoter (data not shown).

Downstream of Hedgehog signaling, we find that *Tbx5* directly regulates the expression of *Ptch1*, *Ptch2*, *Gli1*, *Gli2*, and *Gas1*. Upstream of the Hh pathway, we see overexpression of *Twist1*, a known inhibitor of *Shh*. Moreover, important activators of *Shh* such as *Hand2*, *Hoxa/d11*, and *Hoxa/d13* are underexpressed in *Tbx5* cKO forelimbs. Our comparative ChIP-seq analysis also found that TBX5 binds validated limb enhancers to directly regulate these genes (Fig. 2.6, Fig. S2.4). Overall, our data both support and expand on studies that implicate *Tbx5* as a crucial inhibitor of Hedgehog signaling in the limb (Rallis et al., 2003; H. Xu et al., 2019).

Previous work has shown that *Tbx5* is only required during the earliest phases of limb formation and is dispensable during later outgrowth of the skeletal elements (Hasson et al., 2007). The forelimb disorders we observe in *Tbx5* cKO embryos suggest that *HoxB6-Cre*-mediated deletion of *Tbx5* is occurring early enough to disrupt limb skeletal development (Fig. 2.1). However, it has remained uncertain whether skeletal defects in *Tbx5*-ablated embryos are due to the direct involvement of *Tbx5* in chondrogenesis and ossification or indirect disruption of downstream target genes. Our data suggest that TBX5 directly influences early cartilage and bone formation by regulating components of the BMP and Wnt signaling pathways (Fig. 2.7). BMP and Wnt activity both control crucial developmental processes during morphogenesis of the limb skeleton (Geetha-Loganathan et al., 2008; Pignatti et al., 2014).

Tbx5 is also required for soft tissue patterning of the muscles and tendons in forelimbs (Hasson et al., 2010). In this study, Hasson and colleagues used a tamoxifen-inducible Prx1-Cre line to ablate *Tbx5* in limb mesenchymal cells. Candidate muscle patterning genes were analyzed by whole-mount *in situ* hybridization of *Tbx5* cKO embryos and found to have altered expression patterns in forelimbs. Consistent with this report, we find our *Tbx5* conditional mutants show underexpression of *Cxcl12* (also known as *SDF1*), a gene encoding a chemokine important for migration of muscle progenitors in the limb (Vasyutina et al., 2005). Our mouse TBX5 ChIP-seq data also shows binding sites associated with *Cxcl12*. Furthermore, we observe that TBX5 directly activates *Osr1*, a gene which encodes a transcription factor necessary for the proliferation and survival of myogenic progenitors (Vallecillo-García et al., 2017).

Functional studies in fish, birds, amphibians, and mammals have established that *Tbx5* has a deeply conserved role in growth and development of the vertebrate forelimb (Ahn et al., 2002; Bruneau et al., 2001; Rodriguez-Esteban et al., 1999; M. Suzuki et al., 2018; Tani-Matsuhana et al., 2018). Changes in *Tbx5* expression have been proposed to contribute to the evolution of forelimb size and limb-type-specific morphologies (Bickley & Logan, 2014; Chew et al., 2014; Domyan et al., 2016; Keyte & Smith, 2010; J. Li et al., 2020; J. K. Takeuchi et al., 1999). However, the degree to which TBX5 binding events are conserved in tetrapod forelimbs has remained unknown. Our study provides the first comparison of putative TBX5-bound enhancers in five distantly related species of amniotes. Ancient TBX5 binding events are associated with many genes that have known roles in limb development (Fig. 2.5, Table S2.5, Table S2.6).

Further investigations will reveal how the binding sites of TBX5 have changed in related species that have evolved differences in forelimb morphology.

In conclusion, we have generated a transcriptomic dataset that reveals genes downstream of *Tbx5*. Moreover, we have linked hundreds of TBX5-bound *cis*-regulatory elements to genes with TBX5-dependent expression. These data will allow us to characterize the different mechanisms used by *Tbx5* to pattern the embryonic forelimb. While the roles of individual TBX5-binding sites remain to be investigated, the presence of ancient binding events that are shared between mammals and reptiles strongly suggests that TBX5 directly regulates crucial components of the forelimb regulatory network.

Methods

Animals

Tbx5 cKO mice were generated by crossing *Tbx5*^{flox/flox} mice (Bruneau et al., 2001) with *HoxB6-Cre* mice (Lowe et al., 2000). Both of these mouse strains have a C57BL/6 genetic background. Embryonic day (E) 0.5 was designated at noon of the day a vaginal plug was observed. Eggs were collected from wild-caught brown anole and green anole females. Turtle and alligator samples used were supplied by Martin Cohn and Benjamin Parrott. All animal procedures were performed per guidelines issued by the Institutional Animal Care and Use Committees (IACUC) at the University of Georgia under approved Animal Use Protocols.

RNA-seq

Forelimb pairs were collected from E10.5 mouse embryos, pretreated in RNAlater, and stored at -80°C until further processing. Amniotic sac tissue was collected for genotyping and only XY embryos were used. Total RNA was collected from individual control (*Tbx5^{flox/flox}*) and mutant (*Tbx5^{flox/flox}; HoxB6-Cre*) forelimb samples using the mirVana miRNA Isolation Kit (ThermoFisher Scientific). mRNA libraries from six control and six mutant replicates were prepared using the TruSeq Stranded mRNA Library Prep Kit (Illumina) and sequenced at Georgia Genomics and Bioinformatics Core (50 bp single-end reads). Reads were aligned to the mm10 genome using HISAT2 (v2.1.0) and transcripts were counted using Rsubread (v2.8.2) featureCounts. DEseq2 (v1.34.0) was used to perform differential gene expression analysis.

We used ShinyGO (v0.77) (Ge et al., 2020) to perform gene-set enrichment analysis and to generate lollipop plots. The gene set enrichment analyses initially used all protein coding genes as the background set, but were subsequently reanalyzed using all genes that exhibited an average normalized count (baseMean) greater than five. We utilized BioTapestry to build and visualize the forelimb gene regulatory network (Longabaugh et al., 2005; Paquette et al., 2016).

ChIP-seq

Forelimb pairs were collected from the following embryos: E10.5 mice (outbred ICR; Envigo), stages 3-5 of *A. sagrei* and *A. carolinensis* (Sanger et al., 2008), stage 16 of *A. mississippiensis* (Ferguson, 1985), and stage 12 of *T. scripta elegans* (Greenbaum,

2011). For the mouse, turtle, and *A. sagrei* samples, two independent CHIP and Input replicates were generated. One CHIP and Input replicate were generated from the alligator and *A. carolinensis* samples. Forelimb samples were crosslinked in 1% formaldehyde and stored at -80°C until further processing of chromatin. Roughly 50 µg of chromatin was incubated in Protein G Agarose Columns (Active Motif) with a human/mouse TBX5 polyclonal antibody (R&D Systems AF5918). Libraries were prepared using the NEBNext Ultra II Library Prep Kit and amplified for 15 cycles. Sera-Mag SpeedBeads were used to perform size selection and to remove primer and adapter fragments. Libraries were sequenced by the Georgia Genomics and Bioinformatics Core to generate single-end 75 bp reads.

ChIP-seq data analysis

For species in which we generated two CHIP-seq replicates, we used the ENCODE Transcription Factor and Histone CHIP-Seq processing pipeline (<https://github.com/ENCODE-DCC/chip-seq-pipeline2>) (Landt et al., 2012). Highly reproducible (conservative) peak sets were used with an irreproducible discovery rate (IDR) cutoff of 0.05. For species in which only one CHIP-seq replicate was generated, we used bwa for alignment and MACS2 for peak calling. The following genomes were used for alignment: mm10 (mouse), AnoSag2.0 (brown anole), AnoCar2.0 (green anole), allMis1 (alligator), and *Chrysemys picta belli* - ASM1138683v1 (turtle). We used a multi-species alignment and halliftover (Hickey et al., 2013) to map CHIP-seq peak coordinates from reptile genomes to the mouse genome. To assign putative target genes of each

peak, we used GREAT with default parameters (McLean et al., 2010; Tanigawa et al., 2022). Motif analyses were performed on TBX5 peaks centered 100 bp flanking each summit using HOMER v4.11 (findMotifsGenome.pl) (Heinz et al., 2010). Enrichment heatmaps were generated using Deeptools and genome browser tracks were assembled using pyGenomeTracks. We used bedtools to find peak coordinate intersections.

Data availability

Genomic and transcriptomic data for this manuscript will be uploaded to the Gene Expression Omnibus database (Edgar et al., 2002) and updated accession numbers will be posted to the GitHub page below.

Scripts and bioinformatic pipelines used to analyze data and generate figures are available at <https://github.com/gene-drive/Tbx5-forelimb-genital>.

Public data used

Mouse H3K27ac ChIP-seq data from E11.5 forelimbs was generated by Infante et al. (2015) (Accession GSE64055) and reanalyzed to convert peaks to mm10. Forelimb Capture-C data was obtained from Andrey et al. (2017). Coordinates and embryonic images of experimentally tested enhancers were extracted from the VISTA Enhancer Browser (Visel et al., 2007) and converted to mm10 coordinates using the UCSC Liftover tool.

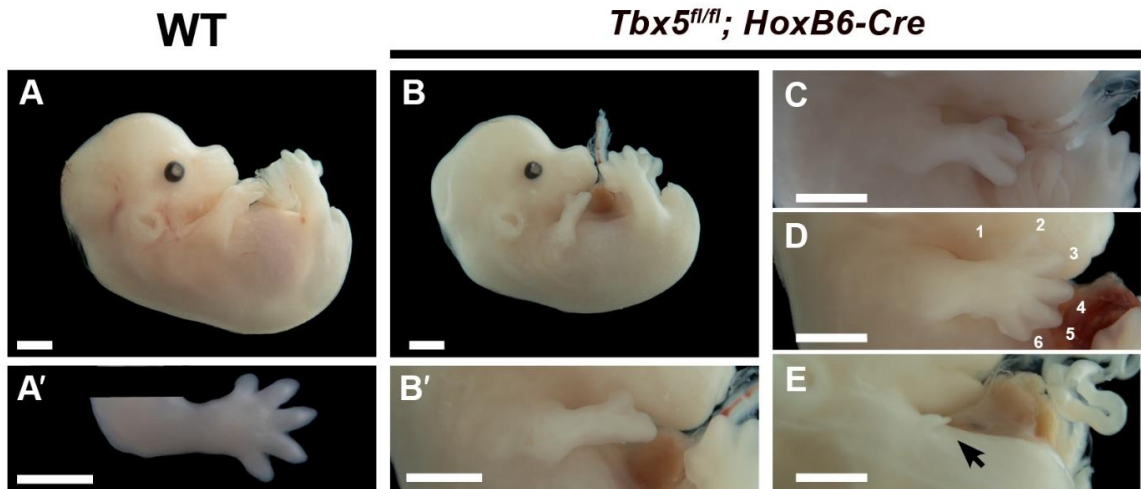


Figure 2.1. *Tbx5* cKO mice display a variety of forelimb disorders

A-E) Morphology of E14.5 embryos (A, B) and forelimbs (A', B', C-E), genotypes as indicated. The forelimb of the WT embryo (A') was dissected to display the pentadactyl digit pattern. *Tbx5* cKO embryos exhibited forelimbs with oligodactyly (B-C, B'), polydactyly (D), and severe truncation (E). Hindlimbs of *Tbx5* mutants showed a wild-type phenotype. Numbers in (D) represent digit count, not identity. The scale bar represents 1 mm.

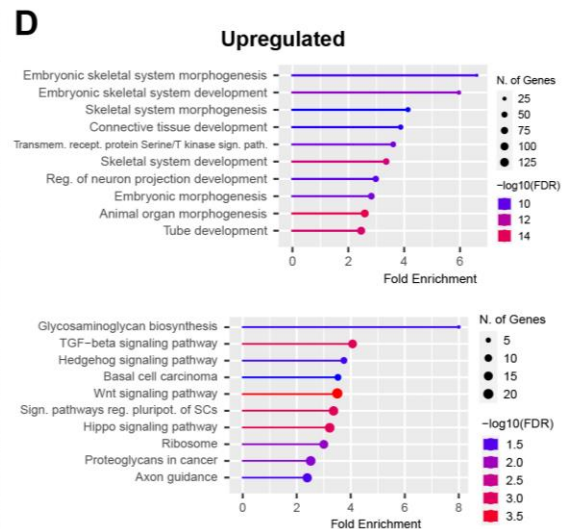
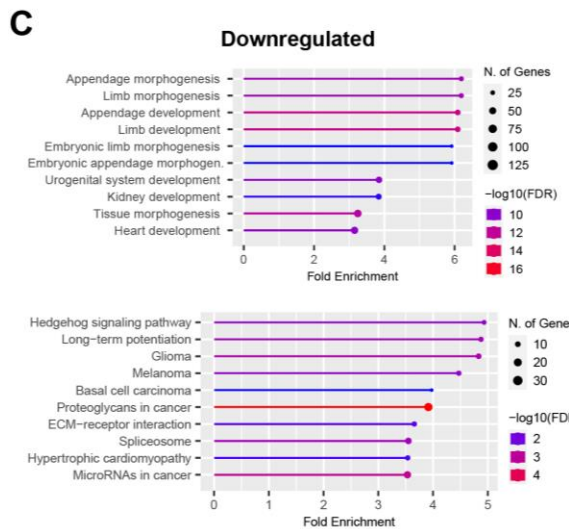
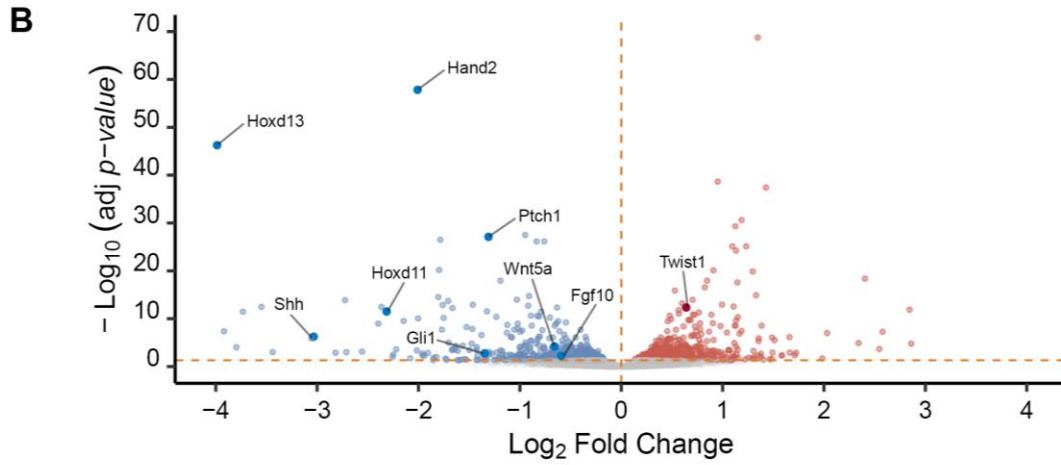
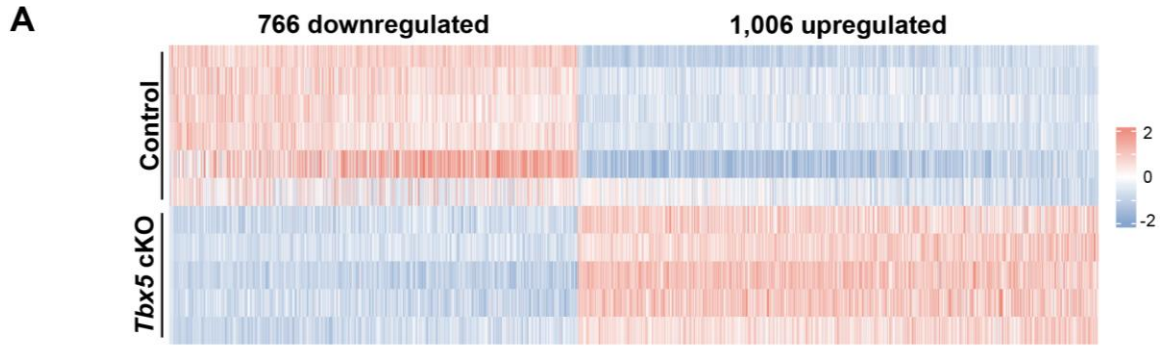


Figure 2.2. Differentially expressed genes (DEGs) in forelimbs of *Tbx5* conditional knockout (cKO) mice at E10.5

A) RNA-seq heatmap of global expression patterns in five replicates of *Tbx5* cKO (*Tbx5*^{flox/flox}; *HoxB6-Cre*) mice compared to six replicates of controls (*Tbx5*^{flox/flox}).

B) Volcano plot showing fold-change and adjusted *p*-value of DEGs output from DESeq2.

Differentially expressed genes (adjusted *p*-value <0.05) are depicted in blue

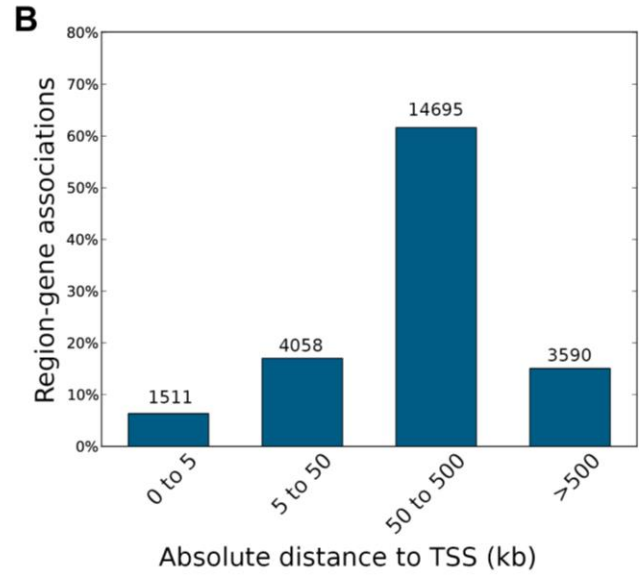
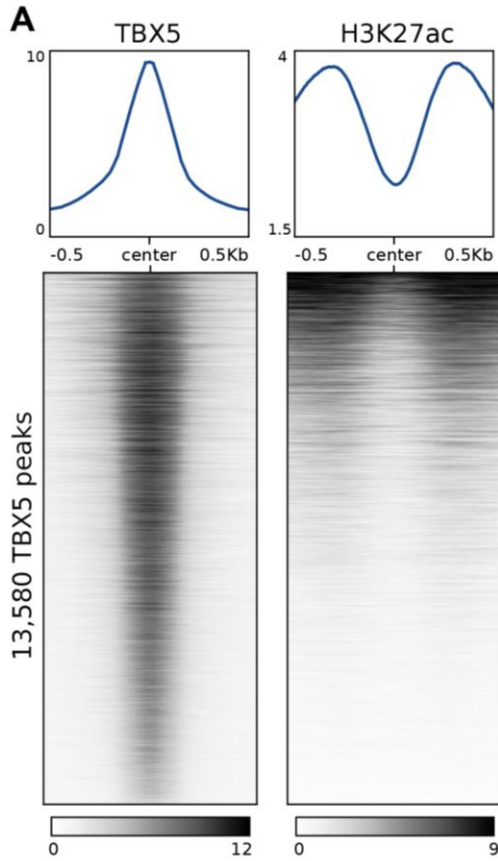
(downregulated) and red (upregulated). Several genes with known roles in limb

development are labeled.

C, D) Lollipop plots showing top enriched gene clusters in the GO Biological Process (top)

(Gene Ontology Consortium, 2021) and KEGG Pathway (bottom) (Kanehisa et al., 2021)

databases for downregulated (C) and upregulated (D) DEGs.



C

Rank	Motif	p-value	Type
1		1e-1341	T-box-Hox
2		1e-756	T-box
3		1e-603	Lhx

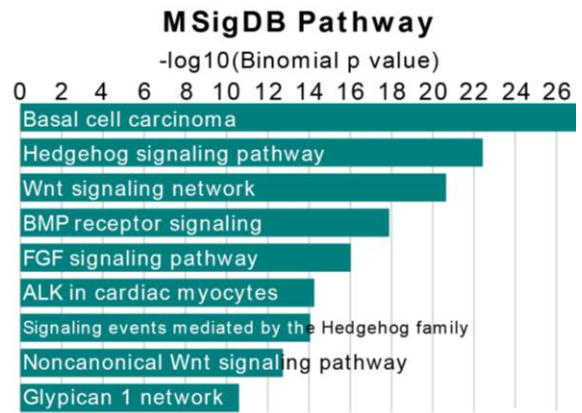
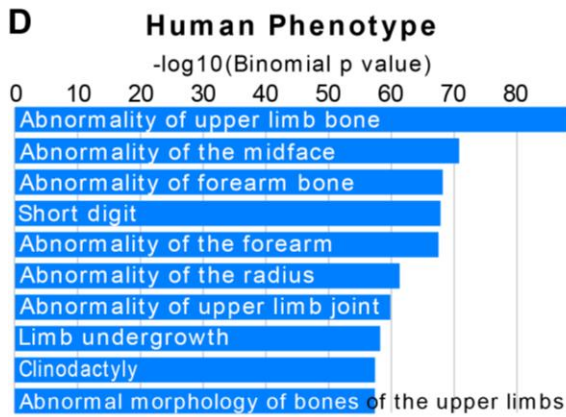


Figure 2.3. Genome-wide enrichment of TBX5 binding in mouse embryonic forelimbs

A) Condensed profiles (top) and heatmaps (bottom) of TBX5 and H3K27ac (Infante et al., 2015) signal in E10.5 and E11.5 forelimbs, respectively. ChIP-seq datasets are centered on TBX5 peak summits in a 1 kb window.

B) Distribution of TBX5 peaks relative to transcriptional start sites (TSS) of associated genes identified using GREAT. The number of peaks counted is listed above each bar in the graph.

C) Top enriched motifs found using HOMER de novo motif analysis in a 100 bp window centered on TBX5 peak summits.

D) Highest-ranked annotation terms of genes associated with TBX5 peaks in the Human Phenotype Ontology (top) and Molecular Signatures Database (bottom).

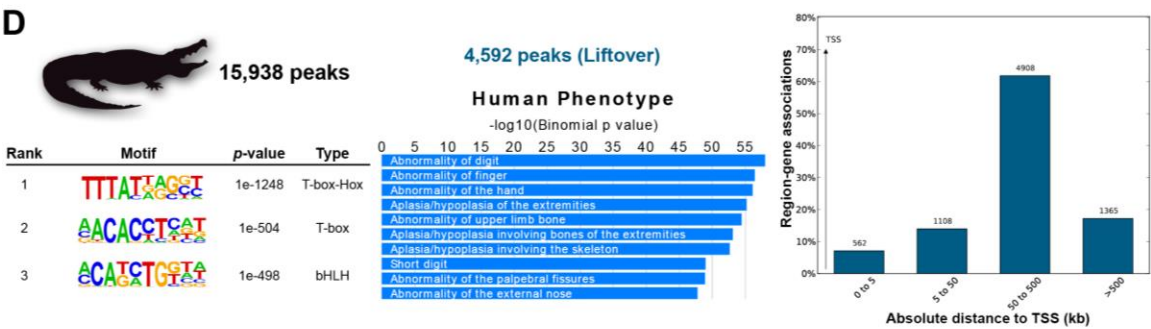
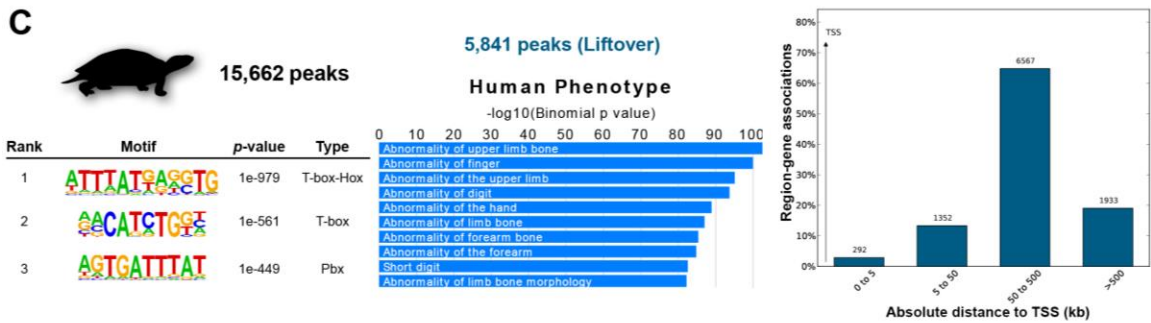
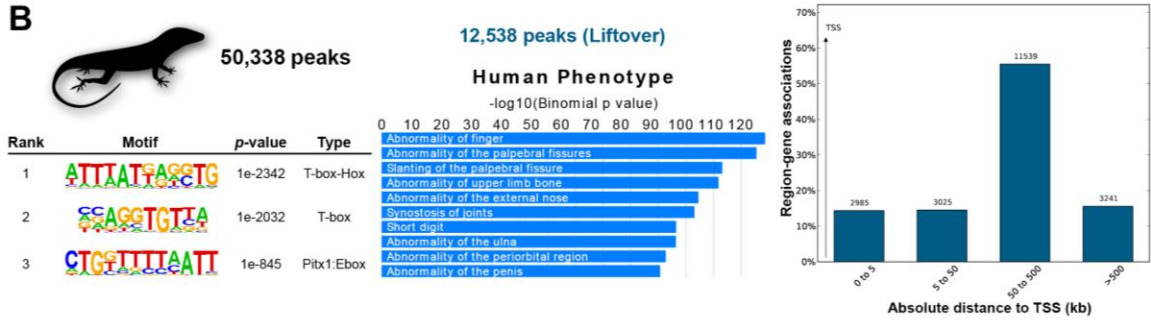
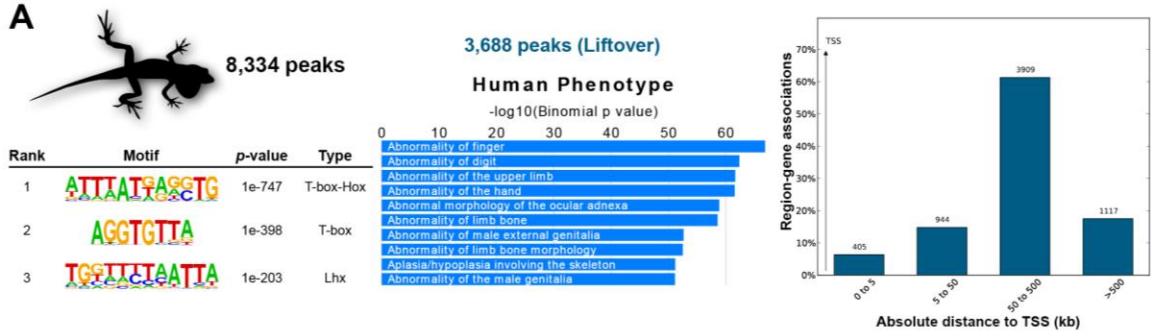


Figure 2.4. Genome-wide occupancy of TBX5 binding events in reptile embryonic forelimbs

A-D) Analysis of TBX5 peaks in brown anole (A), green anole (B), turtle (C), and alligator (D).

Under the peak number identified in each species lists the top enriched motifs found.

Motifs were identified using HOMER *de novo* motif analysis in a 100 bp window

centered on TBX5 peak summits. The peak number in blue lists the number of peaks

that have sequence orthologs in the mouse genome. These peaks were converted into

mouse coordinates using `halLiftover`.

The middle panels show the highest-ranked annotation terms of genes associated with

orthologous TBX5-bound regions in the Human Phenotype Ontology. Each panel on the

right shows the distribution of TBX5 peaks of each species relative to transcriptional

start sites (TSS) of associated genes identified using GREAT. The number of peaks

counted is listed above each bar in the graph.

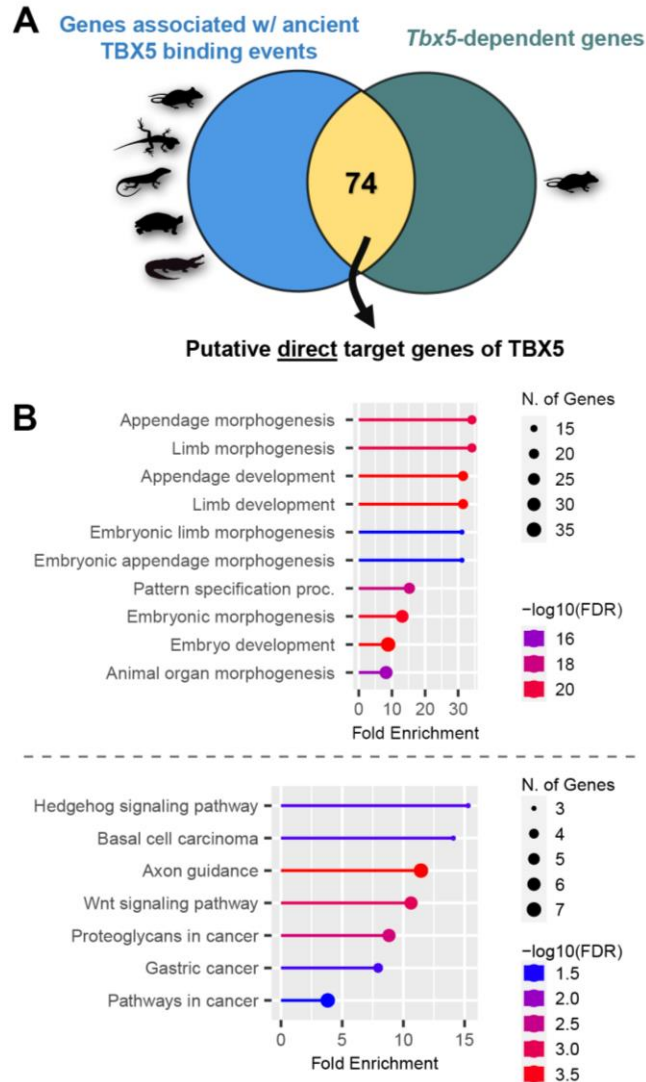
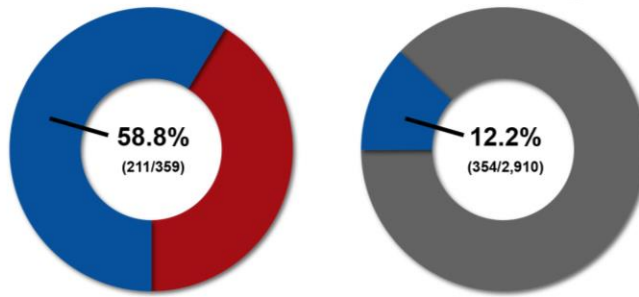


Figure 2.5. Deeply conserved TBX5 binding events in embryonic forelimbs of amniotes

A) Approach for identifying putative direct target genes of TBX5. TBX5 ChIP-seq peaks were compared in five amniote species to find ancient TBX5 binding events. GREAT was used to associate TBX5 peaks with neighboring genes. This gene list was then intersected with misregulated genes identified in *Tbx5* cKO embryos.

B) Lollipop plots showing top enriched gene clusters in the GO Biological Process (top) (Gene Ontology Consortium, 2021) and KEGG Pathway (bottom) (Kanehisa et al., 2021) databases.

A VISTA-limb-positive VISTA-limb-negative



B

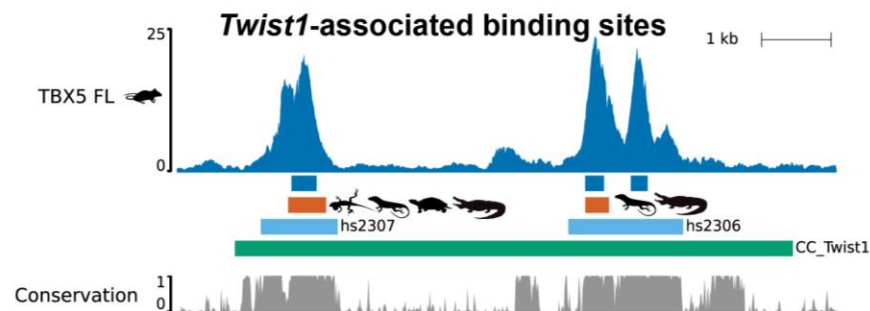
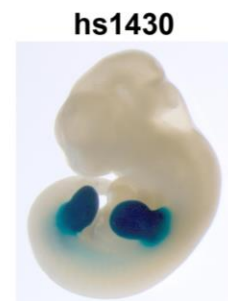
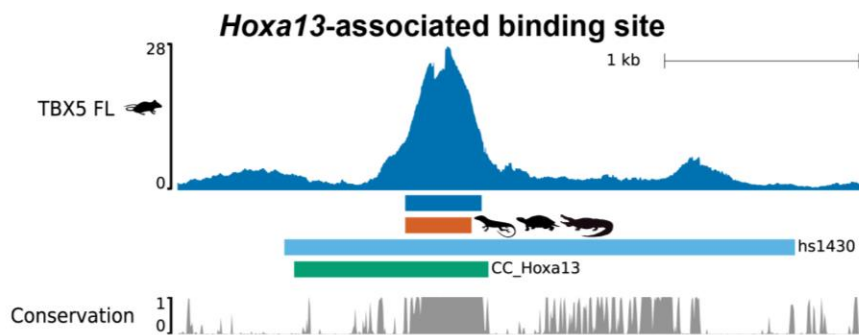
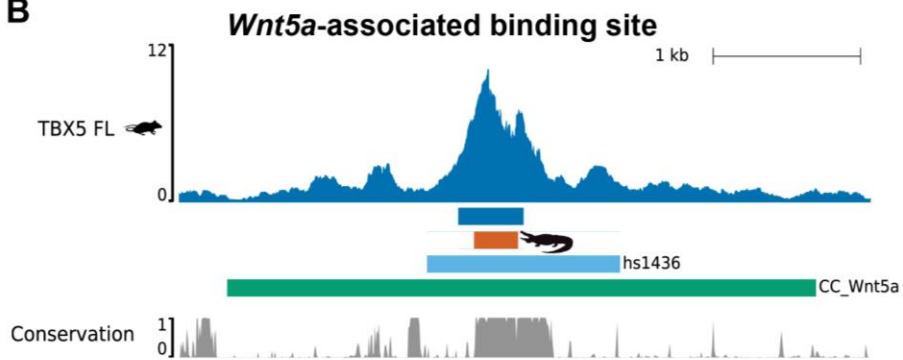


Figure 2.6. TBX5 directly regulates limb genes by binding VISTA-validated enhancers

A) The proportion of TBX5 ChIP-seq peaks that overlap with experimentally validated noncoding fragments of the VISTA Enhancer Browser (Visel et al., 2007). VISTA-limb-positive regions include regulatory elements that display activity in limbs. VISTA-limb-negative regions include negatively tested loci and regions that show activity in non-limb tissue.

B) TBX5-bound *cis*-regulatory elements of limb genes. *Wnt5a* and *Hoxa13* are downregulated in forelimbs of *Tbx5* cKO embryos, while *Twist1* is upregulated. The dark blue graph at the top of each panel shows peak intensity for TBX5 ChIP-seq in mouse embryonic forelimbs. Boxes below the graph represent coordinates for (top to bottom): Mouse TBX5 ChIP-seq peaks (dark blue), conserved TBX5 binding event (orange), validated VISTA enhancer (Visel et al., 2007) (light blue), and Capture-C (CC) peaks indicating interaction with the gene's promoter (Andrey et al., 2017) (green). The orange box marks the minimal mouse sequence conserved in each species indicated that is also bound by TBX5. The conservation graph shows the phastCons score from alignments of 60 vertebrate species (Pollard et al., 2010) obtained from the UCSC Genome Browser (Kent et al., 2002). Photos show *in vivo* enhancer activity in transgenic mice (hs2306 not shown). Genomic coordinates for each region are available in Table S2.4.

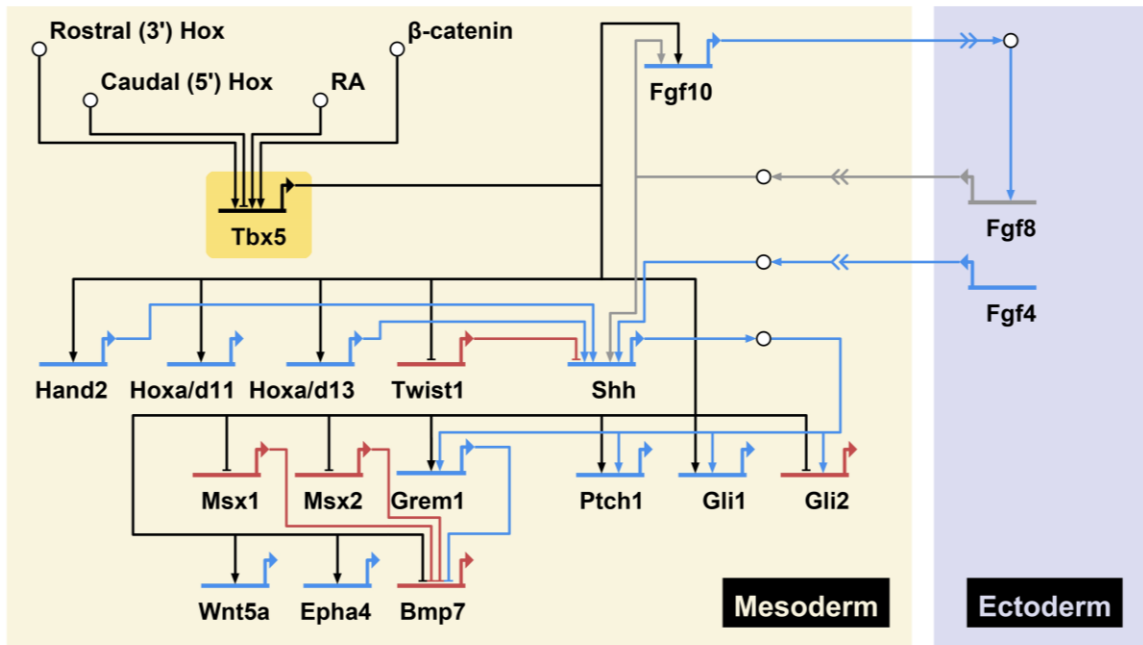


Figure 2.7. Proposed role of *Tbx5* in the gene regulatory network underlying forelimb development

Blue genes are downregulated in *Tbx5* conditional mutants, while red genes are upregulated. Gray genes are not differentially expressed. White circles represent proteins that mediate downstream transcriptional processes. BioTapestry was used to build and visualize the gene regulatory network (Longabaugh et al., 2005; Paquette et al., 2016).

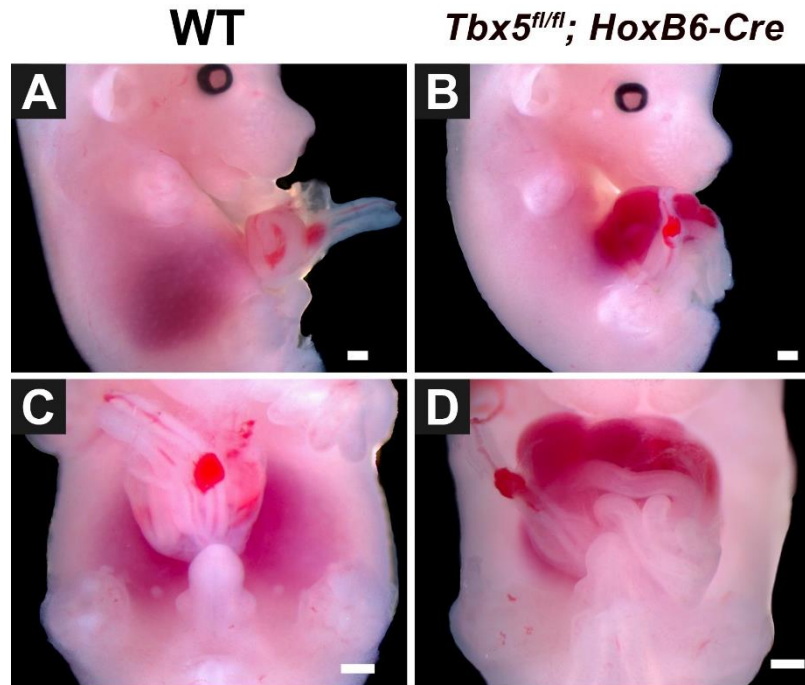


Figure S2.1. *Tbx5* mutants display omphalocele

A-D) Lateral (A, B) and ventral (C, D) views showing the abdominal wall in E14.5 embryos, genotypes as indicated. Limbs were removed to better show the abdomen.

The scale bar represents 500 μm .

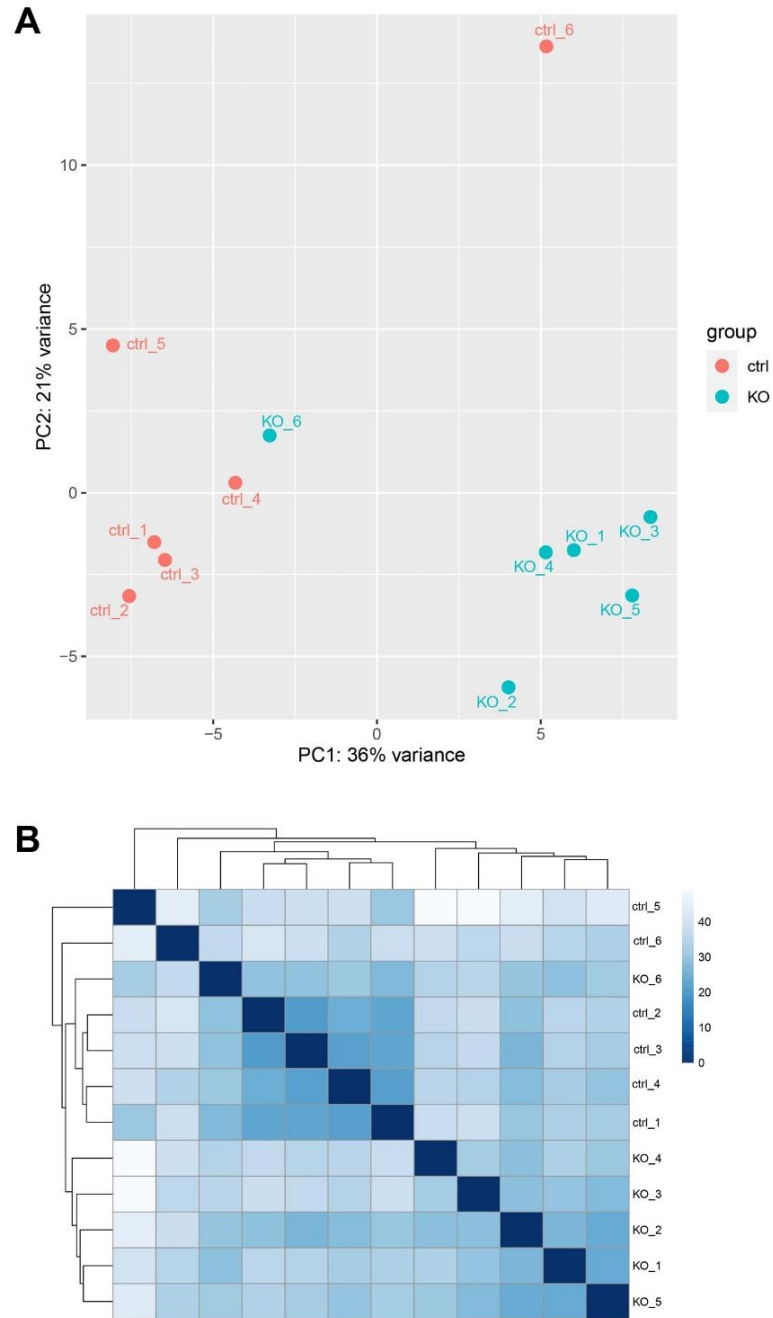


Figure S2.2. RNA-seq data quality assessment by sample clustering

PCA plot (A) and sample-to-sample distances heatmap (B) showing six replicates of *Tbx5* cKO (*Tbx5*^{flox/flox}; HoxB6-Cre) mice compared to six controls (*Tbx5*^{flox/flox}). Sample-to-sample distances were calculated from transformation of count data for overall gene expression.

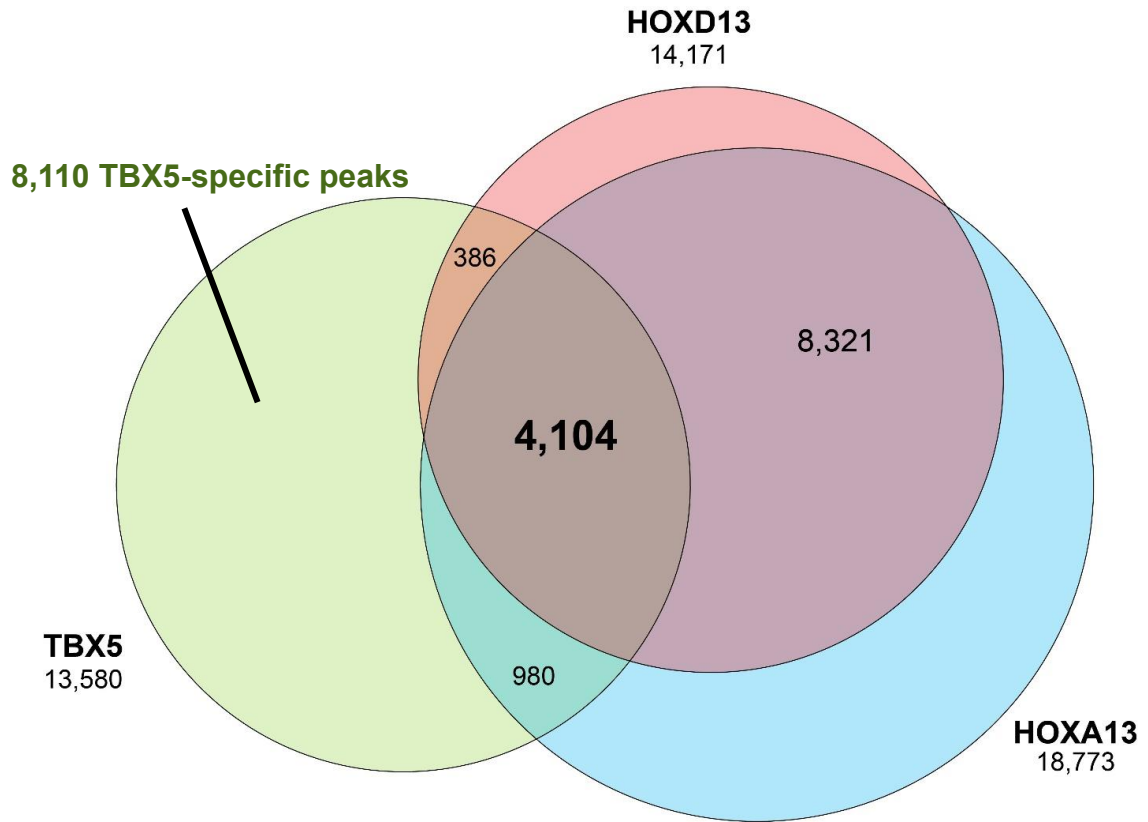


Figure S2.3. TBX5 binds many of the same regions as HOX13

Venn diagram showing overlapping binding regions of TBX5, HOXA13, and HOXD13 in mouse forelimbs. (Sheth et al., 2016). Venn generated using eulerr (Larsson, 2022).

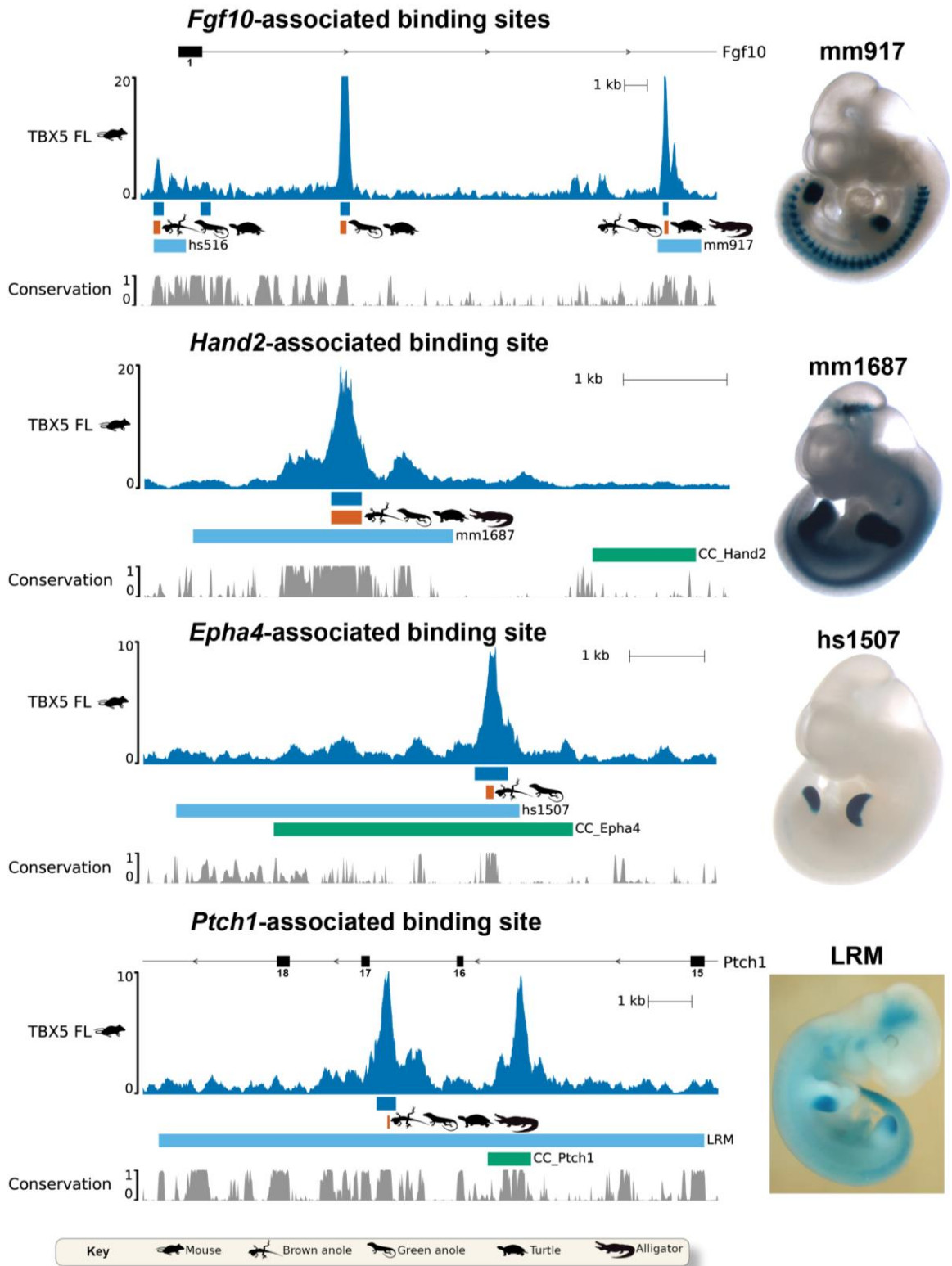


Figure S2.4. Additional examples of TBX5 binding at validated limb enhancers

Fgf10, *Hand2*, *Epha4*, and *Ptch1* are downregulated in forelimbs of *Tbx5* cKO embryos. The dark blue graph at the top of each panel shows peak intensity for TBX5 ChIP-seq in mouse embryonic forelimbs. Boxes below the graph represent coordinates for (top to bottom): Mouse TBX5 ChIP-seq peaks (dark blue), conserved TBX5 binding event (orange), validated VISTA enhancer (Visel et al., 2007) (light blue), and Capture-C (CC) peaks indicating interaction with the gene's promoter (Andrey et al., 2017) (green). The orange box marks the minimal mouse sequence conserved in each species indicated that is also bound by TBX5. The conservation graph shows the phastCons score from alignments of 60 vertebrate species (Pollard et al., 2010) obtained from the UCSC Genome Browser (Kent et al., 2002). Photos show *in vivo* enhancer activity in transgenic mice (hs516 not shown). Photo of limb *cis*-regulatory module (LRM) activity from (Lopez-Rios et al., 2014). Genomic coordinates for each region are available in Table S2.4.

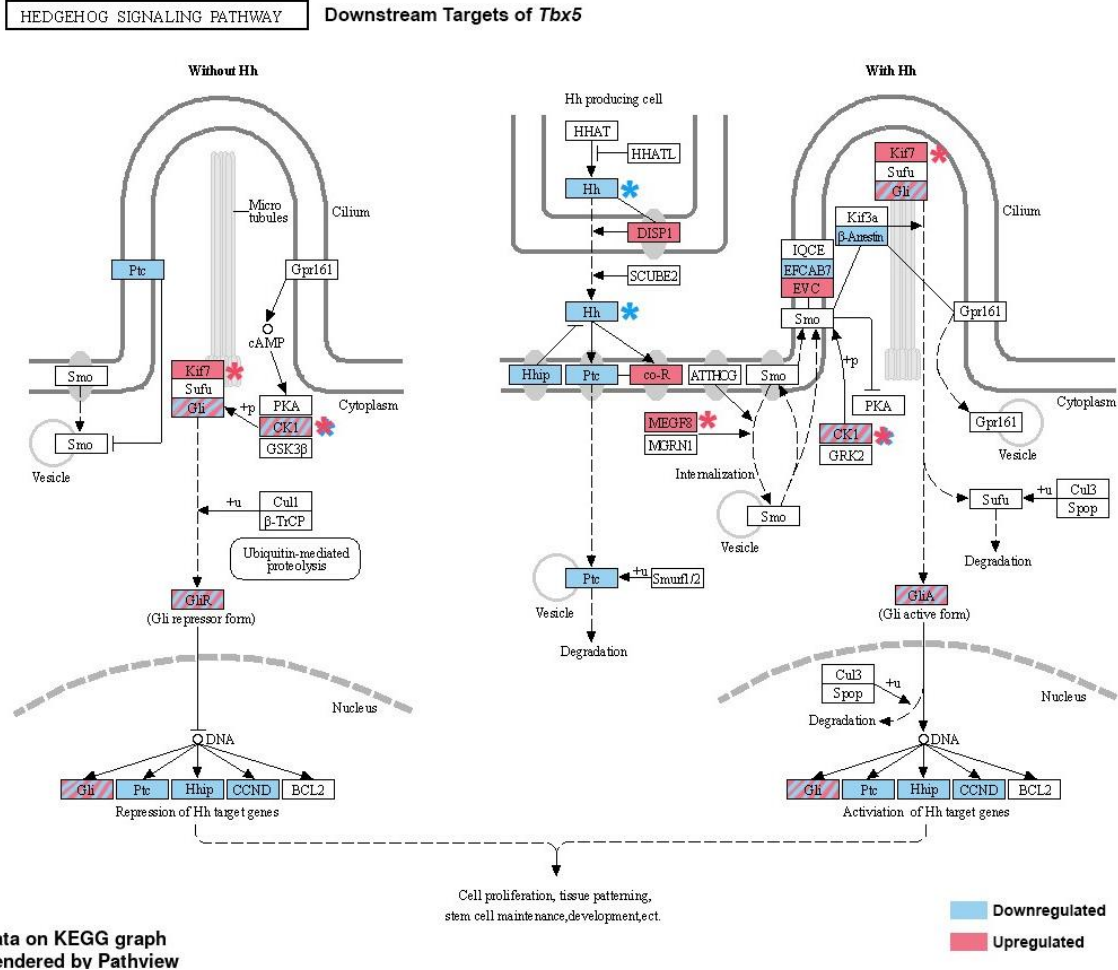


Figure S2.5. *Tbx5* regulates several components of the Hedgehog signaling pathway

Differentially expressed genes in *Tbx5*-depleted forelimbs are highlighted. Striped boxes indicate components that have both upregulated and downregulated genes. Asterisks mark genes that are indirectly regulated by *Tbx5* and are not associated with any TBX5 binding sites. The KEGG pathway diagram was adapted from ShinyGO (Ge et al., 2020) and rendered by Pathview (Kanehisa et al., 2021; W. Luo & Brouwer, 2013).

Table S2.1. Normalized counts of *Tbx5* exons in control and cKO forelimbs

DESeq2 was used to calculate normalized counts of each exon using the median-of-ratios method (Love et al., 2014). Asterisk indicates $p < 0.05$ (one-tailed t -test).

	Exon 1	Exon 2	Exon 3*	Exon 4	Exon 5	Exon 6	Exon 7	Exon 8	Exon 9
Ctrl_1	391.32	397.39	138.83	172.67	289.80	327.11	107.59	541.43	4490.21
Ctrl_2	427.52	377.06	185.32	205.50	310.09	383.48	119.27	470.64	5243.09
Ctrl_3	439.15	435.04	140.90	223.18	328.08	311.62	94.62	559.48	5204.03
Ctrl_4	418.31	371.18	107.73	203.69	284.49	258.40	133.83	569.82	4965.90
Ctrl_5	304.82	356.03	119.49	124.37	241.42	245.08	106.08	384.07	3807.81
Ctrl_6	359.82	424.93	133.65	103.95	316.41	270.72	94.81	504.89	4668.53
KO_1	285.35	390.61	83.70	152.18	272.66	256.18	82.43	533.91	4552.85
KO_2	401.96	494.04	99.01	256.42	317.81	260.38	96.04	653.44	5916.56
KO_3	439.80	456.62	104.54	128.58	276.38	290.80	87.72	710.17	5241.56
KO_4	426.62	462.77	74.72	147.03	395.28	355.51	116.90	533.87	6076.25
KO_5	451.34	334.65	58.71	146.78	367.67	312.63	155.58	563.62	4766.54
KO_6	348.52	404.18	109.61	175.55	247.48	267.17	120.74	447.00	5287.80

Table S2.2. Sample of differentially expressed genes in embryonic forelimbs of *Tbx5***cKO mice**

Gene	baseMean	log2FoldChange	lfcSE	stat	pvalue	padj
Alx4	8769.812	1.44462	0.071458	20.21635	7.02898E-91	1.2139E-86
Irx3	6328.71	1.346562	0.074289	18.1259	1.9906E-73	1.71889E-69
Hand2	5057.112	-2.00898	0.120578	-16.6613	2.50545E-62	1.44231E-58
Hoxd13	2463.938	-3.98709	0.266439	-14.9644	1.25528E-50	5.41966E-47
Alx3	2855.765	0.951851	0.069303	13.73459	6.30092E-43	2.17634E-39
Irx5	1866.729	1.427335	0.105628	13.5129	1.31244E-41	3.77765E-38
Hoxd12	1702.209	-5.676	0.459524	-12.3519	4.75694E-35	1.17361E-31
Hoxc4	1408.938	1.186935	0.096617	12.28498	1.09076E-34	2.35467E-31
Hoxb3	2508.813	1.125819	0.093589	12.02939	2.49006E-33	4.77815E-30
Rnd3	4562.608	-0.94779	0.081245	-11.6658	1.90544E-31	3.2907E-28
Ptch1	4849.923	-1.30976	0.113066	-11.584	4.96792E-31	7.79964E-28
Cntfr	1011.038	-1.78533	0.155885	-11.4528	2.27609E-30	3.27567E-27
Pam	2118.83	-0.83525	0.073452	-11.3715	5.79797E-30	7.15221E-27
Ets2	12695.49	-0.75969	0.066803	-11.3721	5.7554E-30	7.15221E-27
Msx2	3146.509	1.232574	0.110526	11.15186	7.01273E-29	7.56937E-26
Hoxc6	1805.949	1.095737	0.098254	11.15209	6.99422E-29	7.56937E-26
Msx1	14524.67	1.132327	0.103272	10.96451	5.66035E-28	5.75025E-25
Cdc42ep3	407.2145	-1.79606	0.178207	-10.0785	6.87521E-24	6.59638E-21
Hoxb2	1040.299	0.909289	0.090433	10.05478	8.75142E-24	7.95458E-21
Gdf6	458.2878	1.297061	0.12976	9.995816	1.58973E-23	1.37273E-20
Tac1	126.6476	2.403312	0.24916	9.645645	5.12879E-22	4.21782E-19
Pkdcc	21490.32	0.847376	0.088828	9.539473	1.4356E-21	1.12694E-18
Itm2a	4585.435	-1.19163	0.125033	-9.5306	1.56376E-21	1.17418E-18
Rdh10	1374.999	1.145638	0.121309	9.443993	3.58838E-21	2.58214E-18
Tmem59l	957.6818	0.824654	0.089785	9.184808	4.12262E-20	2.8479E-17
Cdon	10743.82	0.528936	0.058677	9.0144	1.97952E-19	1.31486E-16
Hoxb5	788.1774	1.330395	0.151846	8.761496	1.92676E-18	1.23241E-15
Hoxd10	3812.205	-0.90932	0.104398	-8.71013	3.03522E-18	1.87208E-15
Slc8a3	154.8387	-1.80475	0.208558	-8.65351	4.99387E-18	2.97393E-15
Naaa	396.3852	-1.02945	0.121184	-8.49493	1.98045E-17	1.1033E-14
Cdo1	5504.141	0.703569	0.08281	8.49622	1.95865E-17	1.1033E-14
Stra6l	78.09748	-2.72394	0.321751	-8.46597	2.54033E-17	1.37098E-14
Cyp1b1	868.8156	-1.70835	0.202911	-8.41923	3.78966E-17	1.98326E-14
Id3	7008.194	0.600245	0.072472	8.282438	1.20679E-16	6.12978E-14
Lhx2	9710.939	0.994565	0.121264	8.201666	2.37078E-16	1.16981E-13

Table S2.3. Sample of peaks from TBX5 ChIP-seq in forelimbs

Mouse (mm10) TBX5 peaks

Chr	Start	End	Peak name	Fold enrichment	-log10qvalue	Summit
chr8	91713840	91714247	TBX5_FL_mm10_peak_1	450.07	3.94096	91714049
chr1	90119165	90119681	TBX5_FL_mm10_peak_2	407.12	3.94096	90119429
chr17	17486466	17486885	TBX5_FL_mm10_peak_3	402.95	3.94096	17486689
chr5	90162947	90163374	TBX5_FL_mm10_peak_4	401.42	3.94096	90163170
chr2	74380894	74381276	TBX5_FL_mm10_peak_5	386.19	3.94096	74381076
chr7	81176107	81176566	TBX5_FL_mm10_peak_6	369.65	3.94096	81176288
chr6	4557109	4557604	TBX5_FL_mm10_peak_7	366.82	3.94096	4557331
chr14	23523892	23524402	TBX5_FL_mm10_peak_8	363.44	3.94096	23524110
chr5	131855250	131855645	TBX5_FL_mm10_peak_9	359.27	3.94096	131855455
chr15	50664799	50665206	TBX5_FL_mm10_peak_10	357.56	3.94096	50665014
chr1	73363624	73364009	TBX5_FL_mm10_peak_11	354.72	3.94096	73363805
chr16	62468825	62469216	TBX5_FL_mm10_peak_12	352.48	3.94096	62469004
chr2	68404692	68405104	TBX5_FL_mm10_peak_13	347.05	3.94096	68404905
chr8	5482931	5483275	TBX5_FL_mm10_peak_14	345.33	3.94096	5483106
chr3	30018124	30018493	TBX5_FL_mm10_peak_15	344.80	3.94096	30018284
chr2	75439521	75440296	TBX5_FL_mm10_peak_16	344.45	3.94096	75440039
chr3	30227938	30228698	TBX5_FL_mm10_peak_17	342.68	3.94096	30228402
chr1	139092761	139093213	TBX5_FL_mm10_peak_18	342.08	3.94096	139093004
chr13	91187469	91187833	TBX5_FL_mm10_peak_19	340.55	3.94096	91187644
chr9	47846926	47847272	TBX5_FL_mm10_peak_20	333.74	3.94096	47847099
chr8	91679544	91680021	TBX5_FL_mm10_peak_21	332.22	3.94096	91679755
chr13	51259025	51259457	TBX5_FL_mm10_peak_22	328.42	3.94096	51259256
chr8	127809631	127809991	TBX5_FL_mm10_peak_23	328.16	3.94096	127809806
chr16	93272152	93272607	TBX5_FL_mm10_peak_24	328.12	3.94096	93272370
chr16	95935543	95935941	TBX5_FL_mm10_peak_25	327.26	3.94096	95935716
chr4	57738611	57739136	TBX5_FL_mm10_peak_26	324.24	3.94096	57738784
chr3	78594845	78595284	TBX5_FL_mm10_peak_27	319.12	3.94096	78595086
chr18	15253640	15254083	TBX5_FL_mm10_peak_28	316.97	3.94096	15253888
chr4	58670617	58671081	TBX5_FL_mm10_peak_29	315.16	3.94096	58670810
chr2	154973012	154973323	TBX5_FL_mm10_peak_30	314.16	3.94096	154973163
chr7	98956541	98956960	TBX5_FL_mm10_peak_31	312.64	3.94096	98956750
chr6	61216505	61216922	TBX5_FL_mm10_peak_32	312.37	3.94096	61216712
chr13	56159601	56160024	TBX5_FL_mm10_peak_33	311.80	3.94096	56159822
chr3	99665940	99666607	TBX5_FL_mm10_peak_34	311.43	3.94096	99666267
chr10	87867683	87868011	TBX5_FL_mm10_peak_35	311.12	3.94096	87867843

Brown anole TBX5 peaks (AnoSag2.0 Liftover to mm10)

Chr	Start	End	Peak name
chr1	12091766	12091824	Asag_FL_peak_817
chr1	12690557	12690990	Asag_FL_peak_3842
chr1	12691530	12691639	Asag_FL_peak_3842
chr1	13615095	13615180	Asag_FL_peak_7029
chr1	13623648	13623727	Asag_FL_peak_7029,Asag_FL_peak_7476
chr1	13715318	13715752	Asag_FL_peak_56
chr1	14136682	14137123	Asag_FL_peak_5729
chr1	14569920	14569971	Asag_FL_peak_551
chr1	16229743	16230067	Asag_FL_peak_3318
chr1	19231543	19232062	Asag_FL_peak_4222
chr1	23995649	23995712	Asag_FL_peak_7527
chr1	25171149	25171311	Asag_FL_peak_5478
chr1	25830316	25830655	Asag_FL_peak_6410
chr1	26356579	26356755	Asag_FL_peak_1068
chr1	32541048	32541577	Asag_FL_peak_439
chr1	32786002	32786062	Asag_FL_peak_8140
chr1	32786824	32786874	Asag_FL_peak_8140
chr1	33083529	33083839	Asag_FL_peak_3905
chr1	34182570	34183036	Asag_FL_peak_3979
chr1	34238837	34239285	Asag_FL_peak_4494
chr1	34266846	34266963	Asag_FL_peak_6316,Asag_FL_peak_873
chr1	37396059	37396190	Asag_FL_peak_6069
chr1	38261468	38261517	Asag_FL_peak_2457,Asag_FL_peak_4866
chr1	38262325	38262860	Asag_FL_peak_4866
chr1	38545404	38545603	Asag_FL_peak_2572
chr1	39535684	39536132	Asag_FL_peak_3785
chr1	41918472	41919052	Asag_FL_peak_6018
chr1	42357339	42357453	Asag_FL_peak_6544
chr1	43098781	43098880	Asag_FL_peak_5536
chr1	43933995	43934254	Asag_FL_peak_7259
chr1	46123584	46123706	Asag_FL_peak_3854
chr1	46514520	46514642	Asag_FL_peak_3854
chr1	47810681	47810823	Asag_FL_peak_6520
chr1	47854778	47854849	Asag_FL_peak_6520
chr1	48259531	48260205	Asag_FL_peak_4186

Green TBX5 peaks anole (AnoCar2.0 Liftover to mm10)

Chr	Start	End	Peak name
chr1	3671870	3672015	AnoCar2_FL_peak_37454
chr1	4283656	4283703	AnoCar2_FL_peak_38906
chr1	4492047	4492239	AnoCar2_FL_peak_37457
chr1	4492466	4492683	AnoCar2_FL_peak_37458
chr1	4496443	4496507	AnoCar2_FL_peak_37459
chr1	4785664	4785746	AnoCar2_FL_peak_37460
chr1	6583976	6584068	AnoCar2_FL_peak_37477
chr1	6769305	6769420	AnoCar2_FL_peak_37478
chr1	7178545	7178589	AnoCar2_FL_peak_22974
chr1	8051297	8051384	AnoCar2_FL_peak_34650
chr1	8112356	8112405	AnoCar2_FL_peak_34652
chr1	8112855	8113029	AnoCar2_FL_peak_34652
chr1	9548089	9548147	AnoCar2_FL_peak_19901
chr1	9649226	9649340	AnoCar2_FL_peak_19902
chr1	9700373	9700685	AnoCar2_FL_peak_19903
chr1	9748225	9748503	AnoCar2_FL_peak_19905
chr1	10504617	10504670	AnoCar2_FL_peak_19913
chr1	10562981	10563022	AnoCar2_FL_peak_19917
chr1	10994290	10994403	AnoCar2_FL_peak_19920
chr1	11123794	11123880	AnoCar2_FL_peak_19926
chr1	12068129	12068202	AnoCar2_FL_peak_19937
chr1	12091766	12091825	AnoCar2_FL_peak_19939
chr1	12405114	12405155	AnoCar2_FL_peak_19945
chr1	12405983	12406085	AnoCar2_FL_peak_19946
chr1	12409470	12409512	AnoCar2_FL_peak_19947
chr1	12409784	12409831	AnoCar2_FL_peak_19947
chr1	12410209	12410507	AnoCar2_FL_peak_19947
chr1	12510420	12510721	AnoCar2_FL_peak_19948
chr1	12615806	12616057	AnoCar2_FL_peak_19949
chr1	12690557	12691000	AnoCar2_FL_peak_19950
chr1	12691517	12691639	AnoCar2_FL_peak_19950
chr1	12693434	12693624	AnoCar2_FL_peak_19951
chr1	12776140	12776443	AnoCar2_FL_peak_19955
chr1	12914833	12914908	AnoCar2_FL_peak_19961
chr1	13589216	13589469	AnoCar2_FL_peak_19967

Alligator TBX5 peaks (allMis1 Liftover to mm10)

Chr	Start	End	Peak name
chr1	4571822	4572213	allMis1_FL_peak_1951
chr1	6483315	6483366	allMis1_FL_peak_8016
chr1	6767841	6767912	allMis1_FL_peak_8017
chr1	7566186	7566575	allMis1_FL_peak_8021
chr1	11253978	11254129	allMis1_FL_peak_2545
chr1	12092986	12093044	allMis1_FL_peak_2540
chr1	12189835	12190133	allMis1_FL_peak_2539
chr1	12683071	12683119	allMis1_FL_peak_13716
chr1	12838826	12838886	allMis1_FL_peak_12284
chr1	13162513	13162567	allMis1_FL_peak_12281
chr1	13861356	13861598	allMis1_FL_peak_12278
chr1	13927423	13927494	allMis1_FL_peak_12276
chr1	13936044	13936136	allMis1_FL_peak_12274
chr1	14136788	14137070	allMis1_FL_peak_5453
chr1	14192056	14192102	allMis1_FL_peak_5452
chr1	14252329	14252504	allMis1_FL_peak_5451
chr1	14308833	14308928	allMis1_FL_peak_5450
chr1	14370419	14370758	allMis1_FL_peak_5448,allMis1_FL_peak_5449
chr1	14511503	14511879	allMis1_FL_peak_6191
chr1	14567278	14567387	allMis1_FL_peak_6190
chr1	14800081	14800199	allMis1_FL_peak_13839
chr1	14842048	14842519	allMis1_FL_peak_13840
chr1	17601047	17601303	allMis1_FL_peak_9603
chr1	19217473	19217534	allMis1_FL_peak_13007
chr1	19336994	19337559	allMis1_FL_peak_13006
chr1	19389381	19389668	allMis1_FL_peak_13005
chr1	19508348	19508526	allMis1_FL_peak_13431
chr1	19849875	19850070	allMis1_FL_peak_13433
chr1	19888492	19888816	allMis1_FL_peak_3192
chr1	20466832	20467118	allMis1_FL_peak_3190
chr1	23271087	23271154	allMis1_FL_peak_14967
chr1	23864376	23864654	allMis1_FL_peak_7044
chr1	24226700	24226776	allMis1_FL_peak_4389
chr1	24310310	24310423	allMis1_FL_peak_4387
chr1	24587612	24587766	allMis1_FL_peak_4395

Turtle TBX5 peaks

(*T. scripta elegans* aligned to *Chrysemys picta belli* ASM1138683v1; Liftover to mm10)

Chr	Start	End	Peak name
chr1	5162976	5163187	chrPicGB_peak_7124
chr1	6048945	6049089	chrPicGB_peak_6733
chr1	6475200	6475405	chrPicGB_peak_4582
chr1	6744120	6744196	chrPicGB_peak_11594
chr1	8360201	8360250	chrPicGB_peak_782
chr1	10135924	10136253	chrPicGB_peak_13761,chrPicGB_peak_6035
chr1	11925335	11925748	chrPicGB_peak_4262
chr1	11952219	11952562	chrPicGB_peak_3603
chr1	12510438	12510673	chrPicGB_peak_2925
chr1	12776157	12776361	chrPicGB_peak_2791
chr1	12807583	12807972	chrPicGB_peak_2456
chr1	12824787	12825083	chrPicGB_peak_3243
chr1	13081465	13081706	chrPicGB_peak_13475
chr1	13241679	13241736	chrPicGB_peak_12356
chr1	13712948	13713002	chrPicGB_peak_14032
chr1	13715259	13715951	chrPicGB_peak_14032,chrPicGB_peak_626
chr1	13861320	13861501	chrPicGB_peak_2580
chr1	14136715	14137184	chrPicGB_peak_11573
chr1	14184898	14185404	chrPicGB_peak_8365
chr1	14211918	14212005	chrPicGB_peak_7177
chr1	14307020	14307576	chrPicGB_peak_5220
chr1	14370507	14370660	chrPicGB_peak_7429
chr1	14567072	14567391	chrPicGB_peak_14973
chr1	14635585	14636063	chrPicGB_peak_4422
chr1	14842370	14842668	chrPicGB_peak_1231
chr1	14855018	14855415	chrPicGB_peak_8094
chr1	16229701	16230051	chrPicGB_peak_3011,chrPicGB_peak_4098
chr1	16230988	16231096	chrPicGB_peak_12578
chr1	16248867	16249254	chrPicGB_peak_14325
chr1	16997463	16997570	chrPicGB_peak_11217
chr1	17925364	17925617	chrPicGB_peak_1590
chr1	18961431	18961908	chrPicGB_peak_9310
chr1	19217151	19217769	chrPicGB_peak_12969
chr1	19231828	19232064	chrPicGB_peak_12856
chr1	19292005	19292064	chrPicGB_peak_12838

Table S2.4. Coordinates of TBX5 binding at validated limb enhancers

All coordinates are in mm10.

Gene associated with TBX5 binding site	Region shown in Figure	TBX5 ChIP-seq peak in mouse		Species with conserved TBX5 binding	Conserved sequence coordinates (shared among each species)	Published limb-positive enhancer		Capture-C interaction peak coordinates (Andrey et al. 2017)
		Peak Name	Coordinates			Name	Coordinates	
<i>Wnt5a</i>	chr14:28,970,650-28,975,348	TBX5_FL_mm10_peak_4606	chr14:28,972,547-28,972,991	Alligator	chr14:28,972,657-28,972,951	hs1448	chr14:28,972,335-28,973,646	chr14:28,970,978-28,974,977
<i>Hoxa13</i>	chr6:52,966,476-52,970,026	TBX5_FL_mm10_peak_1127	chr6:52,967,648-52,968,040	Green anole, Turtle, Alligator	chr6:52,967,649-52,967,992	hs1430	chr6:52,967,026-52,969,651	chr6:52,967,076-52,968,075
<i>Epha4</i>	chr1:75,768,565-75,776,228	TBX5_FL_mm10_peak_9891	chr1:75,772,994-75,773,438	Brown anole, Green anole	chr1:75,773,146-75,773,275	hs1507	chr1:75,769,003-75,773,592	chr1:75,770,307-75,774,306
<i>Twist1</i>	chr12:34,214,057-34,223,515	TBX5_FL_mm10_peak_2220	chr12:34,219,911-34,220,181	Brown anole, Green anole, Turtle, Alligator	chr12:34,220,049-34,220,100	hs2306	chr12:34,219,910-34,220,181	chr12:34,214,889-34,222,888
		TBX5_FL_mm10_peak_2276	chr12:34,220,566-34,220,805	Green anole, Alligator	chr12:34,220,566-34,220,805			
		TBX5_FL_mm10_peak_965	chr12:34,215,699-34,216,060	Brown anole, Green anole, Turtle, Alligator	chr12:34,215,699-34,216,028	hs2307	chr12:34,215,261-34,216,361	
<i>Fgf10</i>	chr13:118,712,339-118,783,841	TBX5_FL_mm10_peak_5970	chr13:118,713,600-118,714,043	Brown anole, Green anole, Turtle	chr13:118,713,600-118,713,897	hs516	chr13:118,713,611-118,715,013	N/A
		TBX5_FL_mm10_peak_1766	chr13:118,735,749-118,735,982	Brown anole, Green anole, Turtle, Alligator	chr13:118,735,812-118,735,982	mm917	chr13:118,735,524-118,737,413	
<i>Ptch1</i>	chr13:63,519,897-63,533,159	TBX5_FL_mm10_peak_6607	chr13:63,525,294-63,525,737	Brown anole, Green anole, Turtle, Alligator	chr13:63,525,540-63,525,591	LRM	chr13:63,520,270-63,532,846	chr13:63,527,852-63,528,850
<i>Hand2</i>	chr8:56,830,966-56,834,064	TBX5_FL_mm10_peak_828	chr8:56,832,646-56,832,941	Brown anole, Green anole, Turtle, Alligator	chr8:56,832,646-56,832,941	mm1687	chr8:56,831,311-56,833,826	chr8:56,835,175-56,836,174

Table S2.5. Putative direct targets of TBX5 in embryonic forelimbs

Putative direct targets of TBX5 in mouse forelimbs

1700025G04Rik	Calcr1	D330045A20Rik	Fbn1	Hnrnpa3	Letm1	Nav1	Prdx1	Sdc2	Stxbp3	Unc5a
2310009B15Rik	Calm1	D3Erdt751e	Fbxo8	Homer2	Lgals3bp	Ndnf	Prx1	Sdr39u1	Stxbp6	Unc5c
4930427A07Rik	Calml4	D430041D05Rik	Fermt2	Hoxa10	Lhfp	Nefm	Prkcb	Sec24d	Suox	Uqc2
4930453N24Rik	Camk2d	Dab1	Fgd4	Hoxa13	Lhx2	Nfia	Prkx	Sel1l3	Svep1	Usp29
5730596B20Rik	Camk2n1	Dach1	Fgd5	Hoxa2	Lhx9	Ngfr	Prr12	Sema3c	Syk	Usp36
Abcc4	Camk4	Dennd1a	Fgf10	Hoxa4	Limch1	Notch2	Prrt4	Sema3d	Synpo2	Usp46
Abtb2	Caps2	Dgkk	Fgf9	Hoxa7	Lingo1	Nphp4	Prrx2	Sema6d	Tac1	Vac14
Acadsb	Cbfa2t3	Dgkz	Fgfr10p2	Hoxb2	Lmp1	Npr3	Psd2	Serinc5	Taf1c	Vim
Acot11	Cbln1	Disp1	Fhl3	Hoxb3	Lmo2	Nr4a2	Psm14	Sertad4	Tarbp2	Vldlr
Acp6	Ccdc124	Dkk2	Fhod3	Hoxb5	Lmx1b	Nrp1	Psmf1	Sf3a2	Tbcc	Vps13b
Actc1	Ccdc85c	Dlg5	Fip11	Hoxb6	Lpar4	Nsmaf	Ptbp2	Sfrp1	Tbkbp1	Vstm2b
Adamts1	Ccnd1	Dnajb9	Fkbp14	Hoxb8	Lpar6	Ntm	Ptch1	Sfrp2	Tbx2	Wdr18
Adamts5	Ccnj1	Dock10	Fli1	Hoxb9	Lrig1	Ntn4	Ptch2	Sgk3	Tead1	Wdr4
Adgra2	Ccser1	Dock5	Frlt3	Hoxc4	Lrig3	Obsl1	Pth1r	Sgms2	Tenn4	Wdr89
Adgrg6	Cd248	Dock6	Fmn1	Hoxc5	Lrrc32	Olfm1	Ptn	Sh3bgl2	Tfrc	Wif1
Adgrl3	Cd244	Dock7	Fmod	Hoxc6	Lrrc3b	Optn	Ptov1	Sh3bp5	Tgfb2	Wnt2
Adnp	Cd44	Dok1	Fnbp1l	Hoxd10	Lrrn2	Osmr	Ptpn13	Shb	Tgfb1	Wnt4
Al464131	Cd82	Dok4	Fndc3a	Hoxd11	Ltbp1	Osr1	Ptprd	Shisa2	Tgfb2	Wnt5a
Ak5	Cdc40	Dpysl3	Fosl2	Hoxd12	Lum	Osr2	Ptprt	Shox2	Thbs1	Xrcc5
Akap11	Cdc42ep3	Drp2	Foxc1	Hoxd13	Lypd6	Pald	Ptpru	Sim2	Thsd4	Xylyt1
Akap6	Cdh6	Dsel	Foxk1	Hsd11b2	Lypd6b	Pam	Rab11fip3	Sipa112	Thy1	Xylyt1
Alcam	Cdk6	Dsg2	Foxp4	Id1	Macc1	Parm1	Rab38	Six4	Timm21	Zbtb38
Aldh1a2	Cdkal1	Dusp7	Frem1	Id2	Mad11	Parp16	Rap2c	Slc16a7	Timp2	Zcchc4
Alx3	Cdkn1a	Dync11	Frg1	Id3	Magi2	Pbx1	Rapgef1	Slc22a23	Tle1	Zeb1
Alx4	Cdo1	Dync1j2	Fry	Ier5l	Malt1	Pbx3	Rapgef5	Slc27a6	Tle2	Zeb2
Amot	Cdon	Eapp	Fut8	Igdc3	Mamdc2	Pcdh17	Rarb	Slc5a6	Tle6	Zfhx3
Ank3	Cenpi	Ect2	Fzd1	Igf1r	Map3k3	Pesk5	Rassf9	Slc6a17	Tlx1	Zfhx4
Ankrd6	Cetn3	Ednra	G3bp2	Irf2bp2	Map4k3	Pdcd10	Rbck1	Slc8a3	Tmcc3	Zfp51
Ano1	Cgnl1	Efcab7	Gas1	Irf5	Masp1	Pde4b	Rbm20	Slco2a1	Tmed1	Zfp704
Apob	Chn1	Efemp1	Gbf1	Irs1	Mat2b	Pde8a	Rbm25	Slco3a1	Tmeff2	Zwint
App	Chpf	Efna5	Gcat	Irx3	Mcoln3	Pde9a	Rbms3	Slit1	Tmem100	Zyx
Aqp4	Chrd11	Efnb2	Gdf10	Irx4	Mctp2	Pdlim3	Rdh10	Slit2	Tmem104	
Arhgap12	Cic	Eif2b4	Gdf6	Irx5	Mdga1	Pdzd2	Rel1	Smad6	Tmem120a	
Arhgap24	Cited1	Eif3e	Gdnf	Irx6	Mdm4	Pebp1	Rffl	Smad7	Tmem132d	
Arhgap27	Cldn1	Eif4ebp1	Gfra1	Isoc1	Med13l	Peg10	Rgcc	Smc3	Tmem132e	
Arhgap29	Clpb	Emilin2	Gja3	Ispd	Meis1	Phactr3	Rgs9	Smoc1	Tmem200b	
Arl1	Clstn1	Emp1	Gldn	Irga8	Meis2	Phc1	Rnaseh2b	Smyd3	Tmem201	
Arl2	Clstn2	Emx2	Gli1	Irga9	Meox1	Phgdh	Rnd3	Snap91	Tmem26	
Arl4c	Clybl	En1	Gli2	Irgb1	Meox2	Phlda1	Rnf150	Snaip1	Tmem28	
Arl5b	Cmklr1	Engase	Glis1	Irgb5	Mgat4a	Phlda3	Rnf2	Snx14	Tmem56	
Arrb1	Cnot2	Entpd1	Glis3	Iitm2a	Mid1ip1	Piezo2	Ror1	Socs2	Tmct1	
Asb13	Cnr1	Eogt	Gm10320	Jdp2	Mknk2	Pitrm1	Ror2	Sorbs2	Tnc	
Asb4	Cntfr	Epha4	Gm9008	Kat6b	Mlf2	Pkdcc	Rpl13	Sorcs2	Tnik	
Atoh8	Col1a1	Epha7	Gng2	Kcnd2	Mllt3	Pla2g4a	Rpl29	Sorl1	Tns4	
Atp6ap2	Col1a2	Epha8	Gnpnat1	Kcnj5	Mmp16	Plaur	Rplp1	Sost	Tox	
Atp8a1	Col25a1	Ephb1	Gppb1	Kcnk2	Moxd1	Plcl2	Rpp30	Sox6	Tox3	
Atrn1	Col3a1	Ergic2	Gpc3	Kcna1	Mpped2	Plekha6	Rps24	Spag16	Tpbp	
Aup1	Comtd1	Ets2	Grb14	Kcp	Mrpl23	Plxdc2	Rps3a1	Spat6	Tpm1	
Axin2	Cops7a	Eva1b	Grc10	Kctd12	Mrps18a	Plxna1	Rps6ka6	Spon1	Tpra1	
Bahcc1	Cox10	Evx1	Grem1	Kctd15	Mrps24	Plxna2	Rps6kb1	Spry2	Trappc2	
Baz2b	Cox18	Evx2	Gria2	Kctd8	Msantd3	Plxna4	Rspo3	Sptlc3	Trpm1	
Bcat2	Cpa2	Ext2	Gulp1	Kdm3a	Msi2	Plxnc1	Rspo4	Srbd1	Trpm3	
Bcl7b	Cpa4	Extl2	Gyg	Kdm7a	Msx1	Plxnd1	Rsrc1	Srgap3	Trps1	
Begain	Crabp1	Eya1	Gypa	Kirrel3	Msx2	Pmaip1	Rsrc2	Srsf3	Tspan7	
Bhlha9	Crabp2	Fam103a1	Hace1	Klf4	Mtdcl1	Pmp22	Rtl1	St3gal1	Ttc28	
Bmp3	Crif1	Fam111a	Hand2	Klf8	Mtss1	Pomgnt2	Rtn4r1	St3gal2	Ttc7	
Bmp5	Csf2rb2	Fam133b	Hey1	Klf9	Mtus1	Pop5	S1pr3	St3gal6	Ttl11	
Bmp7	Csnk1a1	Fam163b	Hgf	Klhl29	Mtus2	Postn	Sall1	Stag1	Ttl12	
Bnc2	Cxcl12	Fam174b	Hhip	Klhl3	Mybpc1	Pou4f1	Sall3	Stc1	Twist1	
Brip1	Cxxc4	Fam189a2	Hibadh	Ktn1	Myc	Ppp1cb	Sap30l	Stk3	Txing	
Btbd11	Cyfp2	Fam198b	Hif1a	Lamc2	Myh15	Ppp6r3	Sash1	Stk39	Ube2e1	
C1galt1	Cyp1b1	Fam96b	Hist1h2br	Lanc1	Myrf	Prdm1	Satb1	Stra6l	Ubtcl1	
C1qtnf3	Cyth3	Fat3	Hltf	Lbh	Mysm1	Prdm2	Satb2	Strip2	Ubxn7	
Cacna1a	D030056L22Rik	Fbln1	Hmcn1	Lem1	Mzt1	Prdm6	Scn3a	Stx18	Ugp2	

Putative ancient direct targets of TBX5 in amniote forelimbs

Alx4	Dennd1a	Fmn1	Hoxd11	Lrig1	Pbx3	Sema3d	Wif1
Apob	Efna5	Foxc1	Hoxd12	Lrig3	Ptch1	Sox6	Wnt5a
Atoh8	Emx2	Frg1	Hoxd13	Ltbp1	Rab38	Stx18	Zeb2
Calm1	Epha4	Fzd1	Irx3	Med13l	Rarb	Tbx2	Zfhx4
Cdon	Ets2	Gas1	Irx5	Meis1	Rnd3	Tead1	
Cetn3	Evx1	Grem1	Itgb1	Meox2	Ror1	Tle1	
Clybl	Evx2	Hand2	Kat6b	Msx1	Rspo3	Trps1	
Col25a1	Eya1	Hibadh	Kcnma1	Msx2	Rsrc1	Twist1	
Comtd1	Fbxo8	Hnrnpa3	Lhx9	Nr4a2	Sall3	Usp46	
Dach1	Fgf10	Hoxd10	Lmx1b	Nrp1	Satb1	Vps13b	

Upregulated Downregulated

Table S2.6. List of limb genes regulated by TBX5

One triangle next to the gene name indicates the gene is associated with TBX5 binding site(s) in mouse only, while two triangles indicate ancient TBX5 binding in mouse, brown anole, green anole, turtle, and alligator. Output columns are from DEseq2 analysis of RNA-seq data.

	Gene	baseMean	log2FoldChange	lfcSE	stat	pvalue	padj
▶▶	Alx4	8769.81	1.44462	0.07146	20.21635	7.03E-91	1.21E-86
▶▶	Hand2	5057.11	-2.00898	0.12058	-16.66129	2.51E-62	1.44E-58
▶▶	Hoxd13	2463.94	-3.98709	0.26644	-14.96436	1.26E-50	5.42E-47
▶	Alx3	2855.77	0.95185	0.06930	13.73459	6.30E-43	2.18E-39
▶▶	Hoxd12	1702.21	-5.67600	0.45952	-12.35191	4.76E-35	1.17E-31
▶▶	Ptch1	4849.92	-1.30976	0.11307	-11.58399	4.97E-31	7.80E-28
▶	Pam	2118.83	-0.83525	0.07345	-11.37150	5.80E-30	7.15E-27
▶▶	Msx2	3146.51	1.23257	0.11053	11.15186	7.01E-29	7.57E-26
▶▶	Msx1	14524.67	1.13233	0.10327	10.96451	5.66E-28	5.75E-25
▶	Rdh10	1375.00	1.14564	0.12131	9.44399	3.59E-21	2.58E-18
▶▶	Hoxd10	3812.21	-0.90932	0.10440	-8.71013	3.04E-18	1.87E-15
▶	Osr1	838.60	-1.46448	0.17871	-8.19465	2.51E-16	1.21E-13
▶▶	Twist1	14792.76	0.64102	0.08005	8.00797	1.17E-15	4.68E-13
▶▶	Hoxd11	3265.02	-2.31429	0.29840	-7.75563	8.79E-15	3.16E-12
▶	Gli2	6011.05	0.47818	0.06401	7.47085	7.97E-14	2.41E-11
▶	Shox2	8939.75	-1.23272	0.16692	-7.38525	1.52E-13	4.38E-11
▶	Bmp7	6366.59	0.49232	0.06813	7.22574	4.98E-13	1.32E-10
▶▶	Gas1	15672.34	0.72662	0.10847	6.69881	2.10E-11	4.17E-09
▶▶	Grem1	3073.62	-1.01879	0.15544	-6.55434	5.59E-11	1.08E-08
▶	Prrx2	8775.73	0.74028	0.11652	6.35303	2.11E-10	3.68E-08
	Shh	307.91	-3.03416	0.51576	-5.88287	4.03E-09	5.90E-07
▶▶	Rspo3	651.30	-1.08850	0.18556	-5.86612	4.46E-09	6.36726E-07
▶▶	Fmn1	365.31	-0.81694	0.14013	-5.83000	5.54E-09	7.78253E-07
▶▶	Lmx1b	12638.72	0.57606	0.10358	5.56132	2.68E-08	3.16702E-06
▶	Smoc1	2423.94	-1.47621	0.28143	-5.24539	1.56E-07	1.61273E-05
	Fgf4	152.30	-1.56360	0.31007	-5.04273	4.59E-07	4.30759E-05
▶▶	Wnt5a	7263.10	-0.65719	0.13273	-4.95132	7.37106E-07	6.3969E-05
▶	Osr2	520.39	-3.79610	0.78207	-4.85392	1.21042E-06	9.58898E-05
▶	Hoxa11	6582.73	-0.54427	0.11327	-4.80516	1.54627E-06	0.000117123
▶	Hoxa10	8135.24	-0.54252	0.11308	-4.79768	1.60511E-06	0.000119484
▶	En1	258.45	-0.56127	0.12158	-4.61635	3.90557E-06	0.000260421
▶▶	Meox2	1458.26	-1.19179	0.26678	-4.46729	7.92163E-06	0.000456828
▶	Pbx1	22208.84	0.41247	0.09239	4.46460	8.02168E-06	0.000460247
▶	Notch2	9285.56	0.40615	0.09471	4.28830	1.80042E-05	0.00088333
▶	Fgf9	97.40	-0.95999	0.25379	-3.78256	0.000155224	0.004621923
	Gja5	935.26	-0.50477	0.13393	-3.76887	0.000163991	0.004798954
▶	Tgfb2	2626.98	0.57326	0.15450	3.71042	0.00020692	0.005674965
▶▶	Fgf10	1683.67	-0.59267	0.16015	-3.70071	0.000214997	0.005865718

▶	Aldh1a2	30.97	-2.25667	0.64499	-3.49878	0.000467391	0.010335262
▶	Hoxa13	476.87	-4.05435	1.17418	-3.45294	0.000554523	0.011492612
▶	Sfrp2	2373.26	0.30101	0.08784	3.42658	0.000611229	0.012217511
	Kremen2	629.41	0.43279	0.12783	3.38554	0.000710379	0.013631392
▶	Sall1	3949.38	-0.94393	0.28050	-3.36514	0.000765046	0.014376871
▶▶	Tbx2	3265.28	1.08543	0.32333	3.35702	0.000787872	0.014693421
	Ift88	1113.32	-0.27185	0.08229	-3.30332	0.000955484	0.016803673
▶	Fermt2	9175.52	-0.24107	0.07299	-3.30295	0.000956738	0.016808612
	Taf10	5033.48	0.30310	0.09287	3.26378	0.001099379	0.018595765
	Ttbk2	1285.19	-0.38960	0.12021	-3.24094	0.001191376	0.01972504
▶▶	Epha4	7226.13	-0.37666	0.12418	-3.03325	0.002419339	0.03165302
▶	Ror2	6354.94	0.26044	0.08597	3.02934	0.002450909	0.031969186
	Megf8	8403.39	0.25320	0.08600	2.94435	0.003236341	0.037918323
	Reck	3215.68	0.21089	0.07372	2.86056	0.004228888	0.044478008
▶	Crabp2	21330.27	0.20315	0.07177	2.83066	0.004645241	0.047357326

Upregulated Downregulated

CHAPTER 3

TBX5 REGULATES APPENDAGE GENES TO CONTROL PATTERNING OF THE DEVELOPING EXTERNAL GENITALIA²

²Alcala A.J., et al., to be submitted to *bioRxiv*.

Abstract

Abnormalities of the urogenital tract are among the most common human congenital disorders. Studies in both humans and model organisms have shown that disruptions in several genes and signaling pathways can cause morphological defects during development of external genitalia. The TBX5 transcription factor plays a critical role in the growth and patterning of the vertebrate forelimb and is also known to be expressed in the embryonic phallus of several amniote species. While a recent study has identified *TBX5* as a susceptibility gene for posterior urethral valves, it remains unknown what role *Tbx5* plays during development of the external genitalia. We have found that conditional knockout of *Tbx5* in the mouse genital tubercle (GT) causes a reduction of the preputial swellings and urethral hypoplasia. In addition, we have used a combination of CHIP-seq and RNA-seq to investigate enhancer regions and target genes directly regulated by TBX5 in the mouse GT. We intersected our list of misregulated genes with genes that have nearby TBX5 binding sites to identify 39 putative targets of TBX5. Eight of these are associated with ancient TBX5 binding events shared between mouse and brown anole. Lastly, we compare TBX5 occupancy in embryonic appendages and find that approximately 32% of forelimb binding sites are shared with the GT. Together, our findings reveal the role of TBX5 in genital formation and identify the direct transcriptional targets this transcription factor regulates in embryonic genitalia.

Introduction

The external genitalia are sex organs that consist of the clitoris, penis, labia, and scrotum. Molecular and developmental studies in humans and model organisms have revealed the processes underlying the formation of these structures. In mammals and many other species of birds and reptiles, paired genital swellings emerge from the body wall during development and fuse to form an ambisexual genital tubercle (GT), the precursor to the penis and clitoris (Gredler et al., 2014; K. Suzuki et al., 2002).

Differentiation of the mesenchyme and urethra is coordinated during proximodistal outgrowth to generate sexual dimorphic characteristics of the genitalia. While the morphology of external genitalia is incredibly diverse across amniotes (mammals, birds, and reptiles) and between sexes (Gerald R. Cunha et al., 2019, 2014; Weiss et al., 2012), similarities in early development suggest that the phallus evolved from a common ancestor over 310 million years ago (Gredler, 2016; Sanger et al., 2015).

Intriguing parallels are observed between developing limbs and external genitalia, which differ dramatically in both form and function. Interestingly, these appendage types undergo similar phases of development: specification of a growth field along the axis of the embryo, initiation of budding, and coordination of outgrowth and patterning along three dimensions. Furthermore, these appendages use many of the same genes and signaling molecules during embryogenesis (Martin J. Cohn, 2011; Infante et al., 2018). Previous work from our lab has shown that many enhancers active in developing limbs are also active in the genital tubercle (Infante et al., 2015). However,

it remains unknown whether transcription factors expressed in the limbs and phallus interact with the same enhancers to regulate similar suites of target genes.

Prior studies have shown that *Isl1*, a gene that encodes a LIM-homeodomain transcription factor, is essential for the development of urogenital organs (Ching et al., 2018; R. Zhang et al., 2017). Work from our lab has also found that ISL1 directly regulates *Tbx5* in the developing genitalia (Minchey, 2022). The *Tbx5* gene encodes a T-box transcription factor that plays a key role in the patterning and growth of the vertebrate forelimb (Agarwal et al., 2003) and other tissues such as the heart and lungs (Steimle & Moskowitz, 2017; Steimle et al., 2018). Interestingly, *Tbx5* expression has been reported in the developing external genitalia of mice, lizards, snakes, and chickens (Chapman et al., 1996; Douglas et al., 2012; Gibson-Brown et al., 1998; Tschopp et al., 2014). Furthermore, a recent whole-genome sequencing association study has identified *TBX5* as a susceptibility gene for posterior urethral valves (PUV) (Chan et al., 2022). PUV is a disorder of the urogenital tract characterized by membranes forming in the male posterior urethra, which prevent the outflow of urine. Although *Tbx5* exhibits a deeply conserved expression pattern in the amniote phallus, it is unknown what role *Tbx5* plays during the development of the external genitalia.

In this study, we conditionally delete *Tbx5* in the mouse genital tubercle and find that it is required for patterning of the preputial swellings and urethra meatus during embryogenesis. We use a comparative ChIP-seq approach to reveal ancient *TBX5* binding events in embryonic genitalia of mice and *Anolis* lizards. By associating the genomic occupancy of *TBX5* with genes that show *TBX5*-dependent expression, we

reveal putative direct targets of TBX5 in the genitalia. Overall, our results uncover the role of TBX5 in genital morphogenesis and determine the direct targets this transcription factor regulates in embryonic genitalia.

Results

ISL1 directly regulates a conserved enhancer of Tbx5 in developing external genitalia

Previous work from our lab has shown that *Tbx5* is downregulated in genital tubercles (GTs) of *Isl1* conditional knockout mutants (Minchey, 2022). Furthermore, our ISL1 CHIP-seq data show that several ISL1 binding events occur near *Tbx5* in the embryonic phallus of several amniote species. One of these ISL1 binding sites is located at a deeply conserved sequence roughly 77 kb downstream of *Tbx5* (Fig. 3.1). This region is bound by ISL1 in mouse, alligator, and chicken and is flanked by H3K27ac peaks, a pattern that marks enhancers in an active state (Creyghton et al., 2010). To test whether this region is capable of driving reporter gene activity in transgenic mice, we cloned the sequence in front of an *Hsp68* minimal promoter and a *lacZ* reporter. We designate this 953 bp fragment genital tubercle enhancer 1 (GTE1). GTE1 produced strong expression in the GT mesenchyme (Fig. 3.2) in a pattern strikingly similar to *Tbx5* expression observed from *in situ* hybridization experiments (Douglas et al., 2012).

Conditional knockout of Tbx5 leads to reduced size of preputial swellings and urethral hypoplasia.

To investigate the role of *Tbx5* in controlling genital tubercle morphology, we inactivated the gene in the genital mesenchyme by generating mice carrying the *Tbx5* conditional allele, *Tbx5*^{flox/flox} (Bruneau et al., 2001), and a transgene expressing *Cre* recombinase in the limb mesoderm, *HoxB6-Cre* (Lowe et al., 2000). *Tbx5* cKO (*Tbx5*^{flox/flox}; *HoxB6-Cre*) mice displayed reduced size of preputial swellings compared to control mice at E14.5, before sexual differentiation of the GT (Fig. 3.3A-B). In males, preputial swellings (also known as the prepuce) contain accessory sexual glands that secrete an oily substance known as sebum (G. R. Cunha, 1975). The sebum produced by the preputial gland provides lubrication and antibacterial and antifungal properties (Kligman, 1963). It is also thought to contain pheromones that promote aggression (Hucklebridge et al., 1972) and act as a sex attractant (Bronson & Caroom, 1971). The prepuce also grows around the circumference of the glans during development to facilitate the closure of the urethral tube in males (Georgas et al., 2015; K. Suzuki et al., 2002). In females, the glans reduces in size to form the clitoris and the prepuce does not completely surround the genitalia, leading to a urethra that is not fully fused (Georgas et al., 2015).

Gene deletion-gene replacement experiments in mice show that the paralogous *Tbx4* and *Tbx5* genes have similar roles in establishing limb buds (Duboc & Logan, 2011; Minguillon et al., 2005). Genomic studies also find that TBX5 and TBX4 bind many of the same genomic regions in developing limbs (Jain et al., 2018). Furthermore, *Tbx5* and *Tbx4* are co-expressed in embryonic lungs and have partially redundant roles regulating lung branching morphogenesis (Arora et al., 2012). We hypothesized that the subtle

phenotype we observed in *Tbx5* mutant genitalia might be due to genetic compensation by *Tbx4*, which is co-expressed with *Tbx5* in the GT. Interestingly, introduction of a *Tbx4* null allele in the *Tbx5* mutant background did not lead to a more severe phenotype in the GT (Fig. S3.1). Genital tubercles of *Tbx5*^{flox/flox}; *HoxB6-Cre*, *Tbx4*^{null/+} mice had reduced size of preputial swellings, but did not show a distinct phenotype from the *Tbx5*^{flox/flox}; *HoxB6-Cre* mice (Fig. S3.1C,D).

To better characterize the morphological disorders observed and perform quantitative measurements of preputial swelling lengths, we generated high-resolution three-dimensional scans of GTs using light sheet microscopy. Surface renderings of GTs produced by light-sheet microscopy recapitulated the reduced prepuce phenotype we observed in bright field microscopy (Fig. 3.3C-D). Furthermore, lateral lengths of the preputial swellings were shorter in *Tbx5* cKO mutant GTs compared to control embryos (data not shown). To determine the effects of *Tbx5* ablation at the sexually dimorphic stage of GT development, we observed phenotypes in E18.5 mouse embryos using bright field and scanning electron microscopy. In male *Tbx5* mutants, we observe decreased size of the prepuce and more centrally located inflection points of the lateral edges compared to controls (Fig. 3.3G,H,K,L). Furthermore, the urethral meatus improperly forms and appears to be larger in diameter compared to control embryos. In female *Tbx5* mutants, the glans clitoridis is rounder and urethral meatus is also larger in diameter (Fig. 3.3E,F,I,J).

RNA-seq identifies dozens of genes misregulated in genital tubercles of Tbx5 conditional knockout mice

To identify genes with TBX5-dependent expression, we compared global gene expression patterns between GTs of wild-type and *Tbx5* cKO mice at E12.5. A comparison of normalized counts between the five control and three mutant replicates used showed significantly fewer counts at exon 3 of *Tbx5* in mutants compared to controls (Table S3.1). Overall, we found 70 differentially expressed genes; 62 are downregulated, while 8 are upregulated (Fig. 3.4, Table S3.2). To determine whether specific gene categories or molecular pathways are enriched among genes that are differentially expressed in *Tbx5* mutants, we used the gene-set enrichment tool ShinyGO (Ge et al., 2020) with all protein coding genes set as the background set.

Top ranked clusters include genes involved in muscle development and mesenchymal cell differentiation (Fig. 3.4A). These enriched clusters do not differ substantially when using all genes that had an average normalized count (baseMean) greater than five (data not shown). Among upregulated genes is *Fgf8*, which in the limb is known to interact with FGF10 in the limb to form a positive regulatory loop necessary for proximo-distal outgrowth (Ohuchi et al., 1997; Sekine et al., 1999; X. Xu et al., 1998). *Fgf8* is also expressed in the distal tip of the urethral epithelium (Haraguchi et al., 2000), but ablation of the gene in the genital tubercle does not affect its development (Seifert et al., 2009).

We used qPCR to validate several differentially expressed genes identified in our RNA-seq experiments. qPCR assays confirm that *Cxcl12*, *Eya4*, and *Grem2* are

downregulated in *Tbx5*-ablated GTs (Fig. S3.3). *Eya4* encodes a transcriptional coactivator and histone phosphatase that ranks highly as differentially expressed gene in embryonic limbs compared to external genitalia (Tschopp et al., 2014). *Cxcl12* encodes a gene that encodes a chemokine necessary for migration of muscle progenitors in the limb (Vasyutina et al., 2005), but its role in the GT has not been reported. *Grem2* is a BMP antagonist, and BMP signaling has been implicated to play a role during initiation of the GT outgrowth (Kajioka et al., 2019; K. Suzuki et al., 2003).

Hand2 controls *Shh* expression in the zone of polarizing activity in the limb (Galli et al., 2010; Osterwalder et al., 2014) and is directly regulated by TBX5 in embryonic forelimbs (see Chapter 2). *Shh* is expressed in the cloacal epithelium which grows into the urethral epithelium (Haraguchi et al., 2001; Seifert et al., 2008). Deletion of *Shh* leads to early arrest of genital swellings shortly after initiation of genital development (Perriton et al., 2002). While *Hand2* was found to be upregulated in our RNA-seq dataset, it did not show a statistically significant change of expression in our qPCR assays (Fig. S3.3).

Conserved TBX5 binding events in the amniote phallus are enriched near limb genes

To identify genomic targets occupied by TBX5 in mouse external genitalia, we performed TBX5 ChIP-seq on chromatin from E12.5 GTs. Analysis of our TBX5 ChIP-seq replicates in GTs identified 20,728 highly reproducible peaks (Table S3.3). We compared our TBX5 ChIP-seq data with a previously published H3K27ac ChIP-seq dataset performed in mouse genitalia (Infante et al., 2015). We find that many regions flanking

TBX5 binding sites are marked by bimodal H3K27ac peaks (Fig. 3.5A), a pattern that indicates active enhancers (Creyghton et al., 2010). A majority of TBX5 binding sites occur far from transcriptional start sites of their associated genes, suggesting that TBX5 primarily binds at distal enhancers, rather than at promoter regions (Fig. 3.5C). Gene set enrichment analysis shows that TBX5 occupies genomic regions near genes with human orthologs implicated in limb disorders (Fig. 3.5D, top). These peaks are also enriched near genes involved in the Hedgehog, Wnt, and BMP signaling pathways (Fig. 3.4D, bottom).

De novo motif analysis finds that the second top enriched DNA sequence is the known T-box binding motif, AGGTG (Conlon et al., 2001; Wilson & Conlon, 2002) (Fig. 3.5B). Interestingly, the top enriched motif is a Hox motif (Fig. 3.4B). This suggests that TBX5 and HOX proteins may co-bind many of same regions in GTs, similar as what is observed in embryonic forelimbs (Jain et al., 2018) (see Chapter 2). We intersected our TBX5 peaks with published HOXA13 peaks (Amândio et al., 2020) and find that 32.3% (6,691/20,728) overlap (Fig. 3.5A), further supporting the idea that TBX5 and HOX proteins co-occupy a subset of genomic loci in embryonic appendages.

To evaluate the genome-wide enrichment of TBX5 in several different embryonic tissues where it is expressed, we compared TBX5 signal of our data to publicly available ChIP-seq datasets. 4,388/13,580 (32.3%) of forelimb TBX5 binding sites overlap with the 20,728 GT peaks (Figs. 3.6, S3.4, S3.5). We also compared our forelimb and GT TBX5 peaks to published heart and lung ChIP-seq datasets (Figs. 3.6, S3.6, S3.7) (Rankin et al., 2021; Steimle et al., 2018). We find 685/20,728 (3.3%) of our GT peaks overlap with

heart peaks, while 2,492/ 20,728 (12.0%) overlap with lung peaks (Figs. 3.6, S3.5). In context of forelimb TBX5 binding, we observe that 578/13,580 (4.3%) overlap heart peaks, while 2,492/13,580 (18.4%) overlap lung peaks (Figs. 3.6, S3.4). Overall, we find that many regions bound by TBX5 in embryonic forelimbs are also bound in genital tubercles.

While many of these TBX5-bound regions in embryonic genitalia occupy well-conserved non-coding sequences, conservation of DNA sequence does not sufficiently determine that TBX5 binds orthologous elements conserved in other species. To identify deeply conserved TBX5 binding events, we used the same antibody to perform TBX5 ChIP-seq on developing hemiphalluses from the brown anole. The last common ancestor of mammals and reptiles evolved approximately 310 million years ago (Evans, 2009; Pyron, 2010). Therefore, TBX5-binding events that are shared between mice and lizards likely represent ancient binding interactions shared in diverse species of amniotes.

Our ChIP-seq experiments identified 15,415 TBX5 binding sites in external genitalia of the brown anole (Fig. 3.7). *De novo* motif analysis identified a Tbox-Hox composite motif among the highest-ranking sequences (Fig. 3.7A). We used a multi-species alignment and halliftover (Hickey et al., 2013) to map ChIP-seq peak coordinates from the brown anole genome to the mouse genome (Table S3.3). This analysis identified 4,241 brown anole peaks with sequence orthologs in the mouse genome. TBX5 binding events with conserved sequences in the mouse genome are near genes with human orthologs linked to limb disorders (Fig. 3.7B). Like in mice, most of these TBX5-bound regions tend to occur far from the transcriptional start sites of their

associated genes (Fig. 3.7C). Lastly, we intersected our mouse GT TBX5 binding sites (20,278 peaks) with orthologous peak coordinates of the brown anole (4,241 peaks) and find that 869 TBX5-bound regions are deeply conserved in mouse and lizards.

TBX5 binds validated appendage enhancers in developing external genitalia

Although RNA-seq has identified dozens of predicted target genes of TBX5 in developing genital tubercles, a subset of these is likely to be due to indirect downstream effects of *Tbx5* conditional knockout. We used the Genomic Regions Enrichment of Annotations Tool (GREAT) (McLean et al., 2010; Tanigawa et al., 2022) to associate TBX5 peaks with genes they are likely to regulate. This allows us to intersect our differential expression data with our ChIP-seq datasets to identify putative direct targets of TBX5. Integrating the list of genes associated with ancient TBX5 binding events with our RNA-seq dataset identified eight putative direct target genes of TBX5 (Fig. 3.8).

We capitalized on published datasets to narrow down our list of TBX5 binding sites that occur at appendage enhancers. First, we compared our TBX5-occupied sites with experimentally validated, GT-specific enhancers aggregated in the VISTA Enhancer Browser (Visel et al., 2007). We observe that 10 of 17 VISTA-tested enhancers active in the GT are also bound by TBX5 (Table S3.5). We also compared our TBX5 ChIP-seq datasets in forelimbs and genitalia with published Capture-C data from mouse embryonic forelimbs (Andrey et al., 2017). Chromosome Conformation Capture-based technologies such as Capture-C can identify interactions between *cis*-regulatory

elements and the promoters they are associated with (Downes et al., 2022; Hughes et al., 2014).

We find that TBX5 binds conserved enhancers that display highly limb- and genital-specific activity (Fig. 3.9). Several of these regions are also bound by TBX5 in brown anole hemiphalluses. These validated appendage enhancers interact with the promoters of several genes with known functions in the developing limb, including *Msx1*, *Prrx1*, and *Creb5* (Bensoussan-Trigano et al., 2011; Martin et al., 1995; C.-H. Zhang et al., 2022). Interestingly, our CHIP-seq data also reveal that TBX5 binds HLEB – a hindlimb/genital enhancer of *Tbx4* – (Menke et al., 2008) in both mouse and brown anole genitalia (data not shown). However, *Tbx4* was not reported as differentially expressed in *Tbx5*-depleted mice. Overall, our combined CHIP-seq and RNA-seq analyses suggest that TBX5 promotes external genital development by direct and indirect regulation of appendage genes.

Discussion

A variety of transcription factors and signaling molecules govern the outgrowth and patterning of the developing external genitalia. The *Isl1* gene encodes a LIM/Homeobox transcription factor that controls genital tubercle development via regulation of the BMP, FGF, and Wnt signaling pathways (Ching et al., 2018). Conditional deletion of *Isl1* causes external genital hypoplasia and a variety of urethral disorders, and *Isl1* mutant mice also develop swelling of the kidneys and ureter (Ching et al., 2018; Minchey, 2022). Previous work from our lab found that ISL1 directly activates *Tbx5* by

binding a putative enhancer conserved across amniotes (Minchey, 2022). In the current study, we find that this *cis*-regulatory element, GTE1, drives reporter gene activity highly similar to the previously reported expression pattern of *Tbx5* in the GT mesenchyme. We also find that *Tbx5* cKO mice display hypoplasia of the preputial swellings and urethra.

While *Tbx5* has a crucial role in the initiation and patterning of the forelimb bud, we observe that the gene has a more subtle effect on genital tubercle morphology. This further supports the idea that unique molecular mechanisms control the morphological development of the limbs and genitalia despite similarities in the gene expression patterns of these appendage types. However, additional histological analyses of *Tbx5* mutant GTs need to be performed to determine any effects on the development of internal structures such as the urethral epithelium, preputial glands, and mesenchymal swellings (urethral folds). Furthermore, more studies are necessary to reveal any sex-specific effects of *Tbx5* ablation in the GT. Interestingly, *Tbx5* is expressed in the urethral plate epithelium of males but not females at E18.5 (Douglas et al., 2012). In addition to observing sex-specific structures such as the prostate gland, differences in the anogenital (perineum) distance or size of the bulbourethral glands and labioscrotal swellings can also be examined between males and females.

We hypothesized that the subtle phenotype observed in *Tbx5*-ablated genital tubercles might be due to genetic compensation by *Tbx4*. However, *Tbx5*^{flox/flox}; *HoxB6-Cre*, *Tbx4*^{null/+} mice did not display a more apparent phenotypic disruption of GT morphology compared to *Tbx5* cKO mice. It is possible that complete perturbation of

both *Tbx5* and *Tbx4* in the GT would produce a more severe effect on GT development. This would require the use of *Tbx4* flox mice to conditionally delete *Tbx4* in the GT, as the *Tbx4* null allele we used enables a constitutive knockout and is embryonic lethal (Naiche & Papaioannou, 2003, 2007). Because our *Tbx5* cKO mutants die perinatally, it is not possible to observe external genital phenotypes postnatally and at adulthood when more distinct features can be observed. Thus, the use of various Cre driver mouse lines expressed in the GT (Hashimoto et al., 2018) will be required to further investigate the role of *Tbx5* in controlling external genital growth and patterning.

Our RNA-seq analysis of genital development uncovered dozens of misregulated genes in *Tbx5* cKO embryos. Of the 70 differentially expressed genes identified, 39 are associated with nearby TBX5 binding events in mouse GTs (Table S3.2). This list consists of several genes that are also targets of TBX5 in the embryonic forelimb, such as *Cxcl12* and *Hand2* (see Chapter 2). Eight genes are direct targets of TBX5 with nearby ancient binding events in the amniote phallus (Fig. 3.7). One of these includes the homeobox gene *gooseoid* (*Gsc*), which controls proper development of the labioscrotal folds in mice (C. C. Zhu et al., 1998). Another ancient target of TBX5 in external genitalia is *Glis3*, which encodes a GLI-similar zinc finger protein. One study reported a human patient with a mutation in *GLIS3* that presented scrotal hypospadias, bifid scrotum, and chordee, an abnormal bending of the penis (Alghamdi et al., 2017). *Hand2* is another ancient target gene of TBX5 identified in our study. *Hand2* is necessary to regulate Shh signaling during male clasper development in the little skate, *Leucoraja erinacea*

(O'Shaughnessy et al., 2015). Claspers in chondrichthyans (cartilaginous fish) are paired penis-like structures that are used for sperm transfer during copulation.

Using TBX5 ChIP-seq in mouse embryonic forelimbs and GTs, we identified thousands of binding sites in each of these appendage types. Approximately 32% (4,388/13,580 forelimb peaks) of these TBX5 binding sites are shared between the forelimb and GT. Thus, despite the high overlap of active enhancers in embryonic limbs and genitalia (Infante et al., 2015), there are differences in the set of TBX5-bound *cis*-regulatory targets in these tissues. Interestingly, we identify several shared forelimb-GT binding sites that overlap with functionally validated enhancers active in both appendage types (Fig. 3.8). As more of these appendage-specific regulatory elements are discovered, further studies need to be done to investigate the hypothesis that the amniote phallus may have evolved, in part, through co-option of components of an ancient appendage gene regulatory network.

While we find many *cis*-regulatory elements bound by TBX5, some of these are associated with genes that are not misregulated in GTs of *Tbx5* conditional mutants. It is possible that our RNA-seq data are not providing enough resolution of gene expression. Recent advances in single-cell transcriptomics have provided unparalleled insight into the gene expression patterns of cell populations in the developing external genitalia (Amato & Yao, 2021; Armfield & Cohn, 2021). Single-cell analyses of *Tbx5* cKO embryos may reveal rare cell populations that are perturbed in mutant GTs. Furthermore, production of high-resolution enhancer-promoter interaction maps in developing

genitalia using Chromosome Conformation Capture-based technologies will enable higher confident associations of regulatory elements with the genes they regulate.

In conclusion, we describe a novel role of *Tbx5* in properly patterning the urethral meatus and preputial swellings. Moreover, we have linked many TBX5-bound *cis*-regulatory elements to genes with TBX5-dependent expression in developing genitalia. These data provide foundation for future studies of the different mechanisms used by TBX5 to pattern the amniote phallus.

Methods

Animals

Tbx5^{flox/flox} mice (Bruneau et al., 2001) were crossed with *HoxB6-Cre* mice (Lowe et al., 2000) to generate *Tbx5* cKO mice. Each of these mouse strains lies on a C57BL/6 genetic background. Embryonic day (E) 0.5 was defined as noon of the day a vaginal plug was detected. Eggs were collected from wild-caught brown anole. Animal procedures were completed per guidelines issued by the Institutional Animal Care and Use Committees (IACUC) at the University of Georgia under approved Animal Use Protocols.

Microscopy

For light sheet microscopy, embryos were dissected and fixed in 4% PFA then dehydrated in a stepwise series to 100% methanol. Samples were then processed through a modified iDISCO protocol (Renier et al., 2014). In brief, embryos were first trimmed into a small piece containing the pelvic region and genital tubercle and

incubated in 66% dichloromethane (DCM)/33% methanol. Samples were bleached in 5% H₂O₂, rehydrated in a methanol/1X PBS series, and then washed in PTx.2 solution (PBS, TitronX-100). Next, samples were incubated for 30 minutes in DAPI stain, washed in PBS, embedded in 1% agarose, and dehydrated in a series to 100% methanol. The final steps of the clearing process were incubation in DCM and long-term storage in dibenzyl ether (DBE). Cleared samples were imaged using the LaVision BioTec UltraMicroscope II at the University of Georgia Biomedical Microscopy Core. Light sheet scans were compiled using Imaris Stitcher and rendered into a three-dimensional model using the Surface function in the Imaris Microscopy Image Analysis Software (<https://imaris.oxinst.com/>).

For scanning electron microscopy, embryos were fixed in 4% PFA, dehydrated to 100% ethanol, and stored at -20 °C until processing. Samples were prepared by Georgia Electron Microscopy at the University of Georgia and imaged on the Thermo Fisher Scientific (FEI) Teneo (field emission scanning electron microscope).

Transgenic reporter assays and LacZ Staining

To test activity of the *Tbx5* enhancer GTE1, the region (mm10: chr5:119,963,070-119,964,024) was first amplified from BL6 mouse genomic DNA using primers containing 22 bp homology arms flanking the NotI recognition site of Hsp68LacZ. The PCR primers used are as follows:

Tbx5_GTE1_cloning_F1: ATTGGAGCTCCACCGCGGTGGCGACTGCTGATCACTTGTGACATG

Tbx5_GTE1_cloning_R1: ATCCACTAGTTCTAGAGCGGCCTGAACACCTTCTATCAGCTCTTC

The purified PCR product was then cloned into the NotI site of Hsp68LacZ using the NEBuilder HiFi DNA Assembly Cloning Kit. Transgenic vector constructs were sent to Cyagen (<https://www.cyagen.com/us/en/>) for pronuclear injection and transgenic embryo screening.

RNA-seq

GTs were collected from E12.5 mouse embryos, incubated in RNAlater, and stored at -80°C until further processing. Amniotic sac tissue was harvested for genotyping. Only XY embryos were used for RNA-seq, while XX embryos were used for RT-qPCR. Total RNA was collected from individual control (*Tbx5^{flox/flox}*) and mutant (*Tbx5^{flox/flox}; HoxB6-Cre*) GT samples using the mirVana miRNA Isolation Kit (ThermoFisher Scientific). mRNA libraries from five control and three mutant replicates were prepared using the TruSeq Stranded mRNA Library Prep Kit (Illumina) and sequenced at Georgia Genomics and Bioinformatics Core (50 bp single-end reads). Reads were aligned to the mm10 genome using HISAT2 (v2.1.0) and transcripts were counted using Rsubread (v2.8.2) featureCounts. DESeq2 (v1.34.0) was used to perform differential gene expression analysis. We used ShinyGO (v0.77) (Ge et al., 2020) to perform gene-set enrichment analysis and to generate lollipop plots. The gene set enrichment analyses initially used all protein coding genes as the background set, but was subsequently reanalyzed using all genes that exhibited an average normalized count (baseMean) greater than five.

ChIP-seq

External genitalia were collected from the E12.5 mice (outbred ICR; Envigo) and stages 7-9 of *A. sagrei* embryos (Sanger et al., 2008). Two independent ChIP and Input replicates were generated for each experiment. Genital samples were crosslinked in 1% formaldehyde and stored at -80°C until further chromatin processing. Approximately 50 µg of chromatin was incubated in Protein G Agarose Columns (Active Motif) with a human/mouse TBX5 polyclonal antibody (R&D Systems AF5918). Libraries preparation was performed using the NEBNext Ultra II Library Prep Kit and amplified for 15 cycles. Sera-Mag SpeedBeads were utilized to perform size selection and to remove primer and adapter fragments. Libraries were sequenced by the Georgia Genomics and Bioinformatics Core to generate single-end 75 bp reads.

ChIP-seq data analysis

We used the ENCODE Transcription Factor and Histone ChIP-Seq processing pipeline (<https://github.com/ENCODE-DCC/chip-seq-pipeline2>) (Landt et al., 2012) to identify highly reproducible (conservative) peak sets with an irreproducible discovery rate (IDR) cutoff of 0.05. We used mm10 (mouse) and AnoSag2.0 (brown anole) genomes for alignment. We used a multi-species alignment and halliftover (Hickey et al., 2013) to convert ChIP-seq peak coordinates from the lizard genome to the mouse genom. To associate putative target genes with each peak, we used GREAT with default parameters (McLean et al., 2010; Tanigawa et al., 2022). Motif analyses were completed on TBX5 peaks centered 100 bp flanking each summit using HOMER v4.11

(findMotifsGenome.pl) (Heinz et al., 2010). Enrichment heatmaps were produced using Deeptools and genome browser tracks were assembled using pyGenomeTracks. We used bedtools to obtain peak coordinate intersections.

Data availability

Genomic and transcriptomic data for this manuscript will be uploaded to the Gene Expression Omnibus database (Edgar et al., 2002) and updated accession numbers will be posted to the GitHub page below.

Scripts and bioinformatic pipelines used to analyze data and generate figures are available at <https://github.com/gene-drive/Tbx5-forelimb-genital>.

Public data used

Mouse H3K27ac ChIP-seq data from E12.5 genital tubercles was generated by Infante et al. (2015) (Accession GSE64055) and reanalyzed to convert peaks to mm10. HOXA13 CUT&RUN data from mouse GTs was acquired from Amândio et al. (2020) (Accession GSE138514). TBX5 ChIP-seq data from heart and lung were obtained from Steimle et al. (2018) and Rank et al. (2012) (Accessions GSE119885, GSE167207). Capture-C data from mouse embryonic forelimbs was obtained from Andrey et al. (2017) (Accession GSE84792). Embryonic images and genomic coordinates of experimentally tested enhancers were acquired from the VISTA Enhancer Browser (Visel et al., 2007) and converted to mm10 coordinates using the UCSC Liftover tool.

Figures and Tables

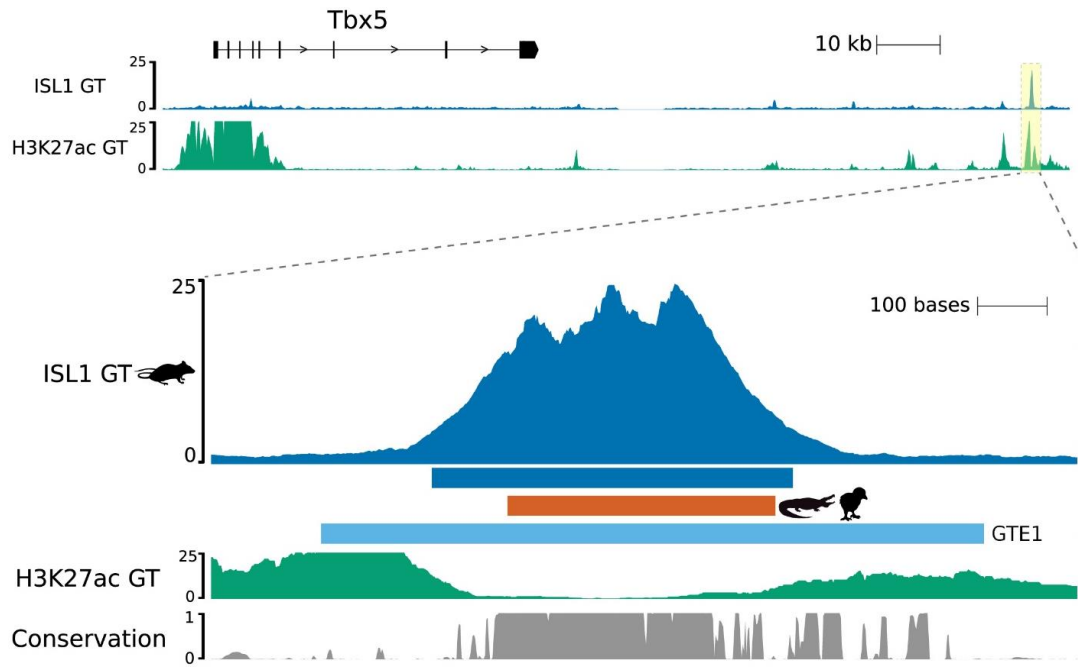


Figure 3.1. ISL1 directly regulates a conserved enhancer of *Tbx5* in the embryonic phallus

Top) Expanded view of the *Tbx5* locus showing CHIP-seq profiles of ISL1 (Minchey, 2022) and H3K27ac (Infante et al., 2015).

Bottom) ISL1 binds GTE1, a putative enhancer of *Tbx5*. *Tbx5* is downregulated in genital tubercles (GTs) of *Isl1* cKO embryos. The dark blue graph in the panel shows peak intensity for TBX5 CHIP-seq in the mouse GT, while the green graph shows peak shows intensity for H3K27ac CHIP-seq. Boxes below the graph represent coordinates for (top to bottom): Mouse TBX5 CHIP-seq peaks (dark blue), conserved TBX5 binding event (orange), and validated GTE1 enhancer (light blue). The orange box marks the minimal mouse sequence conserved that is also bound by TBX5 in alligator and chicken. The conservation graph shows the phastCons score from alignments of 60 vertebrate species (Pollard et al., 2010) obtained from the UCSC Genome Browser (Kent et al., 2002). Genomic coordinates for each region are available in Table S3.4.

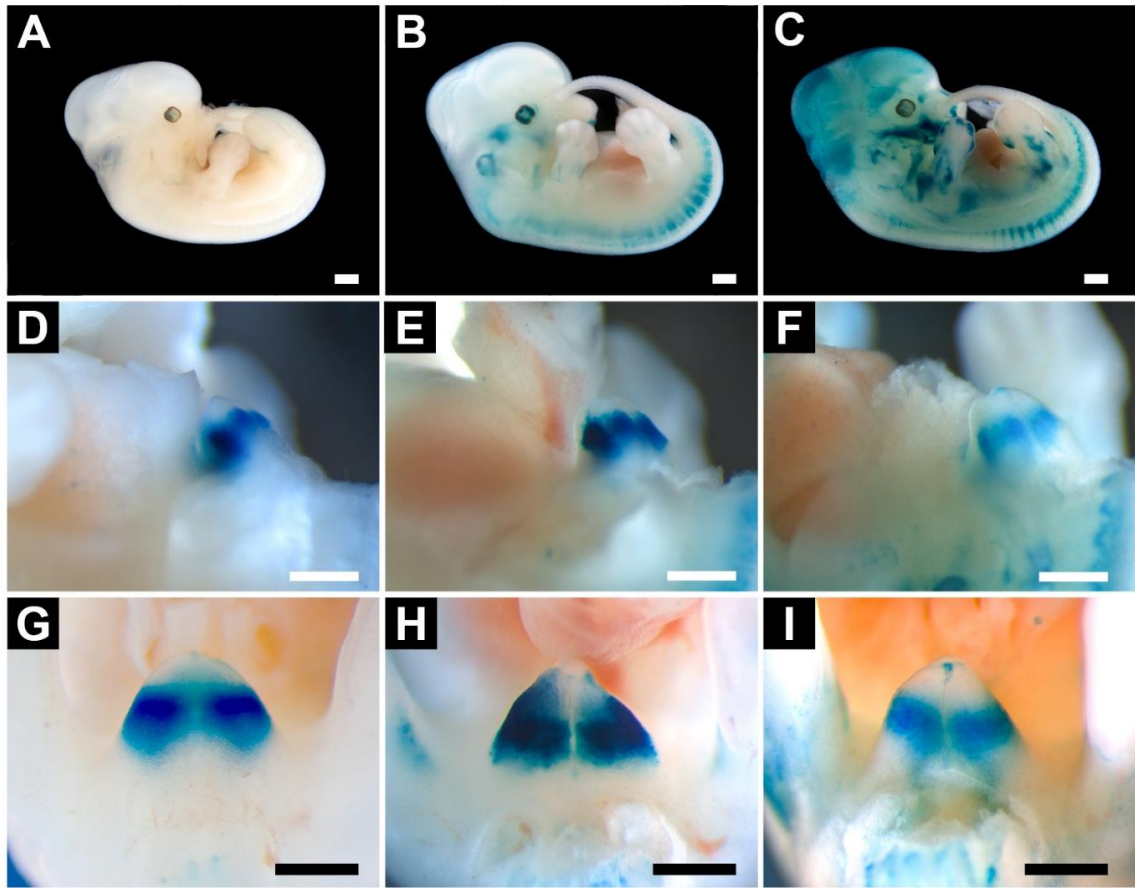


Figure 3.2. GTE1 displays enhancer activity in the mouse genital tubercle

A-I) Three different mouse embryos (~E11.5-E12.5) carrying *GTE1 Hsp68LacZ* transgenes (A, B, C). Activity is shown for lateral (D, E, G) and ventral (G, H, I) views of genital tubercles. The scale bar represents 500 μm .

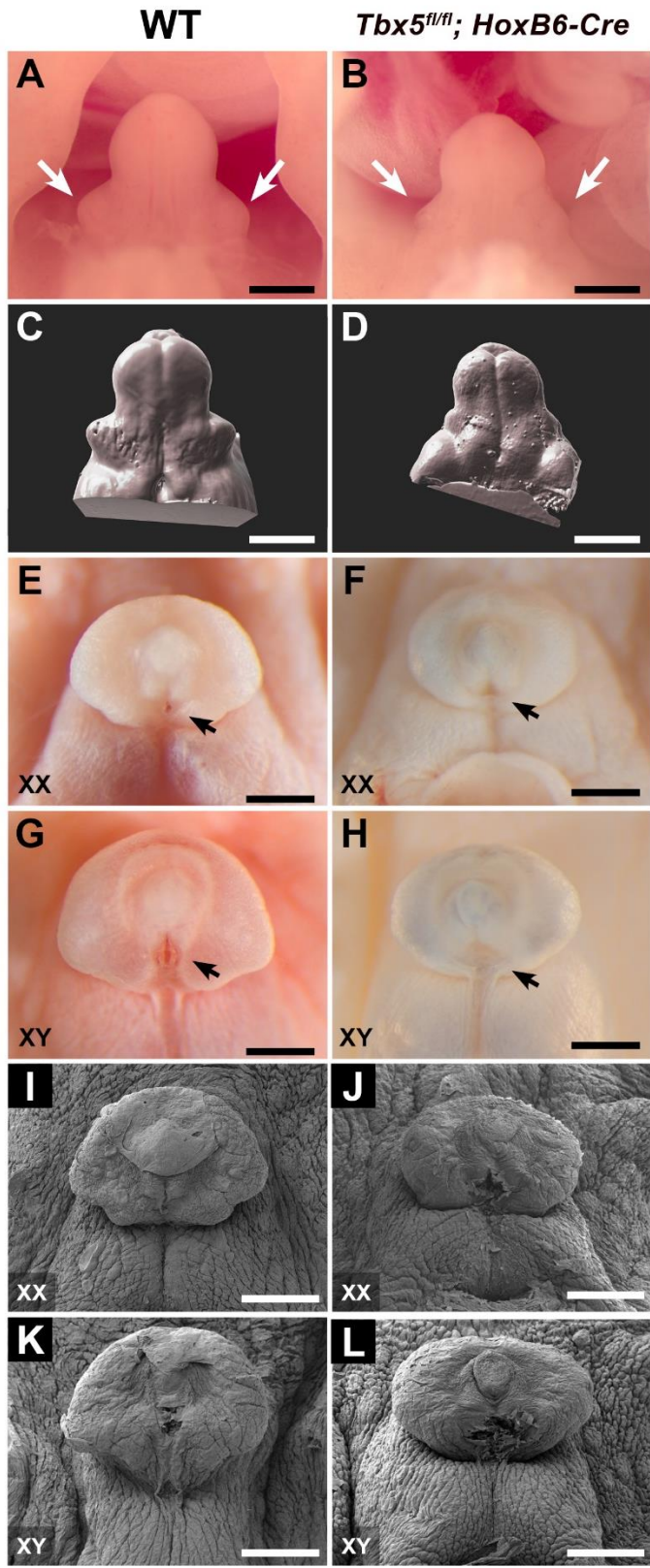


Figure 3.3. Conditional ablation of *Tbx5* leads to reduced size of preputial swellings and urethral hypoplasia

A-D) Bright-field (A, B) and light sheet images (C, D) showing morphology of the GT in E14.5 embryos, genotypes as indicated. White arrows indicate preputial swellings.

E-L) Bright-field images (E-H) and scanning electron micrographs (I-L) showing morphology of the GT in E18.5 embryos, genotypes as indicated. Black arrows indicate the urethral opening (urethral meatus). The scale bar represents 500 μm .

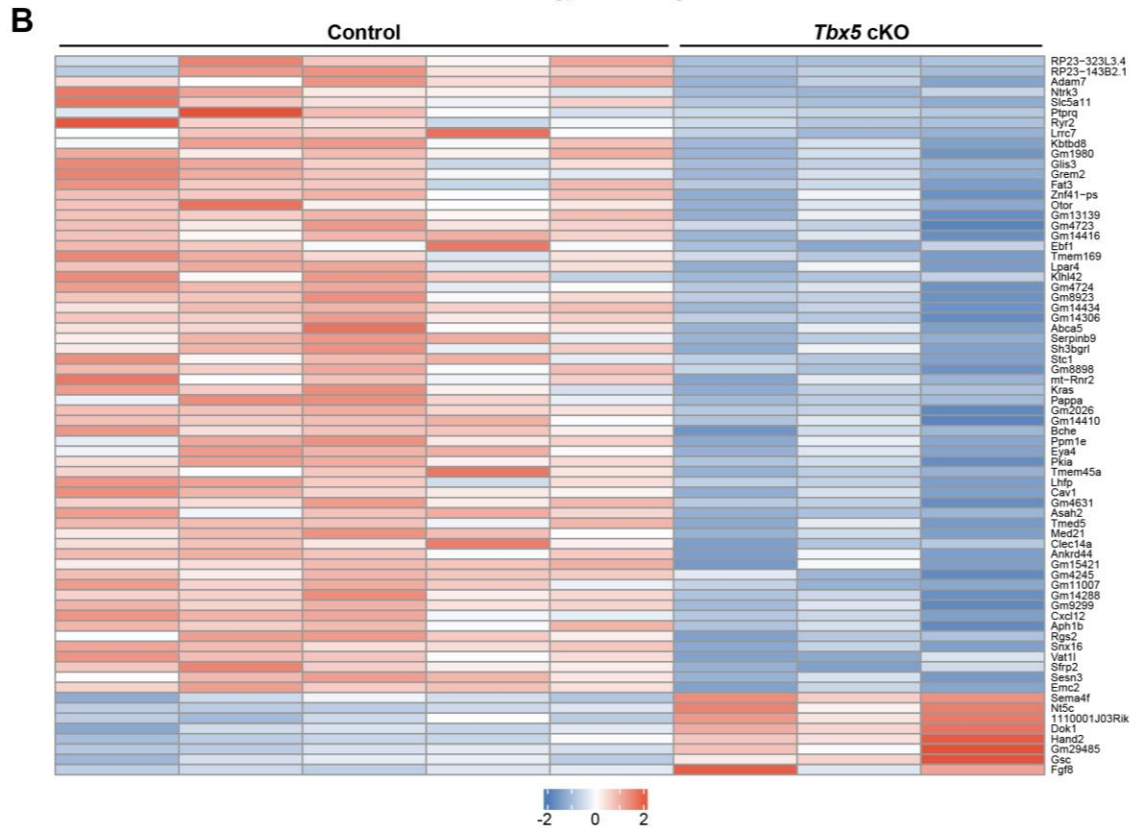
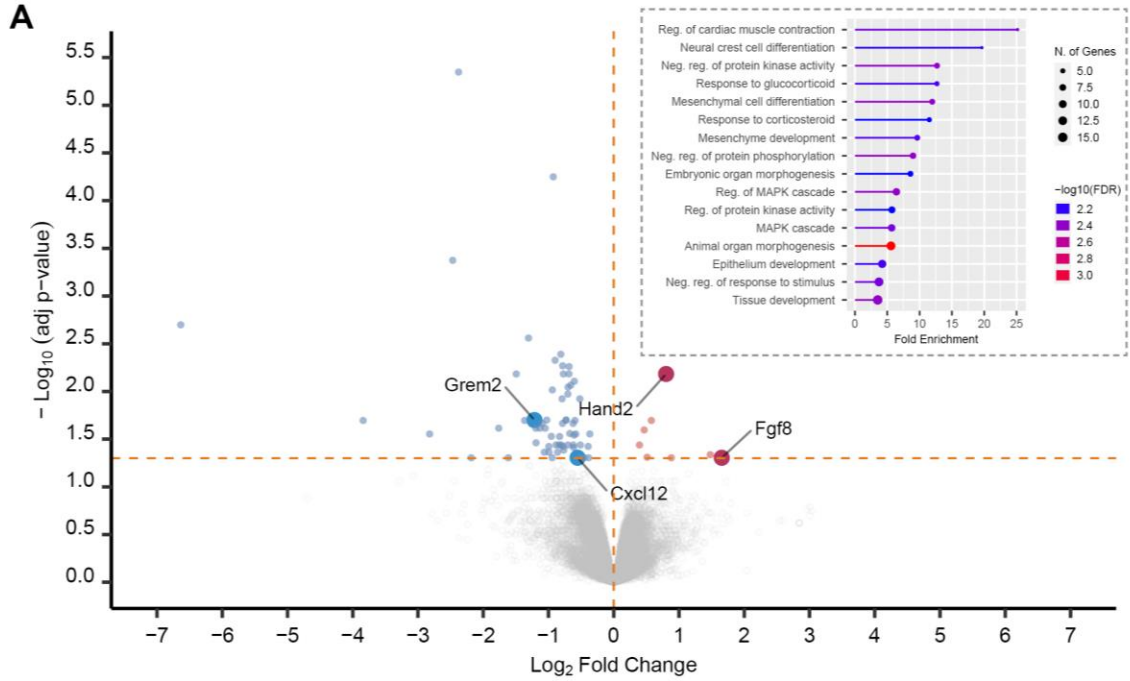


Figure 3.4. Differentially expressed genes (DEGs) in GTs of *Tbx5* conditional knockout (cKO) mice at E12.5

A) Volcano plot showing fold-change and adjusted p -value of DEGs output from DESeq2.

Differentially expressed genes (adjusted p -value < 0.05) are depicted in blue

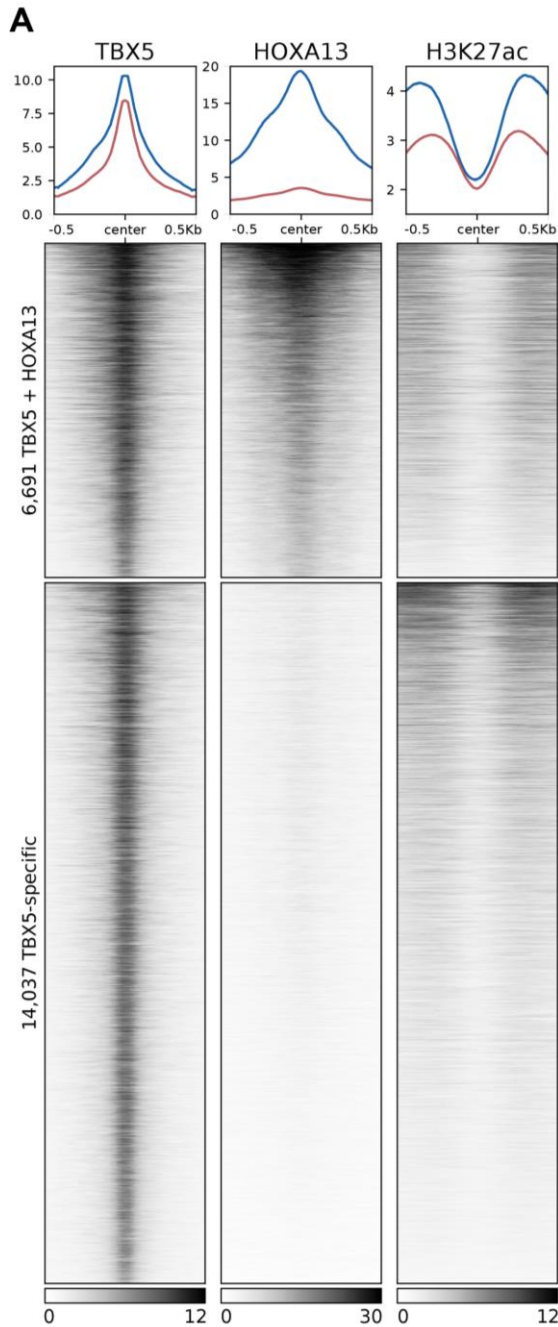
(downregulated) and red (upregulated). Inset: Lollipop plots showing top enriched gene

clusters in the GO Biological Process (Gene Ontology Consortium, 2021) databases for all

DEGs.

B) RNA-seq heatmap of expression patterns in three replicates of *Tbx5* cKO (*Tbx5*^{flox/flox};

HoxB6-Cre) mice compared to five replicates of controls (*Tbx5*^{flox/+}; *HoxB6-Cre*).



B

Rank	Motif	p-value	Type
1		1e-1430	Hox
2		1e-567	T-box

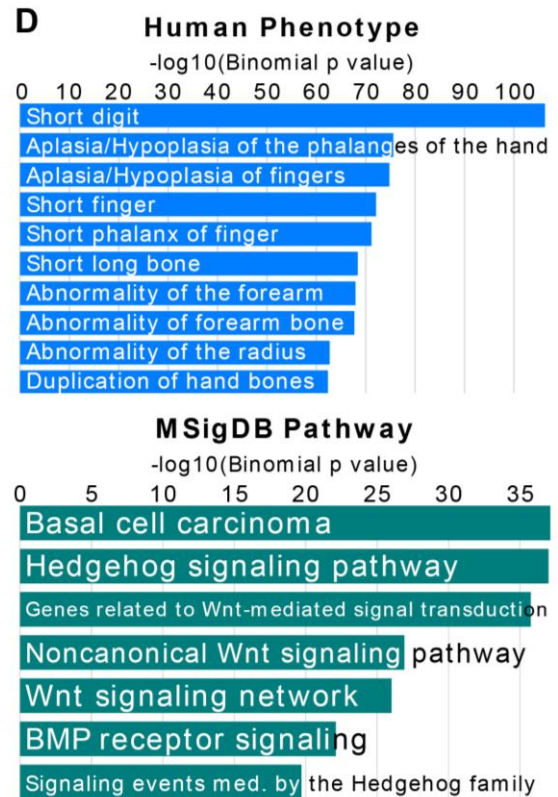
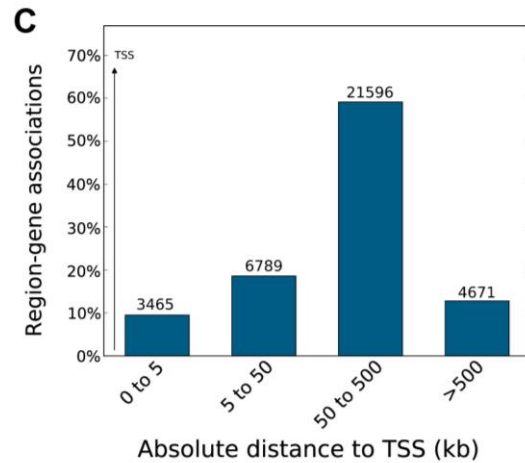


Figure 3.5. Genome-wide enrichment of TBX5 binding in the mouse GT

A) Condensed profiles (top) and heatmaps (bottom) of TBX5, HOXA13 (Amândio et al., 2020), and H3K27ac (Infante et al., 2015) signal in GTs. ChIP-seq datasets are centered on TBX5 peak summits in a 1 kb window. The top heatmaps show enrichment at shared TBX5 + HOXA13 peaks, while the bottom heatmaps show enrichment at TBX5-specific peaks. In the condensed profiles, the blue line represents signal at the TBX5 + HOXA13 peaks, while the red line represents signal at the TBX5-specific peaks. TBX5 and H3K27ac ChIP-seq was performed in E12.5 embryos, while HOXA13 CUT&RUN was performed in E13.5 embryos.

B) Top enriched motifs found using HOMER de novo motif analysis in a 100 bp window centered on TBX5 peak summits.

C) Distribution of TBX5 peaks relative to transcriptional start sites (TSS) of associated genes identified using GREAT. The number of peaks counted is listed above each bar in the graph.

D) Highest-ranked annotation terms of genes associated with TBX5 peaks in the Human Phenotype Ontology (top) and Molecular Signatures Database (bottom).

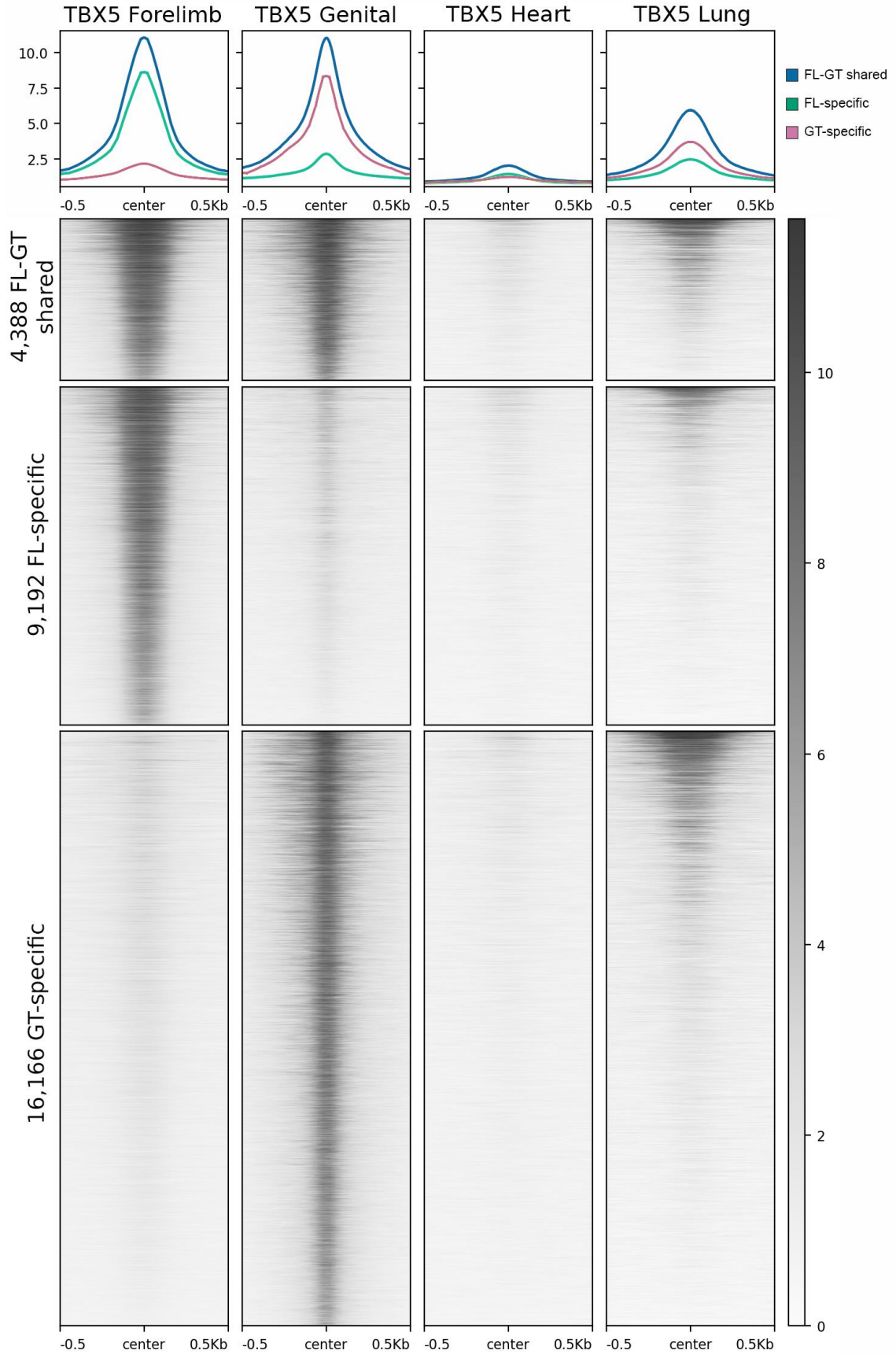
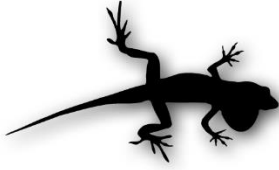


Figure 3.6. Genome-wide enrichment of TBX5 binding in the embryonic mouse forelimb, genital tubercle, heart, and lung

Condensed profiles (top) and heatmaps (bottom) of TBX5 signal in E10.5 forelimbs (FL), E12.5 genital tubercles, E9.5 hearts (Steimle et al., 2018), and E14.5 lungs (Rankin et al., 2021). ChIP-seq datasets are centered on TBX5 peak summits in a 1 kb window. The top heatmaps show enrichment at shared forelimb-GT peaks. The middle and bottom heatmaps show enrichment at forelimb-specific and GT-specific peaks, respectively.

A**15,415 peaks**

Rank	Motif	p-value	Type
1		1e-1038	TCF4 (bHLH)
2		1e-632	Pitx1:Ebox
3		1e-309	Six2
4		1e-245	ETS
5		1e-194	Tbox-Hox

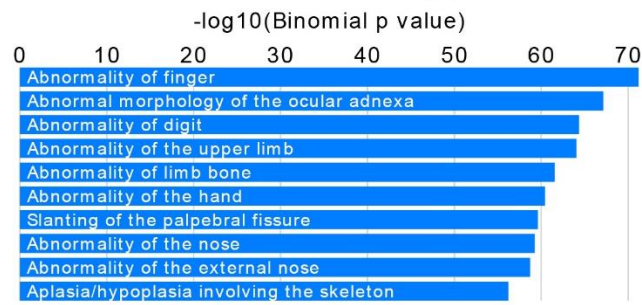
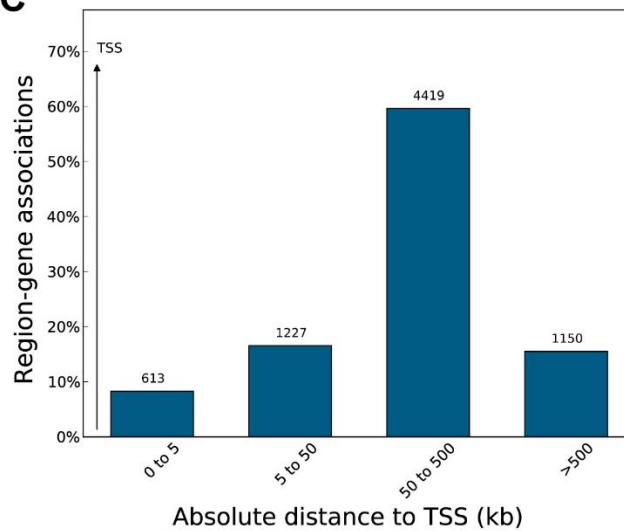
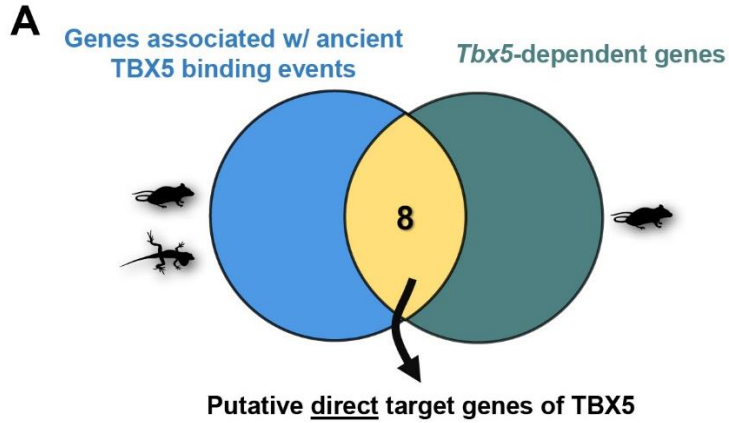
B**4,241 peaks (Liftover)****Human Phenotype****C**

Figure 3.7. Genome-wide occupancy of TBX5 binding events in brown anole embryonic hemiphalluses

A) Top enriched motifs found using HOMER de novo motif analysis in a 100 bp window centered on TBX5 peak summits.

B) Top: brown anole peaks that have sequence orthologs in the mouse genome. These peaks were converted into mouse coordinates using `halLiftover`. Bottom: highest-ranked annotation terms of genes associated with orthologous TBX5-bound regions in the Human Phenotype Ontology.

C) Distribution of TBX5 peaks relative to transcriptional start sites (TSS) of associated genes identified using GREAT. The number of peaks counted is listed above each bar in the graph.



B

Gene associated with TBX5 binding site	Coordinates	Peak Name
Ebf1	chr11:45136790-45137217	TBX5_GT_mm10_peak_619
Emc2	chr15:43545252-43545722	TBX5_GT_mm10_peak_9624
Eya4	chr10:23532182-23532816	TBX5_GT_mm10_peak_1684
	chr10:23450090-23450393	TBX5_GT_mm10_peak_2888
	chr10:23402106-23402576	TBX5_GT_mm10_peak_11266
	chr10:23394248-23394429	TBX5_GT_mm10_peak_4999
Glis3	chr19:28011317-28011787	TBX5_GT_mm10_peak_14136
Gsc	chr12:104678650-104679120	TBX5_GT_mm10_peak_19544
	chr12:104593340-104593810	TBX5_GT_mm10_peak_11461
	chr12:104593237-104593527	TBX5_GT_mm10_peak_2645
Hand2	chr8:56634629-56635099	TBX5_GT_mm10_peak_7926
	chr8:57094961-57095634	TBX5_GT_mm10_peak_14568
	chr8:57094961-57095634	TBX5_GT_mm10_peak_320
Lhfp	chr3:53044230-53044768	TBX5_GT_mm10_peak_150
Sfrp2	chr3:83772427-83772724	TBX5_GT_mm10_peak_6597

Figure 3.8. Deeply conserved TBX5 binding events in the embryonic phallus of amniotes

A) Approach for identifying putative direct target genes of TBX5. TBX5 ChIP-seq peaks were compared in mouse and brown anole to find ancient TBX5 binding events. GREAT was used to associate TBX5 peaks with neighboring genes. This gene list was then intersected with misregulated genes identified in *Tbx5* cKO embryos.

B) Table of putative ancient targets of TBX5 in the embryonic phallus

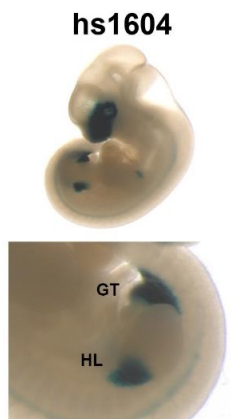
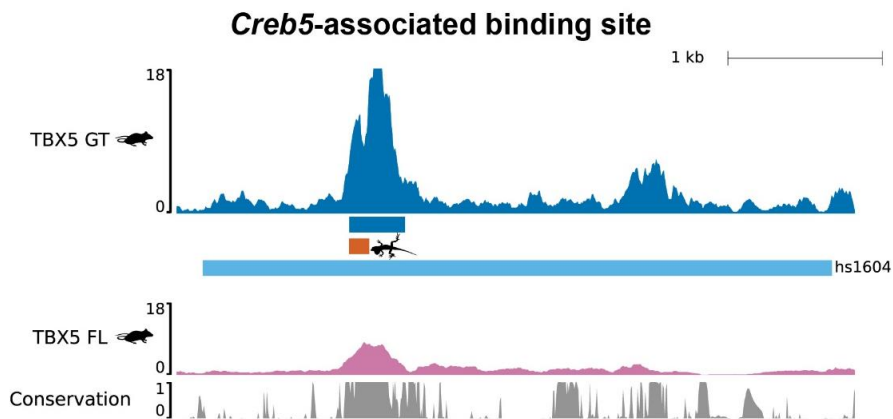
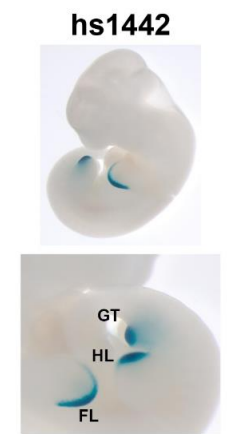
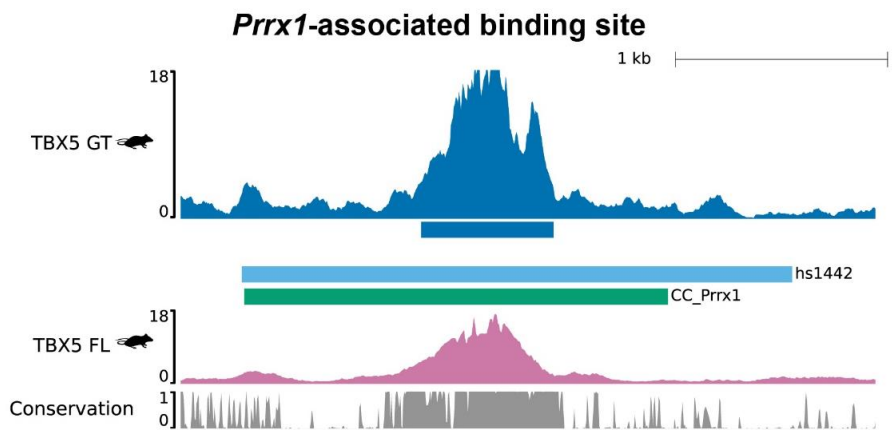
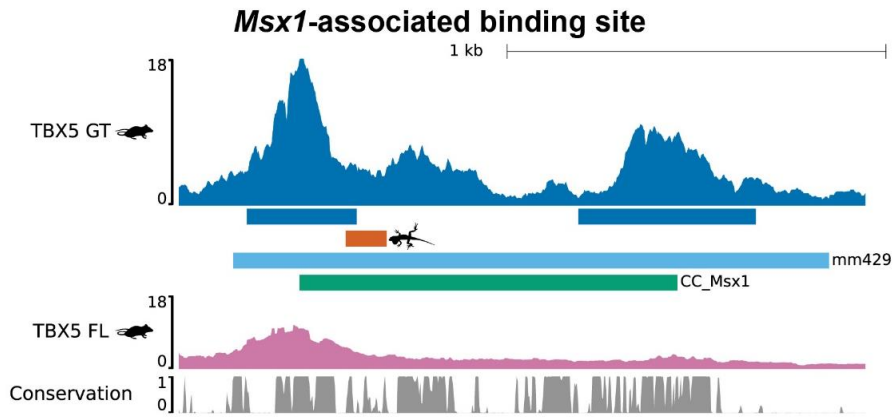


Figure 3.9. TBX5 binds validated appendage enhancers in the forelimb and genital tubercle

Msx1 is upregulated in forelimbs of *Tbx5* cKO embryos. The dark blue graph at the top of each panel shows peak intensity for TBX5 ChIP-seq in the mouse GT. Boxes below the graph represent coordinates for (top to bottom): Mouse TBX5 ChIP-seq peaks in GTs (dark blue), conserved TBX5 binding event (orange), validated VISTA enhancer (Visel et al., 2007) (light blue), and Capture-C (CC) peaks indicating interaction with the gene's promoter in embryonic forelimbs (Andrey et al., 2017) (green). The orange box marks the minimal mouse sequence conserved in each species indicated that is also bound by TBX5. The pink graph shows peak intensity for TBX5 ChIP-seq in mouse embryonic forelimbs. The conservation graph shows the phastCons score from alignments of 60 vertebrate species (Pollard et al., 2010) obtained from the UCSC Genome Browser (Kent et al., 2002). Photos show *in vivo* enhancer activity in transgenic mice. FL: forelimb, HL: hindlimb, GT: genital tubercle. Genomic coordinates for each region are available in Table S3.4. *Creb5* synonym: 9430076C15Rik.

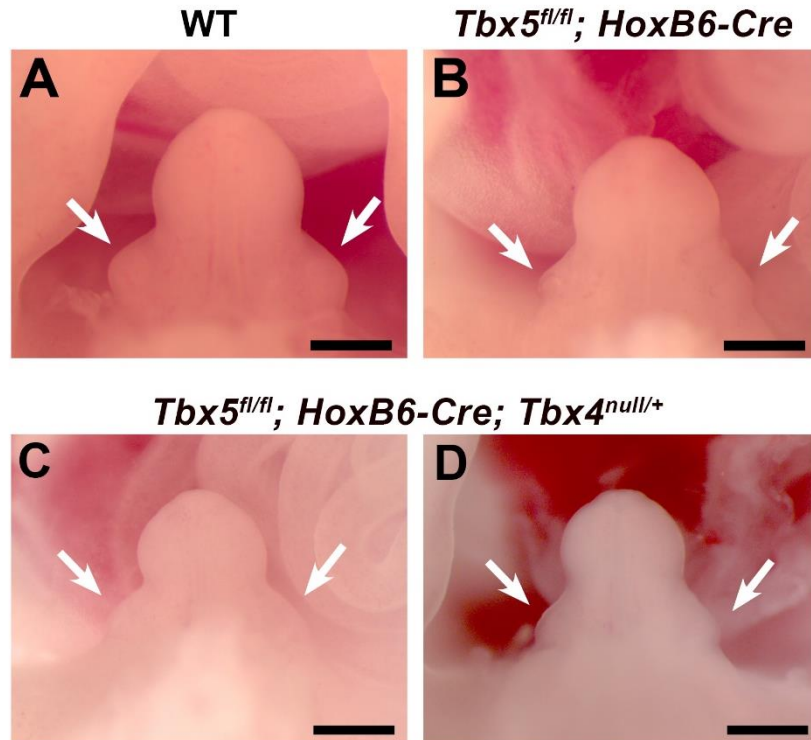


Figure S3.1. Introduction of a *Tbx4* null allele in the *Tbx5* mutant background does not lead to a more severe phenotype in the GT

A-D) Bright-field images showing morphology of the GT in E14.5 embryos, genotypes as indicated. White arrows indicate preputial swellings. The scale bar represents 500 μm.

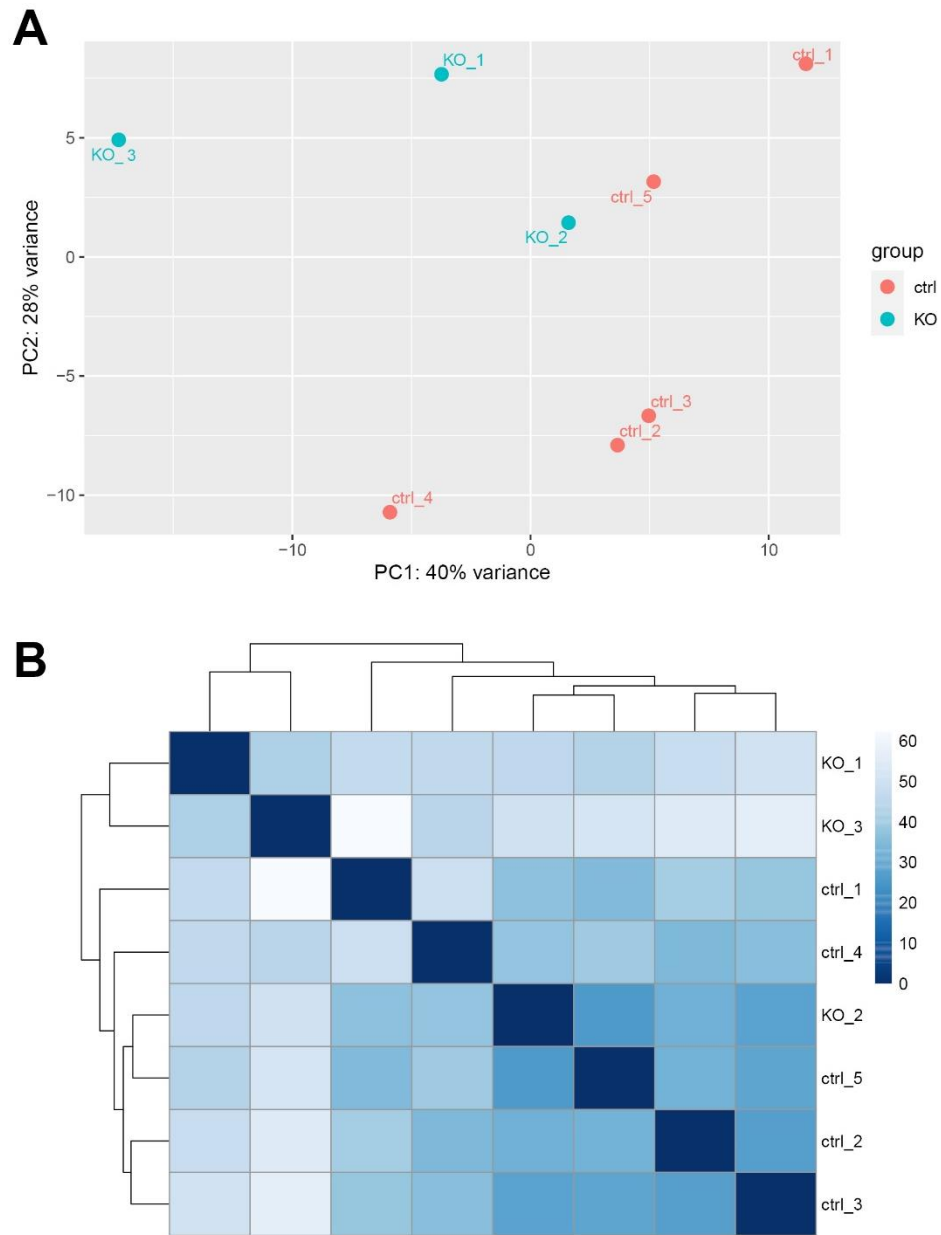


Figure S3.2. RNA-seq data quality assessment by sample clustering (GT)

PCA plot (A) and sample-to-sample distances heatmap (B) showing three replicates of *Tbx5* cKO (*Tbx5*^{fllox/fllox}; HoxB6-Cre) mice compared to five controls (*Tbx5*^{fllox/fllox}). Sample-to-sample distances were calculated from transformation of count data for overall gene expression.

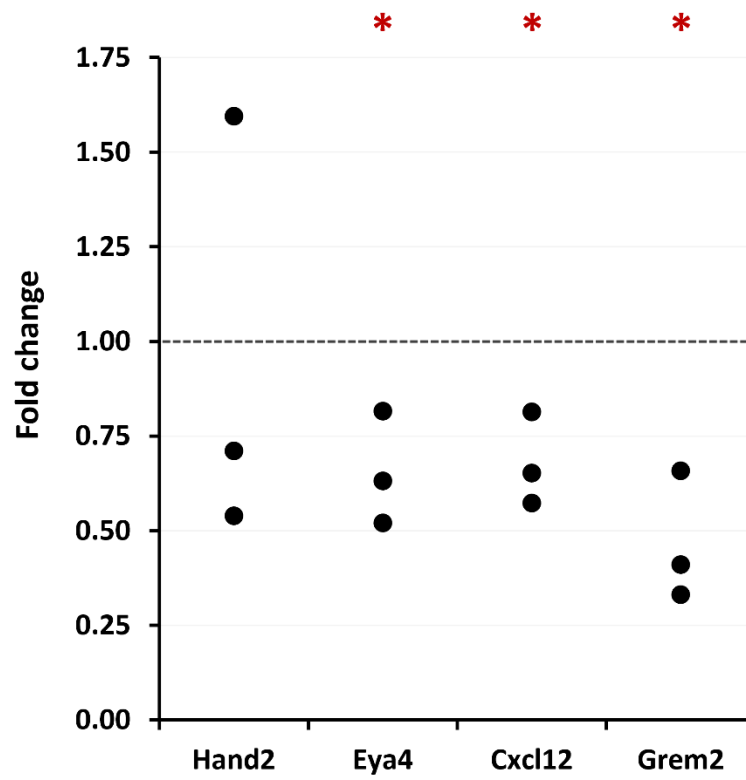


Figure S3.3. qPCR validation of differentially expressed genes identified in RNA-seq analysis

The fold change is the expression ratio of *Tbx5* cKO compared to control GTs. Asterisks indicate $p < 0.05$ (one-tailed t -test).

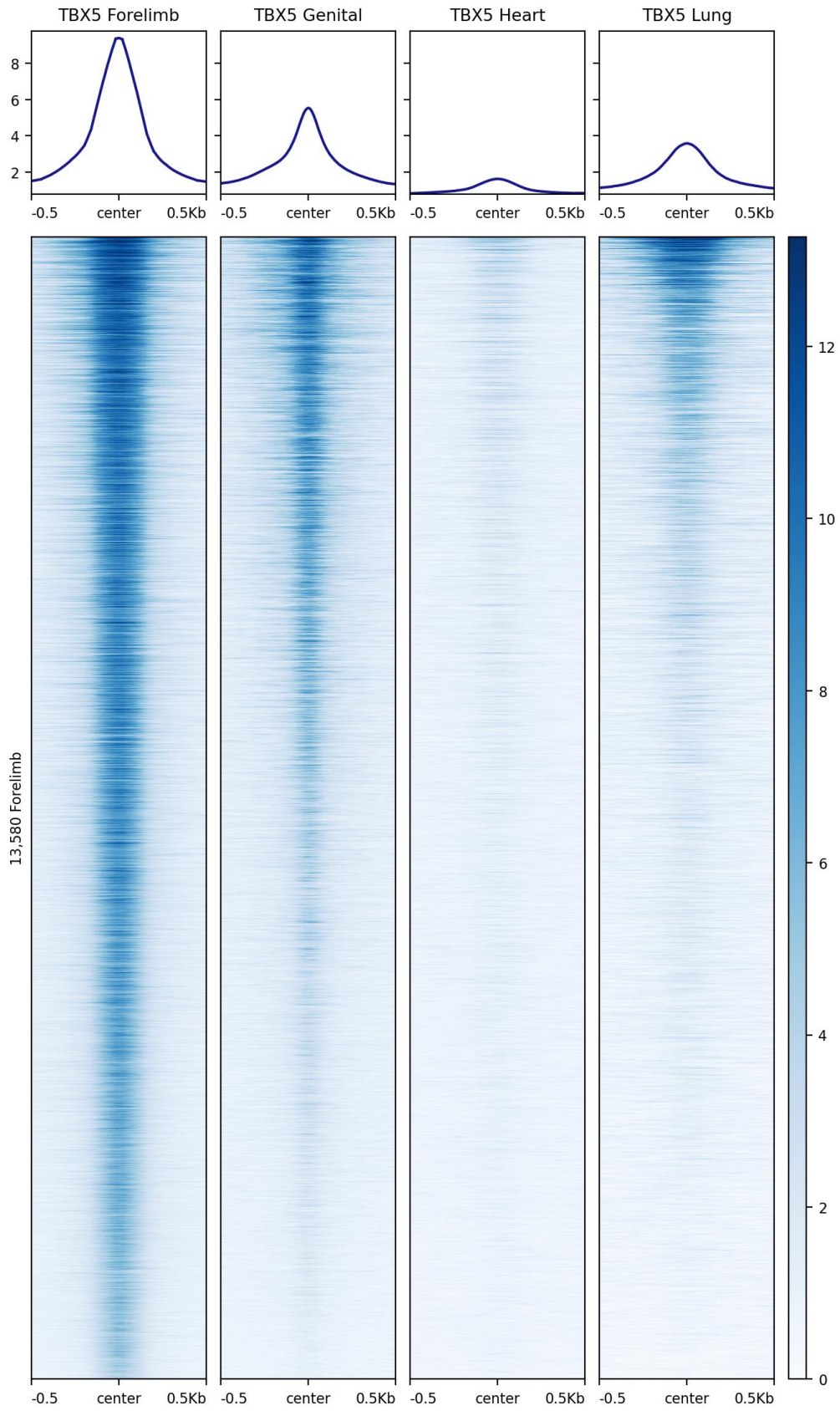


Figure S3.4. Genome-wide enrichment of TBX5, centered on forelimb peaks

Condensed profiles (top) and heatmaps (bottom) of TBX5 signal in E10.5 forelimbs (FL), E12.5 genital tubercles, E9.5 hearts (Steimle et al., 2018), and E14.5 lungs (Steimle et al., 2018). ChIP-seq datasets are centered on TBX5 peak summits in a 1 kb window.

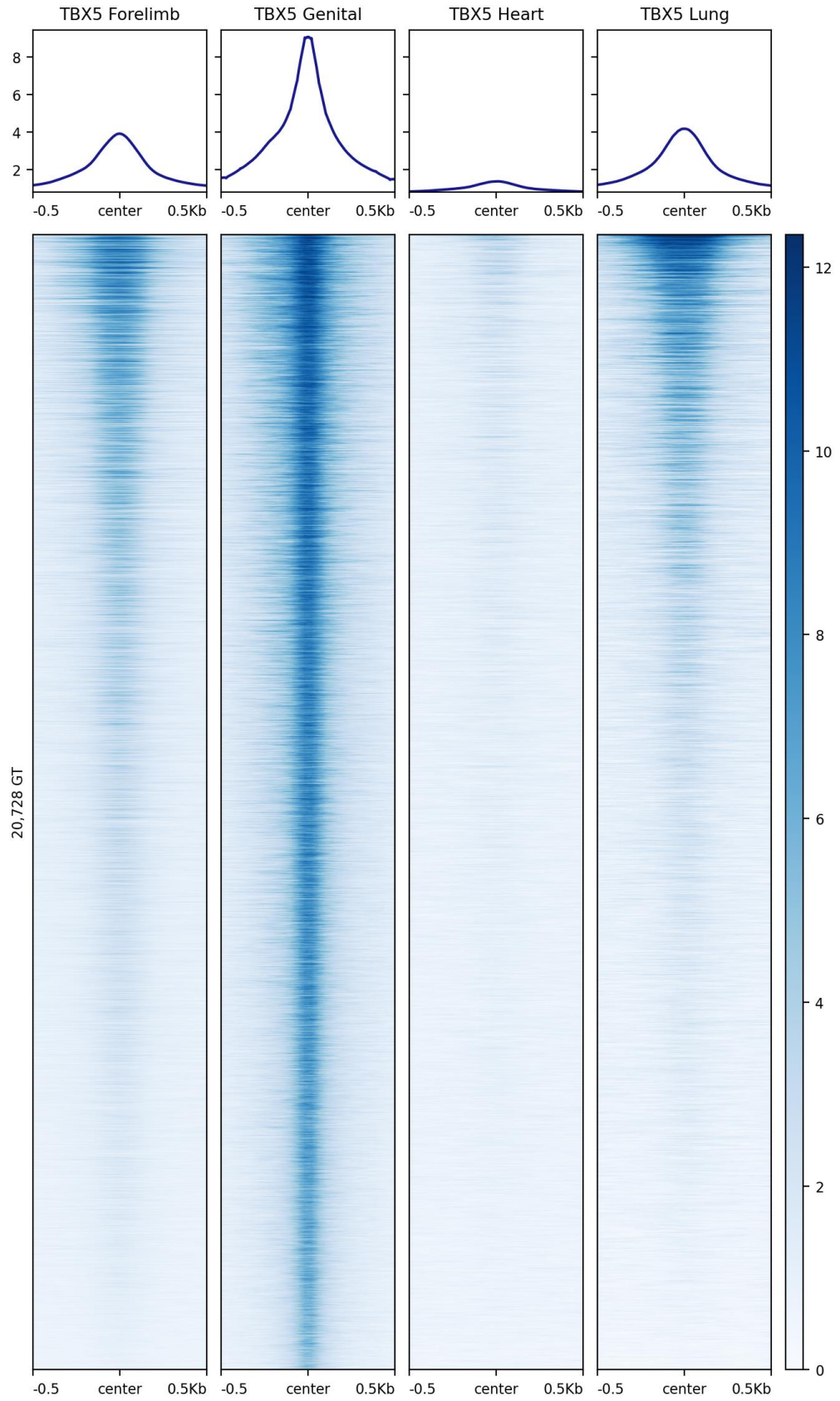


Figure S3.5. Genome-wide enrichment of TBX5, centered on genital peaks

Condensed profiles (top) and heatmaps (bottom) of TBX5 signal in E10.5 forelimbs (FL), E12.5 genital tubercles, E9.5 hearts (Steimle et al., 2018), and E14.5 lungs (Steimle et al., 2018). ChIP-seq datasets are centered on TBX5 peak summits in a 1 kb window.

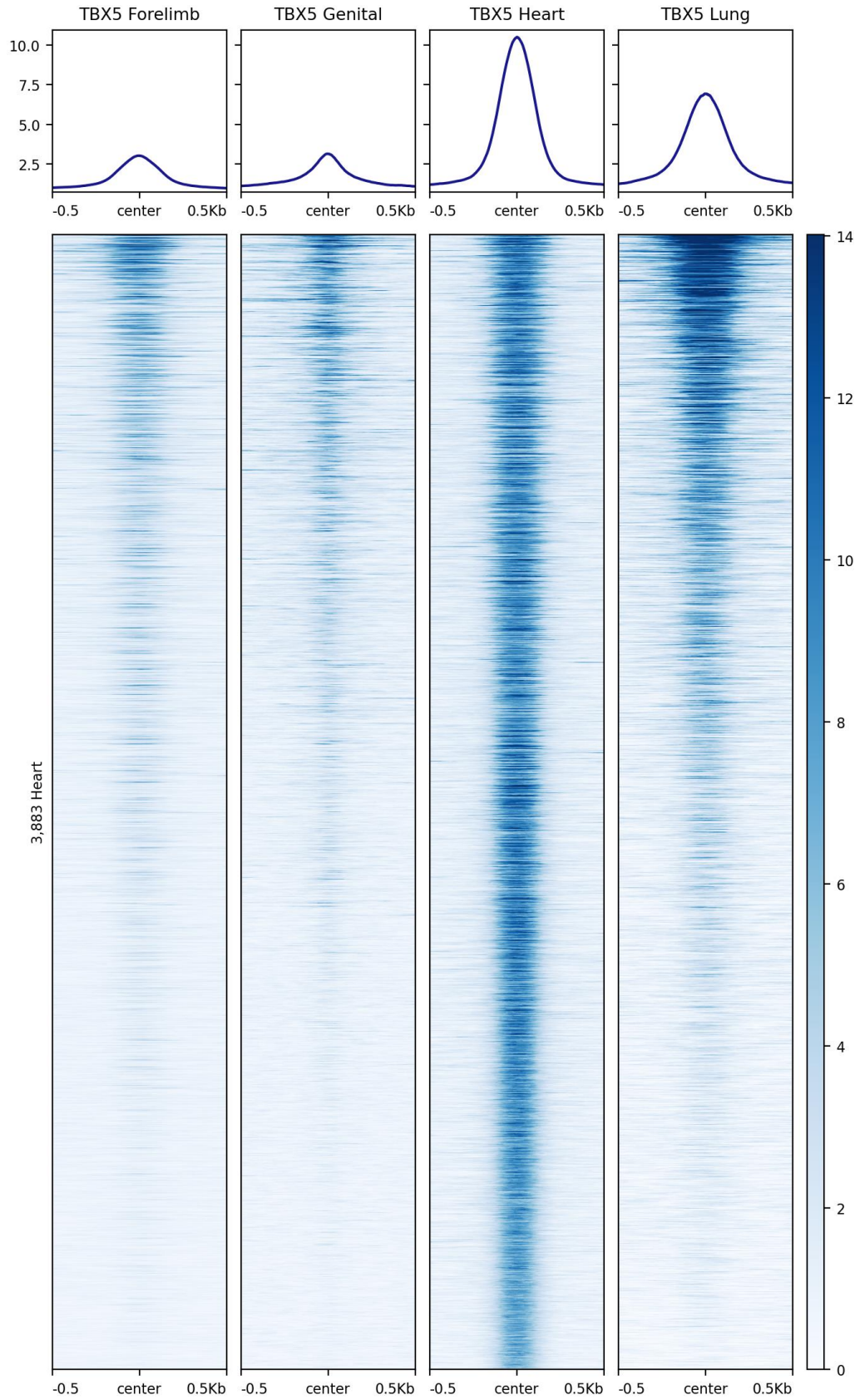


Figure S3.6. Genome-wide enrichment of TBX5, centered on heart peaks

Condensed profiles (top) and heatmaps (bottom) of TBX5 signal in E10.5 forelimbs (FL), E12.5 genital tubercles, E9.5 hearts (Steimle et al., 2018), and E14.5 lungs (Steimle et al., 2018). ChIP-seq datasets are centered on TBX5 peak summits in a 1 kb window.

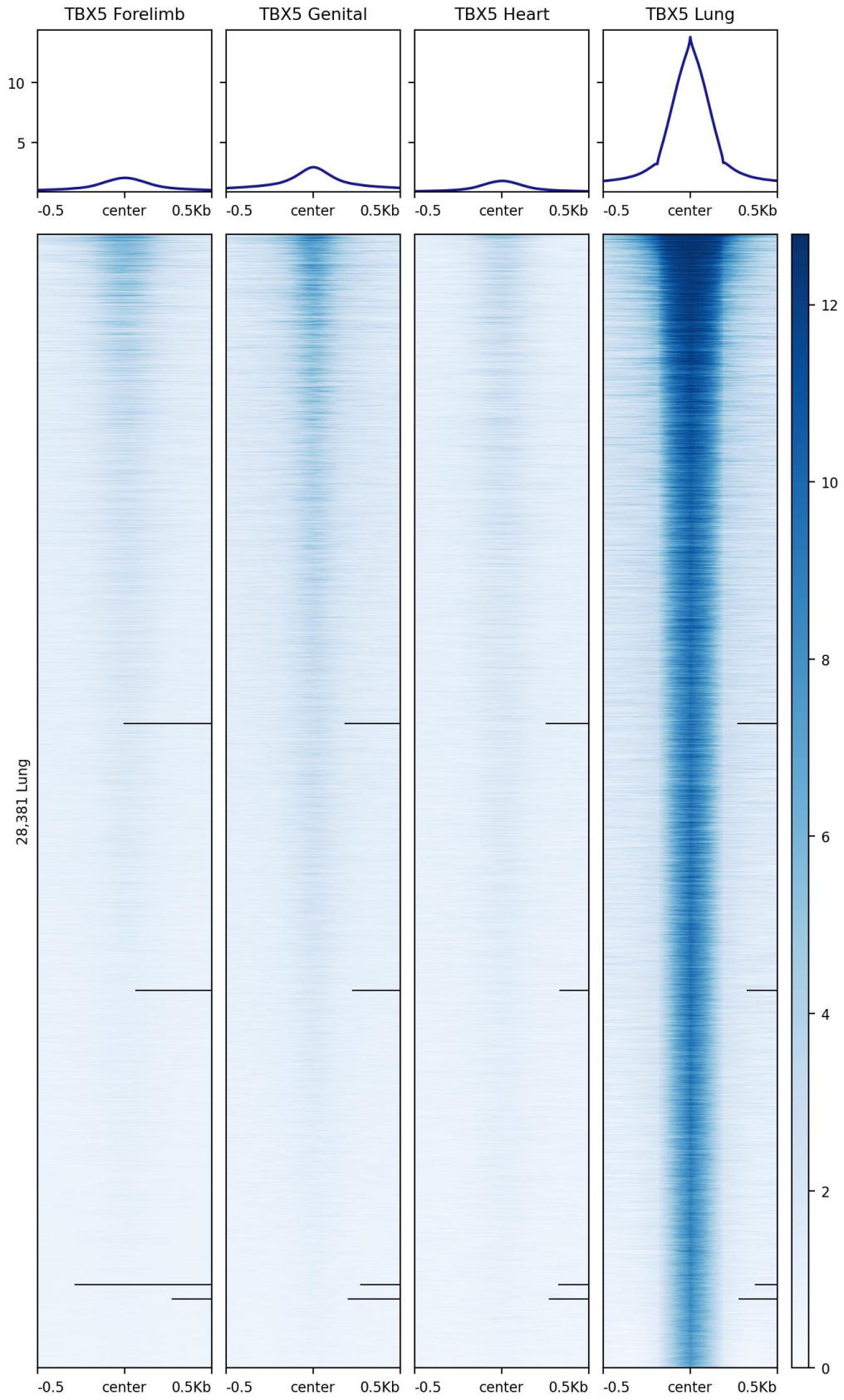


Figure S3.7. Genome-wide enrichment of TBX5, centered on lung peaks

Condensed profiles (top) and heatmaps (bottom) of TBX5 signal in E10.5 forelimbs (FL), E12.5 genital tubercles, E9.5 hearts (Steimle et al., 2018), and E14.5 lungs (Steimle et al., 2018). ChIP-seq datasets are centered on TBX5 peak summits in a 1 kb window. Black lines in heatmaps indicate missing data.

Table S3.1. Normalized counts of *Tbx5* exons in control and cKO genital tubercles

DESeq2 was used to calculate normalized counts of each exon using the median-of-ratios method (Love et al., 2014). Asterisk indicates $p < 0.05$ (one-tailed t -test).

	Exon 1	Exon 2	Exon 3*	Exon 4	Exon 5	Exon 6	Exon 7*	Exon 8	Exon 9
ctrl_1	293.81	330.01	39.31	132.42	227.60	173.80	38.28	467.61	4109.14
ctrl_2	335.20	356.59	37.70	138.56	213.95	176.26	39.73	469.68	4534.81
ctrl_3	313.61	333.81	43.95	161.56	148.49	165.12	41.58	468.04	4403.63
ctrl_4	216.00	231.18	32.69	80.56	147.12	133.11	19.85	324.59	3004.21
ctrl_5	303.72	354.14	34.01	180.59	228.67	177.07	29.32	489.00	4474.84
KO_1	264.10	307.72	2.38	72.96	157.03	129.27	50.76	453.65	3645.86
KO_2	406.71	469.51	3.99	172.45	235.25	244.22	47.85	638.97	5812.51
KO_3	228.51	416.55	0.75	64.43	215.02	166.32	47.95	531.93	4026.19

Table S3.2. Differentially expressed genes in embryonic genitalia of *Tbx5* cKO mice

One triangle next to the gene name indicates the gene is associated with TBX5 binding site(s) in mouse only, while two triangles indicate ancient TBX5 binding in both mouse and brown anole.

	Gene	baseMean	log2FoldChange	lfcSE	stat	pvalue	padj
▶	Slc5a11	234.48	-2.37796	0.37559	-6.33122	2.43236E-10	4.49427E-06
	Gm14434	1163.31	-0.92692	0.15942	-5.81430	6.08895E-09	5.62528E-05
▶	Ntrk3	123.03	-2.46721	0.45732	-5.39499	6.85269E-08	0.000422057
	RP23-323L3.4	18.60	-6.63587	1.31312	-5.05351	4.33761E-07	0.002003651
▶▶	Glis3	472.84	-1.30668	0.26402	-4.94924	7.4505E-07	0.002753256
	Gm8898	821.57	-0.81086	0.16766	-4.83626	1.32306E-06	0.00407437
	Gm14306	474.80	-0.89897	0.18821	-4.77652	1.78352E-06	0.004707727
	Gm2026	1265.45	-0.78307	0.16581	-4.72256	2.32893E-06	0.005378961
▶	Asah2	259.53	-0.68497	0.14590	-4.69471	2.66989E-06	0.005481284
	Gm4631	1502.25	-0.68681	0.14856	-4.62314	3.77974E-06	0.006555969
▶	Bche	398.67	-0.77176	0.16830	-4.58561	4.52655E-06	0.006555969
▶	Kbtbd8	936.24	-1.49371	0.32457	-4.60207	4.18306E-06	0.006555969
▶▶	Hand2	1977.62	0.80218	0.17508	4.58168	4.61263E-06	0.006555969
	Gm11007	708.26	-0.60349	0.13323	-4.52954	5.91111E-06	0.007801397
	Med21	753.50	-0.65846	0.14650	-4.49455	6.97166E-06	0.008587691
	Cav1	826.85	-0.70016	0.15662	-4.47053	7.80261E-06	0.00901055
	Gm8923	456.68	-0.94090	0.21177	-4.44296	8.87286E-06	0.009643756
▶	Tmem45a	311.84	-0.70280	0.15939	-4.40931	1.03701E-05	0.010644957
▶	Rgs2	1057.99	-0.51946	0.11911	-4.36133	1.29277E-05	0.011943255
▶	Kras	2474.95	-0.79161	0.18128	-4.36666	1.26159E-05	0.011943255
▶	Grem2	262.44	-1.21473	0.28791	-4.21906	2.45326E-05	0.019937037
▶	Pkia	758.55	-0.72916	0.17268	-4.22247	2.41636E-05	0.019937037
▶▶	Eya4	1464.41	-0.73262	0.17408	-4.20843	2.57147E-05	0.019937037
▶▶	Ebf1	130.41	-1.02637	0.24398	-4.20684	2.58965E-05	0.019937037
	Gm14288	759.24	-0.59439	0.14179	-4.19211	2.76374E-05	0.020148904
	Gm1980	80.34	-1.36602	0.32688	-4.17901	2.92776E-05	0.020148904
▶	Dok1	666.34	0.57681	0.13834	4.16945	3.05336E-05	0.020148904
	RP23-143B2.1	16.59	-3.84060	0.92084	-4.17077	3.03572E-05	0.020148904
▶	Pappa	454.28	-0.78522	0.18979	-4.13731	3.51408E-05	0.021641098
	Gm13139	823.43	-1.09646	0.26534	-4.13228	3.59188E-05	0.021641098
▶	Clec14a	305.15	-0.62336	0.15094	-4.12980	3.63086E-05	0.021641098
▶	Otor	145.66	-1.13087	0.27748	-4.07542	4.59318E-05	0.024248048
	Gm14416	143.63	-1.05104	0.25768	-4.07892	4.52455E-05	0.024248048
▶	Fat3	3368.44	-1.19500	0.29260	-4.08409	4.42498E-05	0.024248048

▶	Ryr2	122.74	-1.76238	0.43061	-4.09273	4.26323E-05	0.024248048
	Nt5c	779.26	0.46593	0.11480	4.05864	4.93602E-05	0.025334105
▶	Tmed5	560.25	-0.67399	0.16714	-4.03243	5.52022E-05	0.0275668
	Gm9299	605.52	-0.58163	0.14479	-4.01695	5.89568E-05	0.027872614
▶	Adam7	14.00	-2.82157	0.70285	-4.01449	5.95751E-05	0.027872614
▶▶	Emc2	1036.51	-0.36680	0.09144	-4.01148	6.03401E-05	0.027872614
	Gm4245	657.43	-0.61068	0.15270	-3.99920	6.3558E-05	0.028642959
▶	Klhl42	670.50	-0.95669	0.24000	-3.98615	6.71536E-05	0.029542773
▶	Stc1	197.47	-0.82966	0.20848	-3.97965	6.90164E-05	0.02965618
	Znf41-ps	705.24	-1.19128	0.30251	-3.93793	8.21862E-05	0.034512583
	Sh3bgrl	4448.36	-0.83777	0.21370	-3.92029	8.8442E-05	0.03631429
▶	Ankrd44	2609.91	-0.61979	0.15935	-3.88946	0.000100468	0.036399135
▶	Snx16	262.13	-0.51079	0.13069	-3.90843	9.28972E-05	0.036399135
▶▶	Lhfp	1382.13	-0.70159	0.18028	-3.89169	9.95474E-05	0.036399135
	Sema4f	1226.26	0.39420	0.10121	3.89486	9.82569E-05	0.036399135
▶	Abca5	703.16	-0.88439	0.22660	-3.90289	9.5051E-05	0.036399135
	mt-Rnr2	6516.68	-0.80499	0.20614	-3.90496	9.42418E-05	0.036399135
	Gm14410	1002.62	-0.77799	0.20071	-3.87617	0.000106115	0.037657983
▶▶	Sfrp2	4560.31	-0.39226	0.10131	-3.87183	0.000108019	0.037657983
	Tmem169	254.88	-0.99478	0.25725	-3.86695	0.000110204	0.037708244
	Gm15421	1172.39	-0.61575	0.15966	-3.85666	0.000114946	0.038615571
▶	Ppm1e	777.79	-0.76721	0.19997	-3.83664	0.00012473	0.041154169
	Gm4723	570.90	-1.06422	0.27862	-3.81957	0.000133686	0.043278734
	Serpib9	86.25	-0.86009	0.22566	-3.81138	0.000138196	0.043278734
▶	Lpar4	622.17	-0.99291	0.26023	-3.81559	0.000135859	0.043278734
▶▶	Gsc	120.86	1.48019	0.39030	3.79243	0.000149178	0.045939466
	1110001J03Rik	422.68	0.51103	0.13545	3.77292	0.00016135	0.048873171
	Gm29485	152.66	0.88178	0.23498	3.75266	0.000174971	0.049514596
	Gm4724	1209.94	-0.94352	0.25256	-3.73587	0.000187066	0.049514596
▶	Lrrc7	25.19	-1.61563	0.43069	-3.75127	0.000175942	0.049514596
▶	Cxcl12	6708.23	-0.55442	0.14740	-3.76140	0.000168963	0.049514596
▶	Vat1l	875.51	-0.45243	0.12096	-3.74019	0.000183882	0.049514596
▶	Sesn3	6569.92	-0.38550	0.10297	-3.74365	0.000181363	0.049514596
▶	Aph1b	848.39	-0.52504	0.13947	-3.76461	0.000166809	0.049514596
▶	Ptprq	51.14	-2.18446	0.58484	-3.73517	0.000187586	0.049514596
	Fgf8	40.80	1.65509	0.44282	3.73757	0.000185808	0.049514596

Upregulated Downregulated

Table S3.3. Sample of peaks from TBX5 ChIP-seq in external genitalia

Mouse (mm10) TBX5 peaks

Chr	Start	End	Peak name	Fold enrichment	-log10qvalue	Summit
chr5	20133921	20134439	mm10_GT_peak_1	338.01	4.38922	20134125
chr17	83889852	83890290	mm10_GT_peak_2	336.09	4.38922	83890062
chr13	102433206	102433717	mm10_GT_peak_3	335.10	4.38922	102433488
chr13	54837536	54838111	mm10_GT_peak_4	334.27	4.38922	54837745
chr13	51258837	51259473	mm10_GT_peak_5	334.26	4.38922	51259268
chr2	74380597	74381320	mm10_GT_peak_6	326.20	4.38922	74381066
chr6	61216452	61217068	mm10_GT_peak_7	313.65	4.38922	61216729
chr6	122290353	122290869	mm10_GT_peak_8	310.51	4.38922	122290577
chr4	26888483	26889042	mm10_GT_peak_9	310.28	4.38922	26888747
chr11	115259196	115259619	mm10_GT_peak_10	299.09	4.38922	115259388
chr7	68918794	68919351	mm10_GT_peak_11	297.97	4.38922	68919128
chr15	31819214	31819772	mm10_GT_peak_12	297.47	4.38922	31819431
chr4	114716680	114717058	mm10_GT_peak_13	297.21	4.38922	114716866
chr12	31701155	31701756	mm10_GT_peak_14	295.78	4.38922	31701396
chr1	73363473	73364060	mm10_GT_peak_15	295.55	4.38922	73363790
chr6	61215658	61216203	mm10_GT_peak_16	293.77	4.38922	61215916
chr16	66996105	66996787	mm10_GT_peak_17	293.56	4.38922	66996379
chr8	91713822	91714275	mm10_GT_peak_18	292.54	4.38922	91714051
chr12	31026229	31026945	mm10_GT_peak_19	292.02	4.38922	31026615
chr11	53250810	53251234	mm10_GT_peak_20	284.69	4.38922	53251022
chr6	65542943	65543345	mm10_GT_peak_21	278.77	4.38922	65543153
chr19	52355002	52355669	mm10_GT_peak_22	277.56	4.38922	52355373
chr5	118818247	118818757	mm10_GT_peak_23	277.56	4.38922	118818497
chr9	17321100	17321818	mm10_GT_peak_24	277.31	4.38922	17321552
chr10	45229818	45230478	mm10_GT_peak_25	277.15	4.38922	45230165
chr6	16702981	16703854	mm10_GT_peak_26	275.89	4.38922	16703383
chr15	84809507	84809900	mm10_GT_peak_27	275.55	4.38922	84809718
chr5	14228745	14229197	mm10_GT_peak_28	274.93	4.38922	14228949
chr14	60856489	60857005	mm10_GT_peak_29	274.92	4.38922	60856695
chr18	51494262	51494663	mm10_GT_peak_30	272.90	4.38922	51494462
chr2	68442046	68442459	mm10_GT_peak_31	272.73	4.38922	68442262
chr2	128293160	128293562	mm10_GT_peak_32	272.57	4.38922	128293383
chr6	6436436	6436917	mm10_GT_peak_33	270.74	4.38922	6436630
chr12	82848286	82848799	mm10_GT_peak_34	270.64	4.38922	82848464
chr10	122231932	122232691	mm10_GT_peak_35	270.62	4.38922	122232371

Brown anole TBX5 peaks (AnoSag2.0 Liftover to mm10)

Chr	Start	End	Peak name
chr1	6510473	6510578	AnoSag_HP_peak_7082
chr1	6825844	6826344	AnoSag_HP_peak_4376,AnoSag_HP_peak_6745
chr1	7177765	7177842	AnoSag_HP_peak_7238
chr1	7178527	7178589	AnoSag_HP_peak_9229
chr1	10037771	10037812	AnoSag_HP_peak_9303
chr1	10504605	10504670	AnoSag_HP_peak_1369
chr1	10506074	10506144	AnoSag_HP_peak_1369
chr1	10512674	10512720	AnoSag_HP_peak_2617
chr1	11253911	11254232	AnoSag_HP_peak_7967
chr1	12693422	12693624	AnoSag_HP_peak_4886
chr1	12776140	12776504	AnoSag_HP_peak_8688
chr1	13244586	13244920	AnoSag_HP_peak_6424
chr1	13623675	13623727	AnoSag_HP_peak_3977
chr1	13715530	13715748	AnoSag_HP_peak_1099
chr1	13789383	13789615	AnoSag_HP_peak_7984
chr1	13861425	13861571	AnoSag_HP_peak_2405
chr1	14136778	14137123	AnoSag_HP_peak_2674
chr1	14256791	14257011	AnoSag_HP_peak_4216
chr1	14305398	14305714	AnoSag_HP_peak_327
chr1	14306373	14306733	AnoSag_HP_peak_3226
chr1	14774598	14774639	AnoSag_HP_peak_2717
chr1	14842531	14842729	AnoSag_HP_peak_9839
chr1	16229735	16230099	AnoSag_HP_peak_7709
chr1	16248926	16249246	AnoSag_HP_peak_4850
chr1	16294140	16294324	AnoSag_HP_peak_1768,AnoSag_HP_peak_4433
chr1	16375218	16375287	AnoSag_HP_peak_277
chr1	16399282	16399330	AnoSag_HP_peak_5925
chr1	17718120	17718399	AnoSag_HP_peak_11008
chr1	17761062	17761114	AnoSag_HP_peak_8016
chr1	17925333	17925591	AnoSag_HP_peak_12137
chr1	19231722	19232062	AnoSag_HP_peak_11262
chr1	19250965	19251156	AnoSag_HP_peak_8630
chr1	20134992	20135405	AnoSag_HP_peak_7649
chr1	22612904	22613189	AnoSag_HP_peak_4765
chr1	23995654	23995712	AnoSag_HP_peak_7471

Table S3.4. Coordinates of binding at validated appendage enhancers

All coordinates are in mm10.

Gene associated with ISL1 binding site	Region shown in Figure	ISL1 ChIP-seq peak in mouse		Species with conserved ISL1 binding	Conserved sequence coordinates (shared among each species)	Genital-positive enhancer		H2K27ac coordinates (Infante et al. 2015)
		Peak Name	Coordinates			Name	Coordinates	
<i>Tbx5</i>	chr5:119,792,297-119,968,321	ISL1 ChIP-seq peak	chr5:119,963,230-119,963,749	Alligator, Chicken	chr5:119,963,339-119,963,724	GTE1	chr5:119,963,071-119,964,024	chr14:28,970,978-28,974,977

Gene associated with TBX5 binding site	Region shown in Figure	TBX5 ChIP-seq peak in mouse		Species with conserved TBX5 binding	Conserved sequence coordinates (shared among each species)	Published GT-positive enhancer		Capture-C interaction peak coordinates (Andrey et al. 2017)
		Peak Name	Coordinates			Name	Coordinates	
<i>Msx1</i>	chr5:37,967,479-37,969,292	mm10_GT_peak_2446	chr5:37967659-37967949	Brown anole	chr5:37967920-37968028	mm429	chr5:37967624-37969196	chr5:37967798-37968796
		mm10_GT_peak_11320	chr5:37968534-37969003	N/A				
<i>Prrx1</i>	chr1:163,896,934-163,900,211	mm10_GT_peak_142	chr1:163898068-163898693	N/A	N/A	hs1442	chr1:163897222-163899818	chr1:163897234-163899232
<i>Creb5</i>	chr6:53,468,130-53,472,529	mm10_GT_peak_1570	chr6:53469249-53469611	Brown anole	chr6:53469245-53469379	hs1604	chr6:53468300-53472380	N/A

Table S3.5. List of validated genital enhancers bound by TBX5 in the mouse genital tubercle

All coordinates are in mm10. GREAT was used to associate TBX5 peaks with neighboring genes.

VISTA Element	Peak name	Chr	Start	End	Gene(s) associated with TBX5 binding site
hs1442	mm10_GT_peak_142	chr1	163898068	163898693	Scyl3, Kifap3
hs1681	mm10_GT_peak_9055	chr3	5387828	5388297	Zfhx4, Pex2
mm426	mm10_GT_peak_19605	chr5	37825695	37826164	Msx1
mm428	mm10_GT_peak_1242	chr5	37917832	37918288	Msx1, Stx18
mm429	mm10_GT_peak_2446	chr5	37967659	37967949	Msx1, Stx18
	mm10_GT_peak_11320	chr5	37968534	37969003	
hs1604	mm10_GT_peak_1570	chr6	53469249	53469611	Msx1, Stx18
hs906	mm10_GT_peak_6938	chr8	80315011	80315140	Hhip, Gypa
mm569	mm10_GT_peak_2644	chr10	120551903	120552145	Hmga2, Msrb3
hs205	mm10_GT_peak_790	chr11	19350337	19350735	Spred2, Meis1
mm1906	mm10_GT_peak_10605	chr13	15504766	15504971	Inhba, Gli3

CHAPTER 4

CONCLUSIONS AND FUTURE DIRECTIONS

In this dissertation, I expand our understanding of how TBX5 governs appendage formation by investigating the gene regulatory networks underlying forelimb and phallus development. While decades of functional studies have demonstrated the crucial role of *Tbx5* in forelimb outgrowth and morphology across vertebrates, the direct regulatory targets of TBX5 have remained largely unexplored. My combined CHIP-seq and RNA-seq analyses suggest that *Tbx5* directly regulates key components of the Hedgehog, Wnt, and BMP signaling pathways during early patterning of the forelimb. These include genes with known roles in limb development such as *Wnt5a*, *Hoxa13*, *Twist1*, *Hand2*, *Ptch1*, *Epha4*, and *Fgf10*. Furthermore, many of the TBX5 binding sites I identify overlap with functionally validated enhancers active in limbs.

The TBX5 CHIP-seq datasets I have generated in embryonic forelimbs of five diverse amniote species identify thousands of putative enhancers that limb researchers can investigate further. While I was able to capitalize on published chromatin interaction, histone mark profile, and validated enhancer datasets to narrow down interesting candidates, comparing my data with other limb resources can further reveal loci to focus efforts toward. For example, a recent study used ATAC-seq in mouse forelimb and chick wing buds to identify conserved and species-specific profiles of chromatin accessibility (Jhanwar et al., 2021). Another large study used over 50

published limb-specific datasets to train a machine-learning framework to predict active enhancers in developing limbs (Limb-Enhancer Genie) (Monti et al., 2017).

Comparisons of my ChIP-seq data to other datasets will also be necessary to further characterize the role of TBX5 in forelimb development. While my datasets were generated at E10.5 (and comparable stages in other species), it would be valuable to explore TBX5 occupancy at other stages of growth. In addition to the work I have reported in this dissertation, I have generated two TBX5 ChIP-seq replicates in E9.75 forelimbs, which is shortly after forelimb bud initiation. Other labs have compared TBX5 binding in the forelimb to TBX4 and PITX1 binding in the hindlimb (Jain et al., 2018; Nemec et al., 2017). Additional genomic-occupancy comparisons of TBX5 to ISL1, a key regulator of hindlimb initiation (Kawakami et al., 2011; Narkis et al., 2012), can shed light on the regulatory interactions necessary during limb budding. Our lab has previously reported ISL1 ChIP-seq data in several species of amniotes (Minchey, 2022) that can be compared with my TBX5 datasets.

While I report the top enriched motifs found in my various TBX5 ChIP-seq datasets, additional analyses need to be done at specific loci to understand how TBX5 interacts with enhancers it binds to. One approach is to look for evolutionarily conserved enhancers bound by TBX5 that contain DNA binding motifs of interest. Finding changes of motif sequences in limb-reduced or limbless species (such as snakes or leg-reduced lizards) can give hints to the role of an enhancer in the evolution of limb development.

Another interesting avenue to explore is how TBX5 binding in forelimbs has changed in closely related species. *Anolis* lizards are well known for their striking patterns of convergent evolution on different Caribbean islands. The relative forelimb length of *Anolis sagrei*, a trunk-ground anole, is more than 10% larger than *Anolis carolinensis*, a trunk-crown anole. Very little is known about the underlying mechanisms that have contributed to the evolution of different phenotypes in this genus. The TBX5 CHIP-seq datasets I performed in brown anole and green anole forelimbs will enable comparative studies of TBX5 targets in closely related anole species. Furthermore, the data I have generated in turtles and alligators will also act as resources for researchers to understand the role of gene regulation in forelimb growth of reptiles.

By generating mice with *Tbx5*-depleted genitalia and using light sheet and scanning electron microscopy, I discover a novel role of *Tbx5* in the genital tubercle. These *Tbx5* mutant mice exhibit urethral hypoplasia and reduced preputial swellings. While *Tbx5* plays a central role in the initiation and patterning of the forelimb, we find that – overall – the gene has a more subtle effect on genital tubercle morphology. This further supports the suggestion that unique molecular mechanisms regulate the morphological development of the limb and phallus despite parallels in the gene expression patterns of these appendage types.

I further characterize the mechanisms underlying the role of TBX5 in developing genitalia by using CHIP-seq and RNA-seq. Ancient direct targets of TBX5 include *Hand2*, *Glis3*, and *Eya4*. We also describe a new enhancer of *Tbx5* that has genital-specific

activity, GTE1. Further knockout experiments of GTE1 need to be done to reveal its role in genital development and give stronger evidence that it regulates *Tbx5* expression in the GT.

Additional histological assays in *Tbx5* mutant GTs need to be completed to determine any effects on the development of internal structures such as the urethral epithelium, preputial glands, and mesenchymal swellings (urethral folds). Furthermore, more studies are needed to determine any sex-specific effects of *Tbx5* deletion in the GT. Interestingly, *Tbx5* is expressed at E18.5 in the urethral plate epithelium of male but not female mice (Douglas et al., 2012). Along with observing sex-specific structures such as the prostate gland, changes in the anogenital (perineum) length or size of the bulbourethral glands and labioscrotal swellings can also be assessed between males and females. Because the *Tbx5* conditional mutants we generated die perinatally, it is not possible to study external genital phenotypes postnatally and at adulthood when more distinct features can be examined. Therefore, the use of various Cre driver mouse lines expressed in the GT (Hashimoto et al., 2018) will be needed to further characterize the role of *Tbx5* in regulating external genital growth and patterning.

Using TBX5 ChIP-seq in developing mouse forelimbs and GTs, I have identified thousands of candidate binding sites in each of these appendage types. Roughly 32% of forelimb TBX5 binding sites are shared with the GT and are significantly enriched close to genes involved in limb development. More studies will need to be done to explore forelimb-specific, genital-specific, and limb-genital regulatory elements. Global

comparisons of motif sequences and transcription factor co-occupancy can give insight into the distinct and shared roles of TBX5 in these appendage types. While knockout experiments in mice can be useful to test putative enhancers, our lab's established method of CRISPR-Cas9-mediated genome editing in *Anolis* lizards enables the exploration of enhancer function in lizards (Rasys et al., 2019).

My RNA-seq experiments have characterized the global gene expression patterns of the developing forelimbs and external genitalia. However, it is possible that my bulk RNA-seq data are not providing enough resolution of expression profiles in these tissues. Recent innovations in single-cell transcriptomics have provided unparalleled insight into the gene expression patterns of cell populations in the developing limbs (Feregrino et al., 2019; He et al., 2020; Kelly et al., 2019; Markman et al., 2023) and external genitalia (Amato & Yao, 2021; Armfield & Cohn, 2021). Single-cell analyses of *Tbx5*-depleted embryos could reveal rare cell populations that are perturbed in appendages. Furthermore, *in situ* hybridization assays need to be performed to assess the effects of *Tbx5* deletion on spatial gene expression patterns. Spatial transcriptomic technologies are also becoming an essential tool to measure gene activity along with its cellular map within a tissue (Williams et al., 2022). A recent study has developed a new method called TATTOO-seq to spatially resolve single-cell gene expression profiles in the developing mouse forelimb (Bastide et al., 2022). Utilizing these cutting-edge technologies in combination with published datasets will enable further studies of the role of gene regulation in development and evolution.

In conclusion, my studies have shed light on the role of *Tbx5* in the gene regulatory networks orchestrating forelimb and genital development. Overall, the genomic and transcriptomic datasets I have generated serve as foundational resources to form testable hypotheses of the mechanisms underlying the growth of appendages.

REFERENCES

- Agarwal, P., Wylie, J. N., Galceran, J., Arkhitko, O., Li, C., Deng, C., Grosschedl, R., & Bruneau, B. G. (2003). Tbx5 is essential for forelimb bud initiation following patterning of the limb field in the mouse embryo. *Development*, *130*(3), 623–633. <https://doi.org/10.1242/dev.00191>
- Ahn, D.-G., Kourakis, M. J., Rohde, L. A., Silver, L. M., & Ho, R. K. (2002). T-box gene tbx5 is essential for formation of the pectoral limb bud. *Nature*, *417*(6890), 754–758. <https://doi.org/10.1038/nature00814>
- Alghamdi, K. A., Alsaedi, A. B., Aljasser, A., Altawil, A., & Kamal, N. M. (2017). Extended clinical features associated with novel Glis3 mutation: a case report. *BMC Endocrine Disorders*, *17*(1), 14. <https://doi.org/10.1186/s12902-017-0160-z>
- Amândio, A. R., Lopez-Delisle, L., Bolt, C. C., Mascrez, B., & Duboule, D. (2020). A complex regulatory landscape involved in the development of mammalian external genitals. *ELife*, *9*. <https://doi.org/10.7554/eLife.52962>
- Amato, C. M., & Yao, H. H.-C. (2021). Developmental and sexual dimorphic atlas of the prenatal mouse external genitalia at the single-cell level. *Proceedings of the National Academy of Sciences of the United States of America*, *118*(25). <https://doi.org/10.1073/pnas.2103856118>
- Andrey, G., Schöpflin, R., Jerković, I., Heinrich, V., Ibrahim, D. M., Paliou, C., Hochradel, M., Timmermann, B., Haas, S., Vingron, M., & Mundlos, S. (2017). Characterization of hundreds of regulatory landscapes in developing limbs reveals two regimes of chromatin folding. *Genome Research*, *27*(2), 223–233. <https://doi.org/10.1101/gr.213066.116>
- Armfield, B. A., & Cohn, M. J. (2021). Single cell transcriptomic analysis of external genitalia reveals complex and sexually dimorphic cell populations in the early genital tubercle. *Developmental Biology*. <https://doi.org/10.1016/j.ydbio.2021.05.014>
- Arnolds, D. E., Liu, F., Fahrenbach, J. P., Kim, G. H., Schillinger, K. J., Smemo, S., McNally, E. M., Nobrega, M. A., Patel, V. V., & Moskowitz, I. P. (2012). TBX5 drives Scn5a expression to regulate cardiac conduction system function. *The Journal of Clinical Investigation*, *122*(7), 2509–2518. <https://doi.org/10.1172/JCI62617>

- Arora, R., Metzger, R. J., & Papaioannou, V. E. (2012). Multiple roles and interactions of Tbx4 and Tbx5 in development of the respiratory system. *PLoS Genetics*, *8*(8), e1002866. <https://doi.org/10.1371/journal.pgen.1002866>
- Barrow, J. R., Thomas, K. R., Boussadia-Zahui, O., Moore, R., Kemler, R., Capecchi, M. R., & McMahon, A. P. (2003). Ectodermal Wnt3/ β -catenin signaling is required for the establishment and maintenance of the apical ectodermal ridge. *Genes & Development*, *17*(3), 394–409. <https://doi.org/10.1101/gad.1044903>
- Basson, C. T., Bachinsky, D. R., Lin, R. C., Levi, T., Elkins, J. A., Soultz, J., Grayzel, D., Kroumpouzou, E., Traill, T. A., Leblanc-Straceski, J., Renault, B., Kucherlapati, R., Seidman, J. G., & Seidman, C. E. (1997). Mutations in human TBX5 [corrected] cause limb and cardiac malformation in Holt-Oram syndrome. *Nature Genetics*, *15*(1), 30–35. <https://doi.org/10.1038/ng0197-30>
- Bastide, S., Chomsky, E., Saudemont, B., Loe-Mie, Y., Schmutz, S., Novault, S., Marlow, H., Tanay, A., & Spitz, F. (2022). TATTOO-seq delineates spatial and cell type-specific regulatory programs in the developing limb. *Science Advances*, *8*(50), eadd0695. <https://doi.org/10.1126/sciadv.add0695>
- Bensoussan-Trigano, V., Lallemand, Y., Saint Cloment, C., & Robert, B. (2011). Msx1 and Msx2 in limb mesenchyme modulate digit number and identity. *Developmental Dynamics: An Official Publication of the American Association of Anatomists*, *240*(5), 1190–1202. <https://doi.org/10.1002/dvdy.22619>
- Bickley, S. R. B., & Logan, M. P. O. (2014). Regulatory modulation of the T-box gene Tbx5 links development, evolution, and adaptation of the sternum. *Proceedings of the National Academy of Sciences of the United States of America*, *111*(50), 17917–17922. <https://doi.org/10.1073/pnas.1409913111>
- Boulet, A. M., & Capecchi, M. R. (2004). Multiple roles of Hoxa11 and Hoxd11 in the formation of the mammalian forelimb zeugopod. *Development*, *131*(2), 299–309. <https://doi.org/10.1242/dev.00936>
- Bronson, F. H., & Caroom, D. (1971). Preputial gland of the male mouse; attractant function. *Journal of Reproduction and Fertility*, *25*(2), 279–282. <https://doi.org/10.1530/jrf.0.0250279>
- Bruneau, B. G., Logan, M., Davis, N., Levi, T., Tabin, C. J., Seidman, J. G., & Seidman, C. E. (1999). Chamber-specific cardiac expression of Tbx5 and heart defects in Holt-Oram syndrome. *Developmental Biology*, *211*(1), 100–108. <https://doi.org/10.1006/dbio.1999.9298>

- Bruneau, B. G., Nemer, G., Schmitt, J. P., Charron, F., Robitaille, L., Caron, S., Conner, D. A., Gessler, M., Nemer, M., Seidman, C. E., & Seidman, J. G. (2001). A murine model of Holt-Oram syndrome defines roles of the T-box transcription factor Tbx5 in cardiogenesis and disease. *Cell*, *106*(6), 709–721. [https://doi.org/10.1016/S0092-8674\(01\)00493-7](https://doi.org/10.1016/S0092-8674(01)00493-7)
- Buenrostro, J. D., Wu, B., Chang, H. Y., & Greenleaf, W. J. (2015). ATAC-seq: A Method for Assaying Chromatin Accessibility Genome-Wide. *Current Protocols in Molecular Biology / Edited by Frederick M. Ausubel ... [et Al.]*, *109*, 21.29.1-21.29.9. <https://doi.org/10.1002/0471142727.mb2129s109>
- Burke, A. C., Nelson, C. E., Morgan, B. A., & Tabin, C. (1995). Hox genes and the evolution of vertebrate axial morphology. *Development*, *121*(2), 333–346. <https://doi.org/10.1242/dev.121.2.333>
- Butterfield, N. C., Metzis, V., McGlinn, E., Bruce, S. J., Wainwright, B. J., & Wicking, C. (2009). Patched 1 is a crucial determinant of asymmetry and digit number in the vertebrate limb. *Development*, *136*(20), 3515–3524. <https://doi.org/10.1242/dev.037507>
- Chan, M. M. Y., Sadeghi-Alavijeh, O., Lopes, F. M., Hilger, A. C., Stanescu, H. C., Voinescu, C. D., Beaman, G. M., Newman, W. G., Zaniew, M., Weber, S., Ho, Y. M., Connolly, J. O., Wood, D., Maj, C., Stuckey, A., Kousathanas, A., Genomics England Research Consortium, Kleta, R., Woolf, A. S., ... Gale, D. P. (2022). Diverse ancestry whole-genome sequencing association study identifies TBX5 and PTK7 as susceptibility genes for posterior urethral valves. *ELife*, *11*. <https://doi.org/10.7554/eLife.74777>
- Chapman, D. L., Garvey, N., Hancock, S., Alexiou, M., Agulnik, S. I., Gibson-Brown, J. J., Cebra-Thomas, J., Bollag, R. J., Silver, L. M., & Papaioannou, V. E. (1996). Expression of the T-box family genes, Tbx1-Tbx5, during early mouse development. *Developmental Dynamics: An Official Publication of the American Association of Anatomists*, *206*(4), 379–390. [https://doi.org/10.1002/\(SICI\)1097-0177\(199608\)206:4<379::AID-AJA4>3.0.CO;2-F](https://doi.org/10.1002/(SICI)1097-0177(199608)206:4<379::AID-AJA4>3.0.CO;2-F)
- Chen, H., Lun, Y., Ovchinnikov, D., Kokubo, H., Oberg, K. C., Pepicelli, C. V., Gan, L., Lee, B., & Johnson, R. L. (1998). Limb and kidney defects in Lmx1b mutant mice suggest an involvement of LMX1B in human nail patella syndrome. *Nature Genetics*, *19*(1), 51–55. <https://doi.org/10.1038/ng0598-51>
- Chew, K. Y., Shaw, G., Yu, H., Pask, A. J., & Renfree, M. B. (2014). Heterochrony in the regulation of the developing marsupial limb. *Developmental Dynamics: An Official Publication of the American Association of Anatomists*, *243*(2), 324–338. <https://doi.org/10.1002/dvdy.24062>

- Ching, S. T., Infante, C. R., Du, W., Sharir, A., Park, S., Menke, D. B., & Klein, O. D. (2018). Isl1 mediates mesenchymal expansion in the developing external genitalia via regulation of Bmp4, Fgf10 and Wnt5a. *Human Molecular Genetics*, 27(1), 107–119. <https://doi.org/10.1093/hmg/ddx388>
- Cohn, M. J., Patel, K., Krumlauf, R., Wilkinson, D. G., Clarke, J. D., & Tickle, C. (1997). Hox9 genes and vertebrate limb specification. *Nature*, 387(6628), 97–101. <https://doi.org/10.1038/387097a0>
- Cohn, Martin J. (2011). Development of the external genitalia: conserved and divergent mechanisms of appendage patterning. *Developmental Dynamics: An Official Publication of the American Association of Anatomists*, 240(5), 1108–1115. <https://doi.org/10.1002/dvdy.22631>
- Collas, P. (2010). The current state of chromatin immunoprecipitation. *Molecular Biotechnology*, 45(1), 87–100. <https://doi.org/10.1007/s12033-009-9239-8>
- Conlon, F. L., Fairclough, L., Price, B. M., Casey, E. S., & Smith, J. C. (2001). Determinants of T box protein specificity. *Development*, 128(19), 3749–3758. <https://doi.org/10.1242/dev.128.19.3749>
- Cooper, K. L., Sears, K. E., Uygur, A., Maier, J., Baczkowski, K.-S., Brosnahan, M., Antczak, D., Skidmore, J. A., & Tabin, C. J. (2014). Patterning and post-patterning modes of evolutionary digit loss in mammals. *Nature*, 511(7507), 41–45. <https://doi.org/10.1038/nature13496>
- Cotney, J., Leng, J., Oh, S., DeMare, L. E., Reilly, S. K., Gerstein, M. B., & Noonan, J. P. (2012). Chromatin state signatures associated with tissue-specific gene expression and enhancer activity in the embryonic limb. *Genome Research*, 22(6), 1069–1080. <https://doi.org/10.1101/gr.129817.111>
- Cotney, J., Leng, J., Yin, J., Reilly, S. K., DeMare, L. E., Emera, D., Ayoub, A. E., Rakic, P., & Noonan, J. P. (2013). The evolution of lineage-specific regulatory activities in the human embryonic limb. *Cell*, 154(1), 185–196. <https://doi.org/10.1016/j.cell.2013.05.056>
- Crawford, G. E., Holt, I. E., Whittle, J., Webb, B. D., Tai, D., Davis, S., Margulies, E. H., Chen, Y., Bernat, J. A., Ginsburg, D., Zhou, D., Luo, S., Vasicek, T. J., Daly, M. J., Wolfsberg, T. G., & Collins, F. S. (2006). Genome-wide mapping of DNase hypersensitive sites using massively parallel signature sequencing (MPSS). *Genome Research*, 16(1), 123–131. <https://doi.org/10.1101/gr.4074106>
- Creyghton, M. P., Cheng, A. W., Welstead, G. G., Kooistra, T., Carey, B. W., Steine, E. J., Hanna, J., Lodato, M. A., Frampton, G. M., Sharp, P. A., Boyer, L. A., Young, R. A.,

- & Jaenisch, R. (2010). Histone H3K27ac separates active from poised enhancers and predicts developmental state. *Proceedings of the National Academy of Sciences of the United States of America*, *107*(50), 21931–21936. <https://doi.org/10.1073/pnas.1016071107>
- Cunha, G. R. (1975). Hormonal influences on the morphogenesis of the preputial gland of embryonic mice. *The Anatomical Record*, *181*(1), 35–53. <https://doi.org/10.1002/ar.1091810104>
- Cunha, Gerald R., Liu, G., Sinclair, A., Cao, M., Glickman, S., Cooke, P. S., & Baskin, L. (2019). Androgen-independent events in penile development in humans and animals. *Differentiation; Research in Biological Diversity*, *111*, 98–114. <https://doi.org/10.1016/j.diff.2019.07.005>
- Cunha, Gerald R., Risbridger, G., Wang, H., Place, N. J., Grumbach, M., Cunha, T. J., Weldele, M., Conley, A. J., Barcellos, D., Agarwal, S., Bhargava, A., Drea, C., Hammond, G. L., Siiteri, P., Coscia, E. M., McPhaul, M. J., Baskin, L. S., & Glickman, S. E. (2014). Development of the external genitalia: perspectives from the spotted hyena (*Crocuta crocuta*). *Differentiation; Research in Biological Diversity*, *87*(1–2), 4–22. <https://doi.org/10.1016/j.diff.2013.12.003>
- Davis, A. P., Witte, D. P., Hsieh-Li, H. M., Potter, S. S., & Capecchi, M. R. (1995). Absence of radius and ulna in mice lacking *hoxa-11* and *hoxd-11*. *Nature*, *375*(6534), 791–795. <https://doi.org/10.1038/375791a0>
- De Bono, C., Thellier, C., Bertrand, N., Sturny, R., Jullian, E., Cortes, C., Stefanovic, S., Zaffran, S., Théveniau-Ruissy, M., & Kelly, R. G. (2018). T-box genes and retinoic acid signaling regulate the segregation of arterial and venous pole progenitor cells in the murine second heart field. *Human Molecular Genetics*, *27*(21), 3747–3760. <https://doi.org/10.1093/hmg/ddy266>
- De Moerlooze, L., Spencer-Dene, B., Revest, J. M., Hajihosseini, M., Rosewell, I., & Dickson, C. (2000). An important role for the IIIb isoform of fibroblast growth factor receptor 2 (FGFR2) in mesenchymal-epithelial signalling during mouse organogenesis. *Development*, *127*(3), 483–492. <https://doi.org/10.1242/dev.127.3.483>
- Delgado, I., & Torres, M. (2017). Coordination of limb development by crosstalk among axial patterning pathways. *Developmental Biology*, *429*(2), 382–386. <https://doi.org/10.1016/j.ydbio.2017.03.006>
- Delsuc, F., Brinkmann, H., Chourrout, D., & Philippe, H. (2006). Tunicates and not cephalochordates are the closest living relatives of vertebrates. *Nature*,

439(7079), 965–968. <https://doi.org/10.1038/nature04336>

- Desanlis, I., Kherdjemil, Y., Mayran, A., Bouklouch, Y., Gentile, C., Sheth, R., Zeller, R., Drouin, J., & Kmita, M. (2020). HOX13-dependent chromatin accessibility underlies the transition towards the digit development program. *Nature Communications*, *11*(1), 2491. <https://doi.org/10.1038/s41467-020-16317-2>
- Domyan, E. T., Kronenberg, Z., Infante, C. R., Vickrey, A. I., Stringham, S. A., Bruders, R., Guernsey, M. W., Park, S., Payne, J., Beckstead, R. B., Kardon, G., Menke, D. B., Yandell, M., & Shapiro, M. D. (2016). Molecular shifts in limb identity underlie development of feathered feet in two domestic avian species. *ELife*, *5*, e12115. <https://doi.org/10.7554/eLife.12115>
- Domyan, E. T., & Shapiro, M. D. (2017). Pigeonetics takes flight: Evolution, development, and genetics of intraspecific variation. *Developmental Biology*, *427*(2), 241–250. <https://doi.org/10.1016/j.ydbio.2016.11.008>
- Douglas, N. C., Heng, K., Sauer, M. V., & Papaioannou, V. E. (2012). Dynamic expression of Tbx2 subfamily genes in development of the mouse reproductive system. *Developmental Dynamics: An Official Publication of the American Association of Anatomists*, *241*(2), 365–375. <https://doi.org/10.1002/dvdy.23710>
- Downes, D. J., Smith, A. L., Karpinska, M. A., Velychko, T., Rue-Albrecht, K., Sims, D., Milne, T. A., Davies, J. O. J., Oudelaar, A. M., & Hughes, J. R. (2022). Capture-C: a modular and flexible approach for high-resolution chromosome conformation capture. *Nature Protocols*, *17*(2), 445–475. <https://doi.org/10.1038/s41596-021-00651-w>
- Drescher, U. (1997). The Eph family in the patterning of neural development. *Current Biology: CB*, *7*(12), R799-807. [https://doi.org/10.1016/s0960-9822\(06\)00409-x](https://doi.org/10.1016/s0960-9822(06)00409-x)
- Duboc, V., & Logan, M. P. O. (2011). Regulation of limb bud initiation and limb-type morphology. *Developmental Dynamics: An Official Publication of the American Association of Anatomists*, *240*(5), 1017–1027. <https://doi.org/10.1002/dvdy.22582>
- Eckalbar, W. L., Schlebusch, S. A., Mason, M. K., Gill, Z., Parker, A. V., Booker, B. M., Nishizaki, S., Muswamba-Nday, C., Terhune, E., Nevonen, K. A., Makki, N., Friedrich, T., VanderMeer, J. E., Pollard, K. S., Carbone, L., Wall, J. D., Illing, N., & Ahituv, N. (2016). Transcriptomic and epigenomic characterization of the developing bat wing. *Nature Genetics*, *48*(5), 528–536. <https://doi.org/10.1038/ng.3537>

- Eckner, R., Ewen, M. E., Newsome, D., Gerdes, M., DeCaprio, J. A., Lawrence, J. B., & Livingston, D. M. (1994). Molecular cloning and functional analysis of the adenovirus E1A-associated 300-kD protein (p300) reveals a protein with properties of a transcriptional adaptor. *Genes & Development*, *8*(8), 869–884. <https://doi.org/10.1101/gad.8.8.869>
- Edgar, R., Domrachev, M., & Lash, A. E. (2002). Gene Expression Omnibus: NCBI gene expression and hybridization array data repository. *Nucleic Acids Research*, *30*(1), 207–210. <https://doi.org/10.1093/nar/30.1.207>
- Emrich, S. J., Barbazuk, W. B., Li, L., & Schnable, P. S. (2007). Gene discovery and annotation using LCM-454 transcriptome sequencing. *Genome Research*, *17*(1), 69–73. <https://doi.org/10.1101/gr.5145806>
- Evans, S. E. (2009). Evolution and Phylogeny of Amniotes. In M. D. Binder, N. Hirokawa, & U. Windhorst (Eds.), *Encyclopedia of Neuroscience* (pp. 1192–1194). Springer Berlin Heidelberg. https://doi.org/10.1007/978-3-540-29678-2_3113
- Feregrino, C., Sacher, F., Parnas, O., & Tschopp, P. (2019). A single-cell transcriptomic atlas of the developing chicken limb. *BMC Genomics*, *20*(1), 401. <https://doi.org/10.1186/s12864-019-5802-2>
- Ferguson, M. W. (1985). The reproductive biology and embryology of the crocodylians. *Biology of the Reptilia*, *14*, 330–491. http://seaturtle.org/library/FergusonMWJ_1985_InBiologyoftheReptilia_p329-491.pdf
- Fromental-Ramain, C., Warot, X., Messadecq, N., LeMeur, M., Dollé, P., & Chambon, P. (1996). Hoxa-13 and Hoxd-13 play a crucial role in the patterning of the limb autopod. *Development*, *122*(10), 2997–3011. <https://doi.org/10.1242/dev.122.10.2997>
- Galli, A., Robay, D., Osterwalder, M., Bao, X., Bénazet, J.-D., Tariq, M., Paro, R., Mackem, S., & Zeller, R. (2010). Distinct roles of Hand2 in initiating polarity and posterior Shh expression during the onset of mouse limb bud development. *PLoS Genetics*, *6*(4), e1000901. <https://doi.org/10.1371/journal.pgen.1000901>
- Ge, S. X., Jung, D., & Yao, R. (2020). ShinyGO: a graphical gene-set enrichment tool for animals and plants. *Bioinformatics*, *36*(8), 2628–2629. <https://doi.org/10.1093/bioinformatics/btz931>
- Geetha-Loganathan, P., Nimmagadda, S., & Scaal, M. (2008). Wnt signaling in limb organogenesis. *Organogenesis*, *4*(2), 109–115. <https://doi.org/10.4161/org.4.2.5857>

- Gene Ontology Consortium. (2021). The Gene Ontology resource: enriching a GOLD mine. *Nucleic Acids Research*, *49*(D1), D325–D334. <https://doi.org/10.1093/nar/gkaa1113>
- Georgas, K. M., Armstrong, J., Keast, J. R., Larkins, C. E., McHugh, K. M., Southard-Smith, E. M., Cohn, M. J., Batourina, E., Dan, H., Schneider, K., Buehler, D. P., Wiese, C. B., Brennan, J., Davies, J. A., Harding, S. D., Baldock, R. A., Little, M. H., Vezina, C. M., & Mendelsohn, C. (2015). An illustrated anatomical ontology of the developing mouse lower urogenital tract. *Development*, *142*(10), 1893–1908. <https://doi.org/10.1242/dev.117903>
- Gibson-Brown, J. J., I Agulnik S, Silver, L. M., & Papaioannou, V. E. (1998). Expression of T-box genes Tbx2-Tbx5 during chick organogenesis. *Mechanisms of Development*, *74*(1–2), 165–169. [https://doi.org/10.1016/s0925-4773\(98\)00056-2](https://doi.org/10.1016/s0925-4773(98)00056-2)
- Govers, L. C., Phillips, T. R., Mattiske, D. M., Rashoo, N., Black, J. R., Sinclair, A., Baskin, L. S., Risbridger, G. P., & Pask, A. J. (2019). A critical role for estrogen signaling in penis development. *FASEB Journal: Official Publication of the Federation of American Societies for Experimental Biology*, *33*(9), 10383–10392. <https://doi.org/10.1096/fj.201802586RR>
- Gredler, M. L. (2016). Developmental and Evolutionary Origins of the Amniote Phallus. *Integrative and Comparative Biology*, *56*(4), 694–704. <https://doi.org/10.1093/icb/icw102>
- Gredler, M. L., Larkins, C. E., Leal, F., Lewis, A. K., Herrera, A. M., Perriton, C. L., Sanger, T. J., & Cohn, M. J. (2014). Evolution of external genitalia: insights from reptilian development. *Sexual Development: Genetics, Molecular Biology, Evolution, Endocrinology, Embryology, and Pathology of Sex Determination and Differentiation*, *8*(5), 311–326. <https://doi.org/10.1159/000365771>
- Gredler, M. L., Sanger, T. J., & Cohn, M. J. (2015). Development of the cloaca, hemipenes, and hemiclitores in the green anole, *Anolis carolinensis*. *Sexual Development: Genetics, Molecular Biology, Evolution, Endocrinology, Embryology, and Pathology of Sex Determination and Differentiation*, *9*(1), 21–33. <https://doi.org/10.1159/000363757>
- Greenbaum, E. (2011). A standardized series of embryonic stages for the emydid turtle *Trachemys scripta*. *Canadian Journal of Zoology*. <https://doi.org/10.1139/z02-111>
- Gros, J., & Tabin, C. J. (2014). Vertebrate limb bud formation is initiated by localized epithelial-to-mesenchymal transition. *Science*, *343*(6176), 1253–1256.

<https://doi.org/10.1126/science.1248228>

- Halfon, M. S. (2019). Studying Transcriptional Enhancers: The Founder Fallacy, Validation Creep, and Other Biases. *Trends in Genetics: TIG*, 35(2), 93–103. <https://doi.org/10.1016/j.tig.2018.11.004>
- Haraguchi, R., Mo, R., Hui, C., Motoyama, J., Makino, S., Shiroishi, T., Gaffield, W., & Yamada, G. (2001). Unique functions of Sonic hedgehog signaling during external genitalia development. *Development*, 128(21), 4241–4250. <https://www.ncbi.nlm.nih.gov/pubmed/11684660>
- Haraguchi, R., Suzuki, K., Murakami, R., Sakai, M., Kamikawa, M., Kengaku, M., Sekine, K., Kawano, H., Kato, S., Ueno, N., & Yamada, G. (2000). Molecular analysis of external genitalia formation: the role of fibroblast growth factor (Fgf) genes during genital tubercle formation. *Development*, 127(11), 2471–2479. <https://doi.org/10.1242/dev.127.11.2471>
- Hashimoto, D., Hyuga, T., Acebedo, A. R., Alcantara, M. C., Suzuki, K., & Yamada, G. (2018). Developmental mutant mouse models for external genitalia formation. *Congenital Anomalies*. <https://doi.org/10.1111/cga.12319>
- Hasson, P., Del Buono, J., & Logan, M. P. O. (2007). Tbx5 is dispensable for forelimb outgrowth. *Development*, 134(1), 85–92. <https://doi.org/10.1242/dev.02622>
- Hasson, P., DeLaurier, A., Bennett, M., Grigorieva, E., Naiche, L. A., Papaioannou, V. E., Mohun, T. J., & Logan, M. P. O. (2010). Tbx4 and tbx5 acting in connective tissue are required for limb muscle and tendon patterning. *Developmental Cell*, 18(1), 148–156. <https://doi.org/10.1016/j.devcel.2009.11.013>
- He, P., Williams, B. A., Trout, D., Marinov, G. K., Amrhein, H., Berghella, L., Goh, S.-T., Plajzer-Frick, I., Afzal, V., Pennacchio, L. A., Dickel, D. E., Visel, A., Ren, B., Hardison, R. C., Zhang, Y., & Wold, B. J. (2020). The changing mouse embryo transcriptome at whole tissue and single-cell resolution. *Nature*, 583(7818), 760–767. <https://doi.org/10.1038/s41586-020-2536-x>
- Heinz, S., Benner, C., Spann, N., Bertolino, E., Lin, Y. C., Laslo, P., Cheng, J. X., Murre, C., Singh, H., & Glass, C. K. (2010). Simple combinations of lineage-determining transcription factors prime cis-regulatory elements required for macrophage and B cell identities. *Molecular Cell*, 38(4), 576–589. <https://doi.org/10.1016/j.molcel.2010.05.004>
- Helmbacher, F., Schneider-Maunoury, S., Topilko, P., Turet, L., & Charnay, P. (2000). Targeting of the EphA4 tyrosine kinase receptor affects dorsal/ventral pathfinding of limb motor axons. *Development*, 127(15), 3313–3324.

<https://doi.org/10.1242/dev.127.15.3313>

- Herriges, M., & Morrisey, E. E. (2014). Lung development: orchestrating the generation and regeneration of a complex organ. *Development*, *141*(3), 502–513. <https://doi.org/10.1242/dev.098186>
- Hickey, G., Paten, B., Earl, D., Zerbino, D., & Haussler, D. (2013). HAL: a hierarchical format for storing and analyzing multiple genome alignments. *Bioinformatics*, *29*(10), 1341–1342. <https://doi.org/10.1093/bioinformatics/btt128>
- Hoffmann, A. D., Yang, X. H., Burnicka-Turek, O., Bosman, J. D., Ren, X., Steimle, J. D., Vokes, S. A., McMahon, A. P., Kalinichenko, V. V., & Moskowitz, I. P. (2014). Foxf genes integrate tbx5 and hedgehog pathways in the second heart field for cardiac septation. *PLoS Genetics*, *10*(10), e1004604. <https://doi.org/10.1371/journal.pgen.1004604>
- Hucklebridge, F. H., Nowell, N. W., & Wouters, A. (1972). A relationship between social experience and preputial gland function in the albino mouse. *The Journal of Endocrinology*, *55*(2), 449–450. <https://doi.org/10.1677/joe.0.0550449>
- Hughes, J. R., Roberts, N., McGowan, S., Hay, D., Giannoulatou, E., Lynch, M., De Gobbi, M., Taylor, S., Gibbons, R., & Higgs, D. R. (2014). Analysis of hundreds of cis-regulatory landscapes at high resolution in a single, high-throughput experiment. *Nature Genetics*, *46*(2), 205–212. <https://doi.org/10.1038/ng.2871>
- Infante, C. R., Mihala, A. G., Park, S., Wang, J. S., Johnson, K. K., Lauderdale, J. D., & Menke, D. B. (2015). Shared Enhancer Activity in the Limbs and Phallus and Functional Divergence of a Limb-Genital cis-Regulatory Element in Snakes. *Developmental Cell*, *35*(1), 107–119. <https://doi.org/10.1016/j.devcel.2015.09.003>
- Infante, C. R., Park, S., Mihala, A. G., Kingsley, D. M., & Menke, D. B. (2013). Pitx1 broadly associates with limb enhancers and is enriched on hindlimb cis-regulatory elements. *Developmental Biology*, *374*(1), 234–244. <https://doi.org/10.1016/j.ydbio.2012.11.017>
- Infante, C. R., Rasys, A. M., & Menke, D. B. (2018). Appendages and gene regulatory networks: Lessons from the limbless. *Genesis*, *56*(1). <https://doi.org/10.1002/dvg.23078>
- Ingham, P. W., Nystedt, S., Nakano, Y., Brown, W., Stark, D., van den Heuvel, M., & Taylor, A. M. (2000). Patched represses the Hedgehog signalling pathway by promoting modification of the Smoothed protein. *Current Biology: CB*, *10*(20), 1315–1318. [https://doi.org/10.1016/s0960-9822\(00\)00755-7](https://doi.org/10.1016/s0960-9822(00)00755-7)

- Jain, D., Nemec, S., Luxey, M., Gauthier, Y., Bemmo, A., Balsalobre, A., & Drouin, J. (2018). Regulatory integration of Hox factor activity with T-box factors in limb development. *Development*, *145*(6). <https://doi.org/10.1242/dev.159830>
- Jhanwar, S., Malkmus, J., Stolte, J., Romashkina, O., Zuniga, A., & Zeller, R. (2021). Conserved and species-specific chromatin remodeling and regulatory dynamics during mouse and chicken limb bud development. *Nature Communications*, *12*(1), 5685. <https://doi.org/10.1038/s41467-021-25935-3>
- Jin, L., Wu, J., Bellusci, S., & Zhang, J.-S. (2018). Fibroblast Growth Factor 10 and Vertebrate Limb Development. *Frontiers in Genetics*, *9*, 705. <https://doi.org/10.3389/fgene.2018.00705>
- Johnson, E. J., Neely, D. M., Dunn, I. C., & Davey, M. G. (2014). Direct functional consequences of ZRS enhancer mutation combine with secondary long range SHH signalling effects to cause preaxial polydactyly. *Developmental Biology*, *392*(2), 209–220. <https://doi.org/10.1016/j.ydbio.2014.05.025>
- Kajioka, D., Suzuki, K., Nakada, S., Matsushita, S., Miyagawa, S., Takeo, T., Nakagata, N., & Yamada, G. (2019). Bmp4 is an essential growth factor for the initiation of genital tubercle (GT) outgrowth. *Congenital Anomalies*. <https://doi.org/10.1111/cga.12326>
- Kanehisa, M., Furumichi, M., Sato, Y., Ishiguro-Watanabe, M., & Tanabe, M. (2021). KEGG: integrating viruses and cellular organisms. *Nucleic Acids Research*, *49*(D1), D545–D551. <https://doi.org/10.1093/nar/gkaa970>
- Kawakami, Y., Marti, M., Kawakami, H., Itou, J., Quach, T., Johnson, A., Sahara, S., O’Leary, D. D. M., Nakagawa, Y., Lewandoski, M., Pfaff, S., Evans, S. M., & Izpisua Belmonte, J. C. (2011). Islet1-mediated activation of the β -catenin pathway is necessary for hindlimb initiation in mice. *Development*, *138*(20), 4465–4473. <https://doi.org/10.1242/dev.065359>
- Kelly, N. H., Huynh, N. P. T., & Guilak, F. (2019). Single cell RNA-sequencing reveals cellular heterogeneity and trajectories of lineage specification during murine embryonic limb development. *Matrix Biology: Journal of the International Society for Matrix Biology*. <https://doi.org/10.1016/j.matbio.2019.12.004>
- Kent, W. J., Sugnet, C. W., Furey, T. S., Roskin, K. M., Pringle, T. H., Zahler, A. M., & Haussler, D. (2002). The human genome browser at UCSC. *Genome Research*, *12*(6), 996–1006. <https://doi.org/10.1101/gr.229102>
- Keyte, A. L., & Smith, K. K. (2010). Developmental origins of precocial forelimbs in marsupial neonates. *Development*, *137*(24), 4283–4294.

<https://doi.org/10.1242/dev.049445>

- Kidder, B. L., Hu, G., & Zhao, K. (2011). ChIP-Seq: technical considerations for obtaining high-quality data. *Nature Immunology*, *12*(10), 918–922. <https://doi.org/10.1038/ni.2117>
- Kligman, A. M. (1963). THE USES OF SEBUM. *The British Journal of Dermatology*, *75*, 307–319. <https://doi.org/10.1111/j.1365-2133.1963.tb13567.x>
- Kmita, M., Tarchini, B., Zàkány, J., Logan, M., Tabin, C. J., & Duboule, D. (2005). Early developmental arrest of mammalian limbs lacking HoxA/HoxD gene function. *Nature*, *435*(7045), 1113–1116. <https://doi.org/10.1038/nature03648>
- Knezevic, V., De Santo, R., Schughart, K., Huffstadt, U., Chiang, C., Mahon, K. A., & Mackem, S. (1997). Hoxd-12 differentially affects preaxial and postaxial chondrogenic branches in the limb and regulates Sonic hedgehog in a positive feedback loop. *Development*, *124*(22), 4523–4536. <https://doi.org/10.1242/dev.124.22.4523>
- Koshiba-Takeuchi, K., Mori, A. D., Kaynak, B. L., Cebra-Thomas, J., Sukonnik, T., Georges, R. O., Latham, S., Beck, L., Henkelman, R. M., Black, B. L., Olson, E. N., Wade, J., Takeuchi, J. K., Nemer, M., Gilbert, S. F., & Bruneau, B. G. (2009). Reptilian heart development and the molecular basis of cardiac chamber evolution. *Nature*, *461*(7260), 95–98. <https://doi.org/10.1038/nature08324>
- Kumawat, K., & Gosens, R. (2016). WNT-5A: signaling and functions in health and disease. *Cellular and Molecular Life Sciences: CMLS*, *73*(3), 567–587. <https://doi.org/10.1007/s00018-015-2076-y>
- Kvon, E. Z., Kamneva, O. K., Melo, U. S., Barozzi, I., Osterwalder, M., Mannion, B. J., Tissières, V., Pickle, C. S., Plajzer-Frick, I., Lee, E. A., Kato, M., Garvin, T. H., Akiyama, J. A., Afzal, V., Lopez-Rios, J., Rubin, E. M., Dickel, D. E., Pennacchio, L. A., & Visel, A. (2016). Progressive Loss of Function in a Limb Enhancer during Snake Evolution. *Cell*, *167*(3), 633–642.e11. <https://doi.org/10.1016/j.cell.2016.09.028>
- Lanctôt, C., Moreau, A., Chamberland, M., Tremblay, M. L., & Drouin, J. (1999). Hindlimb patterning and mandible development require the Ptx1 gene. *Development*, *126*(9), 1805–1810. <https://doi.org/10.1242/dev.126.9.1805>
- Landt, S. G., Marinov, G. K., Kundaje, A., Kheradpour, P., Pauli, F., Batzoglou, S., Bernstein, B. E., Bickel, P., Brown, J. B., Cayting, P., Chen, Y., DeSalvo, G., Epstein, C., Fisher-Aylor, K. I., Euskirchen, G., Gerstein, M., Gertz, J., Hartemink, A. J., Hoffman, M. M., ... Snyder, M. (2012). ChIP-seq guidelines and practices of the

ENCODE and modENCODE consortia. *Genome Research*, 22(9), 1813–1831.
<https://doi.org/10.1101/gr.136184.111>

- Larsson, J. (2022). *Area-Proportional Euler and Venn Diagrams with Ellipses [R package eulerr version 7.0.0]*. <https://CRAN.R-project.org/package=eulerr>
- Laufer, E., Nelson, C. E., Johnson, R. L., Morgan, B. A., & Tabin, C. (1994). Sonic hedgehog and Fgf-4 act through a signaling cascade and feedback loop to integrate growth and patterning of the developing limb bud. *Cell*, 79(6), 993–1003.
[https://doi.org/10.1016/0092-8674\(94\)90030-2](https://doi.org/10.1016/0092-8674(94)90030-2)
- Leal, F., & Cohn, M. J. (2015). Development of hemipenes in the ball python snake *Python regius*. *Sexual Development: Genetics, Molecular Biology, Evolution, Endocrinology, Embryology, and Pathology of Sex Determination and Differentiation*, 9(1), 6–20. <https://doi.org/10.1159/000363758>
- Leal, F., & Cohn, M. J. (2016). Loss and Re-emergence of Legs in Snakes by Modular Evolution of Sonic hedgehog and HOXD Enhancers. *Current Biology: CB*, 26(21), 2966–2973. <https://doi.org/10.1016/j.cub.2016.09.020>
- Lettice, L. A., Horikoshi, T., Heaney, S. J. H., van Baren, M. J., van der Linde, H. C., Breedveld, G. J., Joosse, M., Akarsu, N., Oostra, B. A., Endo, N., Shibata, M., Suzuki, M., Takahashi, E., Shinka, T., Nakahori, Y., Ayusawa, D., Nakabayashi, K., Scherer, S. W., Heutink, P., ... Noji, S. (2002). Disruption of a long-range cis-acting regulator for *Shh* causes preaxial polydactyly. *Proceedings of the National Academy of Sciences of the United States of America*, 99(11), 7548–7553.
<https://doi.org/10.1073/pnas.112212199>
- Li, J., Lee, M., Davis, B. W., Lamichhaney, S., Dorshorst, B. J., Siegel, P. B., & Andersson, L. (2020). Mutations upstream of the TBX5 and PITX1 transcription factor genes are associated with feathered legs in the domestic chicken. *Molecular Biology and Evolution*. <https://doi.org/10.1093/molbev/msaa093>
- Li, Q. Y., Newbury-Ecob, R. A., Terrett, J. A., Wilson, D. I., Curtis, A. R., Yi, C. H., Gebuhr, T., Bullen, P. J., Robson, S. C., Strachan, T., Bonnet, D., Lyonnet, S., Young, I. D., Raeburn, J. A., Buckler, A. J., Law, D. J., & Brook, J. D. (1997). Holt-Oram syndrome is caused by mutations in TBX5, a member of the Brachyury (T) gene family. *Nature Genetics*, 15(1), 21–29. <https://doi.org/10.1038/ng0197-21>
- Liberatore, C. M., Searcy-Schrick, R. D., & Yutzey, K. E. (2000). Ventricular expression of *tbx5* inhibits normal heart chamber development. *Developmental Biology*, 223(1), 169–180. <https://doi.org/10.1006/dbio.2000.9748>

- Lister, R., O'Malley, R. C., Tonti-Filippini, J., Gregory, B. D., Berry, C. C., Millar, A. H., & Ecker, J. R. (2008). Highly integrated single-base resolution maps of the epigenome in Arabidopsis. *Cell*, *133*(3), 523–536. <https://doi.org/10.1016/j.cell.2008.03.029>
- Liu, Y., Liu, C., Yamada, Y., & Fan, C.-M. (2002). Growth arrest specific gene 1 acts as a region-specific mediator of the Fgf10/Fgf8 regulatory loop in the limb. *Development*, *129*(22), 5289–5300. <https://doi.org/10.1242/dev.129.22.5289>
- Loebel, D. A. F., Hor, A. C. C., Bildsoe, H., Jones, V., Chen, Y.-T., Behringer, R. R., & Tam, P. P. L. (2012). Regionalized Twist1 activity in the forelimb bud drives the morphogenesis of the proximal and preaxial skeleton. *Developmental Biology*, *362*(2), 132–140. <https://doi.org/10.1016/j.ydbio.2011.11.020>
- Logan, M. (2003). Finger or toe: the molecular basis of limb identity. *Development*, *130*(26), 6401–6410. <https://doi.org/10.1242/dev.00956>
- Longabaugh, W. J. R., Davidson, E. H., & Bolouri, H. (2005). Computational representation of developmental genetic regulatory networks. *Developmental Biology*, *283*(1), 1–16. <https://doi.org/10.1016/j.ydbio.2005.04.023>
- Lopez-Rios, J., Duchesne, A., Speziale, D., Andrey, G., Peterson, K. A., Germann, P., Unal, E., Liu, J., Floriot, S., Barbey, S., Gallard, Y., Müller-Gerbl, M., Courtney, A. D., Klopp, C., Rodriguez, S., Ivanek, R., Beisel, C., Wicking, C., Iber, D., ... Zeller, R. (2014). Attenuated sensing of SHH by Ptch1 underlies evolution of bovine limbs. *Nature*, *511*(7507), 46–51. <https://doi.org/10.1038/nature13289>
- Love, M. I., Huber, W., & Anders, S. (2014). Moderated estimation of fold change and dispersion for RNA-seq data with DESeq2. *Genome Biology*, *15*(12), 550. <https://doi.org/10.1186/s13059-014-0550-8>
- Lowe, L. A., Yamada, S., & Kuehn, M. R. (2000). HoxB6-Cre transgenic mice express Cre recombinase in extra-embryonic mesoderm, in lateral plate and limb mesoderm and at the midbrain/hindbrain junction. *Genesis*, *26*(2), 118–120. <https://www.ncbi.nlm.nih.gov/pubmed/10686603>
- Luo, G., Hofmann, C., Bronckers, A. L., Sohocki, M., Bradley, A., & Karsenty, G. (1995). BMP-7 is an inducer of nephrogenesis, and is also required for eye development and skeletal patterning. *Genes & Development*, *9*(22), 2808–2820. <https://doi.org/10.1101/gad.9.22.2808>
- Luo, W., & Brouwer, C. (2013). Pathview: an R/Bioconductor package for pathway-based data integration and visualization. *Bioinformatics*, *29*(14), 1830–1831. <https://doi.org/10.1093/bioinformatics/btt285>

- Maatouk, D. M., Choi, K.-S., Bouldin, C. M., & Harfe, B. D. (2009). In the limb AER *Bmp2* and *Bmp4* are required for dorsal-ventral patterning and interdigital cell death but not limb outgrowth. *Developmental Biology*, *327*(2), 516–523. <https://doi.org/10.1016/j.ydbio.2009.01.004>
- Maier, J. A., Rivas-Astroza, M., Deng, J., Dowling, A., Oboikovitz, P., Cao, X., Behringer, R. R., Cretokos, C. J., Rasweiler, J. J., 4th, Zhong, S., & Sears, K. E. (2017). Transcriptomic insights into the genetic basis of mammalian limb diversity. *BMC Evolutionary Biology*, *17*(1), 86. <https://doi.org/10.1186/s12862-017-0902-6>
- Markman, S., Zada, M., David, E., Giladi, A., Amit, I., & Zelzer, E. (2023). A single-cell census of mouse limb development identifies complex spatiotemporal dynamics of skeleton formation. *Developmental Cell*. <https://doi.org/10.1016/j.devcel.2023.02.013>
- Martin, J. F., Bradley, A., & Olson, E. N. (1995). The paired-like homeo box gene *MHox* is required for early events of skeletogenesis in multiple lineages. *Genes & Development*, *9*(10), 1237–1249. <https://doi.org/10.1101/gad.9.10.1237>
- McLean, C. Y., Bristor, D., Hiller, M., Clarke, S. L., Schaar, B. T., Lowe, C. B., Wenger, A. M., & Bejerano, G. (2010). GREAT improves functional interpretation of cis-regulatory regions. *Nature Biotechnology*, *28*(5), 495–501. <https://doi.org/10.1038/nbt.1630>
- Menke, D. B., Guenther, C., & Kingsley, D. M. (2008). Dual hindlimb control elements in the *Tbx4* gene and region-specific control of bone size in vertebrate limbs. *Development*, *135*(15), 2543–2553. <https://doi.org/10.1242/dev.017384>
- Merino, R., Rodriguez-Leon, J., Macias, D., Gañan, Y., Economides, A. N., & Hurler, J. M. (1999). The BMP antagonist Gremlin regulates outgrowth, chondrogenesis and programmed cell death in the developing limb. *Development*, *126*(23), 5515–5522. <https://doi.org/10.1242/dev.126.23.5515>
- Min, H., Danilenko, D. M., Scully, S. A., Bolon, B., Ring, B. D., Tarpley, J. E., DeRose, M., & Simonet, W. S. (1998). *Fgf-10* is required for both limb and lung development and exhibits striking functional similarity to *Drosophila* branchless. *Genes & Development*, *12*(20), 3156–3161. <https://doi.org/10.1101/gad.12.20.3156>
- Minchey, S. (2022). *CONSERVED TARGETS OF ISL1 DURING HINDLIMB INITIATION AND OUTGROWTH OF THE EXTERNAL GENITALIA* [University of Georgia]. <https://esploro.libs.uga.edu/esploro/outputs/doctoral/CONSERVED-TARGETS-OF-ISL1-DURING-HINDLIMB/9949450430602959>

- Minguillon, C., Del Buono, J., & Logan, M. P. (2005). Tbx5 and Tbx4 are not sufficient to determine limb-specific morphologies but have common roles in initiating limb outgrowth. *Developmental Cell*, *8*(1), 75–84. <https://doi.org/10.1016/j.devcel.2004.11.013>
- Minguillon, C., Gibson-Brown, J. J., & Logan, M. P. (2009). Tbx4/5 gene duplication and the origin of vertebrate paired appendages. *Proceedings of the National Academy of Sciences of the United States of America*, *106*(51), 21726–21730. <https://doi.org/10.1073/pnas.0910153106>
- Minguillon, C., Nishimoto, S., Wood, S., Vendrell, E., Gibson-Brown, J. J., & Logan, M. P. O. (2012). Hox genes regulate the onset of Tbx5 expression in the forelimb. *Development*, *139*(17), 3180–3188. <https://doi.org/10.1242/dev.084814>
- Monti, R., Barozzi, I., Osterwalder, M., Lee, E., Kato, M., Garvin, T. H., Plajzer-Frick, I., Pickle, C. S., Akiyama, J. A., Afzal, V., Beerenwinkel, N., Dickel, D. E., Visel, A., & Pennacchio, L. A. (2017). Limb-Enhancer Genie: An accessible resource of accurate enhancer predictions in the developing limb. *PLoS Computational Biology*, *13*(8), e1005720. <https://doi.org/10.1371/journal.pcbi.1005720>
- Moreau, C., Caldarelli, P., Rocancourt, D., Roussel, J., Denans, N., Pourquie, O., & Gros, J. (2018). Timed Collinear Activation of Hox Genes during Gastrulation Controls the Avian Forelimb Position. *Current Biology: CB*. <https://doi.org/10.1016/j.cub.2018.11.009>
- Moskowitz, I. P. G., Kim, J. B., Moore, M. L., Wolf, C. M., Peterson, M. A., Shendure, J., Nobrega, M. A., Yokota, Y., Berul, C., Izumo, S., Seidman, J. G., & Seidman, C. E. (2007). A molecular pathway including Id2, Tbx5, and Nkx2-5 required for cardiac conduction system development. *Cell*, *129*(7), 1365–1376. <https://doi.org/10.1016/j.cell.2007.04.036>
- Moskowitz, I. P. G., Pizard, A., Patel, V. V., Bruneau, B. G., Kim, J. B., Kupersmidt, S., Roden, D., Berul, C. I., Seidman, C. E., & Seidman, J. G. (2004). The T-Box transcription factor Tbx5 is required for the patterning and maturation of the murine cardiac conduction system. *Development*, *131*(16), 4107–4116. <https://doi.org/10.1242/dev.01265>
- Naiche, L. A., & Papaioannou, V. E. (2003). Loss of Tbx4 blocks hindlimb development and affects vascularization and fusion of the allantois. *Development*, *130*(12), 2681–2693. <https://doi.org/10.1242/dev.00504>
- Naiche, L. A., & Papaioannou, V. E. (2007). Tbx4 is not required for hindlimb identity or post-bud hindlimb outgrowth. *Development*, *134*(1), 93–103. <https://doi.org/10.1242/dev.02712>

- Narkis, G., Tzchori, I., Cohen, T., Holtz, A., Wier, E., & Westphal, H. (2012). Isl1 and Ldb Co-regulators of transcription are essential early determinants of mouse limb development. *Developmental Dynamics: An Official Publication of the American Association of Anatomists*, 241(4), 787–791. <https://doi.org/10.1002/dvdy.23761>
- Nemec, S., Luxey, M., Jain, D., Huang Sung, A., Pastinen, T., & Drouin, J. (2017). Pitx1 directly modulates the core limb development program to implement hindlimb identity. *Development*, 144(18), 3325–3335. <https://doi.org/10.1242/dev.154864>
- Newbury-Ecob, R. A., Leanage, R., Raeburn, J. A., & Young, I. D. (1996). Holt-Oram syndrome: a clinical genetic study. *Journal of Medical Genetics*, 33(4), 300–307. <https://doi.org/10.1136/jmg.33.4.300>
- Ng, J. K., Kawakami, Y., Büscher, D., Raya, A., Itoh, T., Koth, C. M., Rodríguez Esteban, C., Rodríguez-León, J., Garrity, D. M., Fishman, M. C., & Izpisua Belmonte, J. C. (2002). The limb identity gene Tbx5 promotes limb initiation by interacting with Wnt2b and Fgf10. *Development*, 129(22), 5161–5170. <https://www.ncbi.nlm.nih.gov/pubmed/12399308>
- Nishimoto, S., Minguillon, C., Wood, S., & Logan, M. P. O. (2014). A combination of activation and repression by a colinear Hox code controls forelimb-restricted expression of Tbx5 and reveals Hox protein specificity. *PLoS Genetics*, 10(3), e1004245. <https://doi.org/10.1371/journal.pgen.1004245>
- Nishimoto, S., Wilde, S. M., Wood, S., & Logan, M. P. O. (2015). RA Acts in a Coherent Feed-Forward Mechanism with Tbx5 to Control Limb Bud Induction and Initiation. *Cell Reports*, 12(5), 879–891. <https://doi.org/10.1016/j.celrep.2015.06.068>
- Niswander, L., Jeffrey, S., Martin, G. R., & Tickle, C. (1994). A positive feedback loop coordinates growth and patterning in the vertebrate limb. *Nature*, 371(6498), 609–612. <https://doi.org/10.1038/371609a0>
- Ohta, K., Nakamura, M., Hirokawa, K., Tanaka, S., Iwama, A., Suda, T., Ando, M., & Tanaka, H. (1996). The receptor tyrosine kinase, Cdk8, is transiently expressed on subtypes of motoneurons in the spinal cord during development. *Mechanisms of Development*, 54(1), 59–69. [https://doi.org/10.1016/0925-4773\(95\)00461-0](https://doi.org/10.1016/0925-4773(95)00461-0)
- Ohuchi, H., Nakagawa, T., Yamamoto, A., Araga, A., Ohata, T., Ishimaru, Y., Yoshioka, H., Kuwana, T., Nohno, T., Yamasaki, M., Itoh, N., & Noji, S. (1997). The mesenchymal factor, FGF10, initiates and maintains the outgrowth of the chick limb bud through interaction with FGF8, an apical ectodermal factor. *Development*, 124(11), 2235–2244. <https://doi.org/10.1242/dev.124.11.2235>

- O'Shaughnessy, K. L., Dahn, R. D., & Cohn, M. J. (2015). Molecular development of chondrichthyan claspers and the evolution of copulatory organs. *Nature Communications*, *6*, 6698. <https://doi.org/10.1038/ncomms7698>
- Osterwalder, M., Speziale, D., Shoukry, M., Mohan, R., Ivanek, R., Kohler, M., Beisel, C., Wen, X., Scales, S. J., Christoffels, V. M., Visel, A., Lopez-Rios, J., & Zeller, R. (2014). HAND2 targets define a network of transcriptional regulators that compartmentalize the early limb bud mesenchyme. *Developmental Cell*, *31*(3), 345–357. <https://doi.org/10.1016/j.devcel.2014.09.018>
- Ouimette, J.-F., Jolin, M. L., L'honoré, A., Gifuni, A., & Drouin, J. (2010). Divergent transcriptional activities determine limb identity. *Nature Communications*, *1*, 35. <https://doi.org/10.1038/ncomms1036>
- Paquette, S. M., Leinonen, K., & Longabaugh, W. J. R. (2016). BioTapestry now provides a web application and improved drawing and layout tools. *F1000Research*, *5*, 39. <https://doi.org/10.12688/f1000research.7620.1>
- Parr, B. A., Shea, M. J., Vassileva, G., & McMahon, A. P. (1993). Mouse Wnt genes exhibit discrete domains of expression in the early embryonic CNS and limb buds. *Development*, *119*(1), 247–261. <https://doi.org/10.1242/dev.119.1.247>
- Parr, Brian A., & McMahon, A. P. (1995). Dorsalizing signal Wnt-7a required for normal polarity of D–V and A–P axes of mouse limb. *Nature*, *374*(6520), 350–353. <https://doi.org/10.1038/374350a0>
- Peng, T., Tian, Y., Boogerd, C. J., Lu, M. M., Kadzik, R. S., Stewart, K. M., Evans, S. M., & Morrisey, E. E. (2013). Coordination of heart and lung co-development by a multipotent cardiopulmonary progenitor. *Nature*, *500*(7464), 589–592. <https://doi.org/10.1038/nature12358>
- Perriton, C. L., Powles, N., Chiang, C., Maconochie, M. K., & Cohn, M. J. (2002). Sonic hedgehog signaling from the urethral epithelium controls external genital development. *Developmental Biology*, *247*(1), 26–46. <https://doi.org/10.1006/dbio.2002.0668>
- Petit, F., Sears, K. E., & Ahituv, N. (2017). Limb development: a paradigm of gene regulation. *Nature Reviews. Genetics*, *18*(4), 245–258. <https://doi.org/10.1038/nrg.2016.167>
- Pignatti, E., Zeller, R., & Zuniga, A. (2014). To BMP or not to BMP during vertebrate limb bud development. *Seminars in Cell & Developmental Biology*, *32*, 119–127. <https://doi.org/10.1016/j.semcd.2014.04.004>

- Pineault, K. M., & Wellik, D. M. (2014). Hox genes and limb musculoskeletal development. *Current Osteoporosis Reports*, *12*(4), 420–427. <https://doi.org/10.1007/s11914-014-0241-0>
- Pollard, K. S., Hubisz, M. J., Rosenbloom, K. R., & Siepel, A. (2010). Detection of nonneutral substitution rates on mammalian phylogenies. *Genome Research*, *20*(1), 110–121. <https://doi.org/10.1101/gr.097857.109>
- Pyron, R. A. (2010). A likelihood method for assessing molecular divergence time estimates and the placement of fossil calibrations. *Systematic Biology*, *59*(2), 185–194. <https://doi.org/10.1093/sysbio/syp090>
- Rallis, C., Bruneau, B. G., Del Buono, J., Seidman, C. E., Seidman, J. G., Nissim, S., Tabin, C. J., & Logan, M. P. O. (2003). Tbx5 is required for forelimb bud formation and continued outgrowth. *Development*, *130*(12), 2741–2751. <https://www.ncbi.nlm.nih.gov/pubmed/12736217>
- Rankin, S. A., Steimle, J. D., Yang, X. H., Rydeen, A. B., Agarwal, K., Chaturvedi, P., Ikegami, K., Herriges, M. J., Moskowitz, I. P., & Zorn, A. M. (2021). Tbx5 drives aldh1a2 expression to regulate a RA-Hedgehog-Wnt gene regulatory network coordinating cardiopulmonary development. *ELife*, *10*, e69288. <https://doi.org/10.7554/eLife.69288>
- Rasys, A. M., Park, S., Ball, R. E., Alcalá, A. J., Lauderdale, J. D., & Menke, D. B. (2019). CRISPR-Cas9 Gene Editing in Lizards through Microinjection of Unfertilized Oocytes. *Cell Reports*, *28*(9), 2288–2292.e3. <https://doi.org/10.1016/j.celrep.2019.07.089>
- Renier, N., Wu, Z., Simon, D. J., Yang, J., Ariel, P., & Tessier-Lavigne, M. (2014). iDISCO: a simple, rapid method to immunolabel large tissue samples for volume imaging. *Cell*, *159*(4), 896–910. <https://doi.org/10.1016/j.cell.2014.10.010>
- Riddle, R. D., Ensini, M., Nelson, C., Tsuchida, T., Jessell, T. M., & Tabin, C. (1995). Induction of the LIM homeobox gene Lmx1 by WNT7a establishes dorsoventral pattern in the vertebrate limb. *Cell*, *83*(4), 631–640. [https://doi.org/10.1016/0092-8674\(95\)90103-5](https://doi.org/10.1016/0092-8674(95)90103-5)
- Riddle, R. D., Johnson, R. L., Laufer, E., & Tabin, C. (1993). Sonic hedgehog mediates the polarizing activity of the ZPA. *Cell*, *75*(7), 1401–1416. [https://doi.org/10.1016/0092-8674\(93\)90626-2](https://doi.org/10.1016/0092-8674(93)90626-2)
- Rodriguez-Esteban, C., Tsukui, T., Yonei, S., Magallon, J., Tamura, K., & Izpisua Belmonte, J. C. (1999). The T-box genes Tbx4 and Tbx5 regulate limb outgrowth and identity. *Nature*, *398*(6730), 814–818. <https://doi.org/10.1038/19769>

- Roscito, J. G., Sameith, K., Kirilenko, B. M., Hecker, N., Winkler, S., Dahl, A., Rodrigues, M. T., & Hiller, M. (2022). Convergent and lineage-specific genomic differences in limb regulatory elements in limbless reptile lineages. *Cell Reports*, *38*(3). <https://doi.org/10.1016/j.celrep.2021.110280>
- Ruvinsky, I., Silver, L. M., & Gibson-Brown, J. J. (2000). Phylogenetic analysis of T-Box genes demonstrates the importance of amphioxus for understanding evolution of the vertebrate genome. *Genetics*, *156*(3), 1249–1257. <https://doi.org/10.1093/genetics/156.3.1249>
- Sagai, T., Hosoya, M., Mizushina, Y., Tamura, M., & Shiroishi, T. (2005). Elimination of a long-range cis-regulatory module causes complete loss of limb-specific Shh expression and truncation of the mouse limb. *Development*, *132*(4), 797–803. <https://doi.org/10.1242/dev.01613>
- Sanger, T. J., Gredler, M. L., & Cohn, M. J. (2015). Resurrecting embryos of the tuatara, *Sphenodon punctatus*, to resolve vertebrate phallus evolution. *Biology Letters*, *11*(10). <https://doi.org/10.1098/rsbl.2015.0694>
- Sanger, T. J., Losos, J. B., & Gibson-Brown, J. J. (2008). A developmental staging series for the lizard genus *Anolis*: a new system for the integration of evolution, development, and ecology. *Journal of Morphology*, *269*(2), 129–137. <https://doi.org/10.1002/jmor.10563>
- Saunders, J. W. (1968). Ectodermal-mesenchymal interactions in the origins of limb symmetry. *Epithelial-Mesenchymal Interactions*, 78–97. <https://ci.nii.ac.jp/naid/10024201092/>
- Saunders, J. W., Jr. (1948). The proximo-distal sequence of origin of the parts of the chick wing and the role of the ectoderm. *The Journal of Experimental Zoology*, *108*(3), 363–403. <https://doi.org/10.1002/jez.1401080304>
- Seifert, A. W., Harfe, B. D., & Cohn, M. J. (2008). Cell lineage analysis demonstrates an endodermal origin of the distal urethra and perineum. *Developmental Biology*, *318*(1), 143–152. <https://doi.org/10.1016/j.ydbio.2008.03.017>
- Seifert, A. W., Yamaguchi, T., & Cohn, M. J. (2009). Functional and phylogenetic analysis shows that *Fgf8* is a marker of genital induction in mammals but is not required for external genital development. *Development*, *136*(15), 2643–2651. <https://doi.org/10.1242/dev.036830>
- Sekine, K., Ohuchi, H., Fujiwara, M., Yamasaki, M., Yoshizawa, T., Sato, T., Yagishita, N., Matsui, D., Koga, Y., Itoh, N., & Kato, S. (1999). *Fgf10* is essential for limb and lung formation. *Nature Genetics*, *21*(1), 138–141. <https://doi.org/10.1038/5096>

- Sheeba, C. J., & Logan, M. P. O. (2017). The Roles of T-Box Genes in Vertebrate Limb Development. *Current Topics in Developmental Biology*, *122*, 355–381. <https://doi.org/10.1016/bs.ctdb.2016.08.009>
- Sheth, R., Barozzi, I., Langlais, D., Osterwalder, M., Nemec, S., Carlson, H. L., Stadler, H. S., Visel, A., Drouin, J., & Kmita, M. (2016). Distal Limb Patterning Requires Modulation of cis-Regulatory Activities by HOX13. *Cell Reports*, *17*(11), 2913–2926. <https://doi.org/10.1016/j.celrep.2016.11.039>
- Sheth, R., Marcon, L., Bastida, M. F., Junco, M., Quintana, L., Dahn, R., Kmita, M., Sharpe, J., & Ros, M. A. (2012). Hox genes regulate digit patterning by controlling the wavelength of a Turing-type mechanism. *Science*, *338*(6113), 1476–1480. <https://doi.org/10.1126/science.1226804>
- Smith, J. C., & Wolpert, L. (1981). Pattern formation along the anteroposterior axis of the chick wing: the increase in width following a polarizing region graft and the effect of X-irradiation. *Journal of Embryology and Experimental Morphology*, *63*, 127–144. <https://www.ncbi.nlm.nih.gov/pubmed/7310285>
- Song, L., & Crawford, G. E. (2010). DNase-seq: a high-resolution technique for mapping active gene regulatory elements across the genome from mammalian cells. *Cold Spring Harbor Protocols*, *2010*(2), db.prot5384. <https://doi.org/10.1101/pdb.prot5384>
- Steimle, & Moskowitz, I. P. (2017). TBX5: A Key Regulator of Heart Development. *Current Topics in Developmental Biology*, *122*, 195–221. <https://doi.org/10.1016/bs.ctdb.2016.08.008>
- Steimle, Rankin, S. A., Slagle, C. E., Bekeny, J., Rydeen, A. B., Chan, S. S.-K., Kweon, J., Yang, X. H., Ikegami, K., Nadadur, R. D., Rowton, M., Hoffmann, A. D., Lazarevic, S., Thomas, W., Boyle Anderson, E. A. T., Horb, M. E., Luna-Zurita, L., Ho, R. K., Kyba, M., ... Moskowitz, I. P. (2018). Evolutionarily conserved Tbx5-Wnt2/2b pathway orchestrates cardiopulmonary development. *Proceedings of the National Academy of Sciences of the United States of America*, *115*(45), E10615–E10624. <https://doi.org/10.1073/pnas.1811624115>
- Sulaiman, F. A., Nishimoto, S., Murphy, G. R. F., Kucharska, A., Butterfield, N. C., Newbury-Ecob, R., & Logan, M. P. O. (2016). Tbx5 Buffers Inherent Left/Right Asymmetry Ensuring Symmetric Forelimb Formation. *PLoS Genetics*, *12*(12), e1006521. <https://doi.org/10.1371/journal.pgen.1006521>
- Sun, X., Mariani, F. V., & Martin, G. R. (2002). Functions of FGF signalling from the apical ectodermal ridge in limb development. *Nature*, *418*(6897), 501–508. <https://doi.org/10.1038/nature00902>

- Suzuki, K., Bachiller, D., Chen, Y. P., Kamikawa, M., Ogi, H., Haraguchi, R., Ogino, Y., Minami, Y., Mishina, Y., Ahn, K., Crenshaw, E. B., 3rd, & Yamada, G. (2003). Regulation of outgrowth and apoptosis for the terminal appendage: external genitalia development by concerted actions of BMP signaling [corrected]. *Development*, *130*(25), 6209–6220. <https://doi.org/10.1242/dev.00846>
- Suzuki, K., Ogino, Y., Murakami, R., Satoh, Y., Bachiller, D., & Yamada, G. (2002). Embryonic development of mouse external genitalia: insights into a unique mode of organogenesis. *Evolution & Development*, *4*(2), 133–141. <https://doi.org/10.1046/j.1525-142X.2002.01061.x>
- Suzuki, M., Hayashi, T., Inoue, T., Agata, K., Hirayama, M., Suzuki, M., Shigenobu, S., Takeuchi, T., Yamamoto, T., & Suzuki, K.-I. T. (2018). Cas9 ribonucleoprotein complex allows direct and rapid analysis of coding and noncoding regions of target genes in *Pleurodeles waltl* development and regeneration. *Developmental Biology*, *443*(2), 127–136. <https://doi.org/10.1016/j.ydbio.2018.09.008>
- Takeuchi, J. K., Koshiba-Takeuchi, K., Matsumoto, K., Vogel-Höpker, A., Naitoh-Matsuo, M., Ogura, K., Takahashi, N., Yasuda, K., & Ogura, T. (1999). Tbx5 and Tbx4 genes determine the wing/leg identity of limb buds. *Nature*, *398*(6730), 810–814. <https://doi.org/10.1038/19762>
- Takeuchi, J. K., Ohgi, M., Koshiba-Takeuchi, K., Shiratori, H., Sakaki, I., Ogura, K., Saijoh, Y., & Ogura, T. (2003). Tbx5 specifies the left/right ventricles and ventricular septum position during cardiogenesis. *Development*, *130*(24), 5953–5964. <https://doi.org/10.1242/dev.00797>
- Takeuchi, Jun K., Koshiba-Takeuchi, K., Suzuki, T., Kamimura, M., Ogura, K., & Ogura, T. (2003). Tbx5 and Tbx4 trigger limb initiation through activation of the Wnt/Fgf signaling cascade. *Development*, *130*(12), 2729–2739. <https://www.ncbi.nlm.nih.gov/pubmed/12736216>
- Tanigawa, Y., Dyer, E. S., & Bejerano, G. (2022). WhichTF is functionally important in your open chromatin data? *PLoS Computational Biology*, *18*(8), e1010378. <https://doi.org/10.1371/journal.pcbi.1010378>
- Tani-Matsuhana, S., Kusakabe, R., & Inoue, K. (2018). Developmental mechanisms of migratory muscle precursors in medaka pectoral fin formation. *Development Genes and Evolution*, *228*(5), 189–196. <https://doi.org/10.1007/s00427-018-0616-9>
- Tickle, C., Summerbell, D., & Wolpert, L. (1975). Positional signalling and specification of digits in chick limb morphogenesis. *Nature*, *254*(5497), 199–202. <https://doi.org/10.1038/254199a0>

- Tickle, Cheryll, & Towers, M. (2017). Sonic Hedgehog Signaling in Limb Development. *Frontiers in Cell and Developmental Biology*, 5, 14. <https://doi.org/10.3389/fcell.2017.00014>
- Timmons, J. A., Szkop, K. J., & Gallagher, I. J. (2015). Multiple sources of bias confound functional enrichment analysis of global -omics data. *Genome Biology*, 16(1), 186. <https://doi.org/10.1186/s13059-015-0761-7>
- Towers, M., Mahood, R., Yin, Y., & Tickle, C. (2008). Integration of growth and specification in chick wing digit-patterning. *Nature*, 452(7189), 882–886. <https://doi.org/10.1038/nature06718>
- Tschopp, P., Sherratt, E., Sanger, T. J., Groner, A. C., Aspiras, A. C., Hu, J. K., Pourquié, O., Gros, J., & Tabin, C. J. (2014). A relative shift in cloacal location repositions external genitalia in amniote evolution. *Nature*, 516(7531), 391–394. <https://doi.org/10.1038/nature13819>
- Tschopp, P., & Tabin, C. J. (2017). Deep homology in the age of next-generation sequencing. *Philosophical Transactions of the Royal Society of London. Series B, Biological Sciences*, 372(1713). <https://doi.org/10.1098/rstb.2015.0475>
- Twigg, S. R. F., Lloyd, D., Jenkins, D., Elçioğlu, N. E., Cooper, C. D. O., Al-Sannaa, N., Annagür, A., Gillissen-Kaesbach, G., Hüning, I., Knight, S. J. L., Goodship, J. A., Keavney, B. D., Beales, P. L., Gileadi, O., McGowan, S. J., & Wilkie, A. O. M. (2012). Mutations in multidomain protein MEGF8 identify a Carpenter syndrome subtype associated with defective lateralization. *American Journal of Human Genetics*, 91(5), 897–905. <https://doi.org/10.1016/j.ajhg.2012.08.027>
- Vallecillo-García, P., Orgeur, M., Vom Hofe-Schneider, S., Stumm, J., Kappert, V., Ibrahim, D. M., Börno, S. T., Hayashi, S., Relaix, F., Hildebrandt, K., Sengle, G., Koch, M., Timmermann, B., Marazzi, G., Sassoon, D. A., Duprez, D., & Stricker, S. (2017). Odd skipped-related 1 identifies a population of embryonic fibro-adipogenic progenitors regulating myogenesis during limb development. *Nature Communications*, 8(1), 1218. <https://doi.org/10.1038/s41467-017-01120-3>
- Vasyutina, E., Stebler, J., Brand-Saberi, B., Schulz, S., Raz, E., & Birchmeier, C. (2005). CXCR4 and Gab1 cooperate to control the development of migrating muscle progenitor cells. *Genes & Development*, 19(18), 2187–2198. <https://doi.org/10.1101/gad.346205>
- Visel, A., Blow, M. J., Li, Z., Zhang, T., Akiyama, J. A., Holt, A., Plajzer-Frick, I., Shoukry, M., Wright, C., Chen, F., Afzal, V., Ren, B., Rubin, E. M., & Pennacchio, L. A. (2009). ChIP-seq accurately predicts tissue-specific activity of enhancers. *Nature*, 457(7231), 854–858. <https://doi.org/10.1038/nature07730>

- Visel, A., Minovitsky, S., Dubchak, I., & Pennacchio, L. A. (2007). VISTA Enhancer Browser--a database of tissue-specific human enhancers. *Nucleic Acids Research*, 35(Database issue), D88-92. <https://doi.org/10.1093/nar/gkl822>
- Waldron, L., Steimle, J. D., Greco, T. M., Gomez, N. C., Dorr, K. M., Kweon, J., Temple, B., Yang, X. H., Wilczewski, C. M., Davis, I. J., Cristea, I. M., Moskowitz, I. P., & Conlon, F. L. (2016). The Cardiac TBX5 Interactome Reveals a Chromatin Remodeling Network Essential for Cardiac Septation. *Developmental Cell*, 36(3), 262–275. <https://doi.org/10.1016/j.devcel.2016.01.009>
- Wanek, N., Muneoka, K., Holler-Dinsmore, G., Burton, R., & Bryant, S. V. (1989). A staging system for mouse limb development. *The Journal of Experimental Zoology*, 249(1), 41–49. <https://doi.org/10.1002/jez.1402490109>
- Wang, J. S., Infante, C. R., Park, S., & Menke, D. B. (2018). PITX1 promotes chondrogenesis and myogenesis in mouse hindlimbs through conserved regulatory targets. *Developmental Biology*, 434(1), 186–195. <https://doi.org/10.1016/j.ydbio.2017.12.013>
- Weatherbee, S. D., Behringer, R. R., Rasweiler, J. J., 4th, & Niswander, L. A. (2006). Interdigital webbing retention in bat wings illustrates genetic changes underlying amniote limb diversification. *Proceedings of the National Academy of Sciences of the United States of America*, 103(41), 15103–15107. <https://doi.org/10.1073/pnas.0604934103>
- Weiss, D. A., Rodriguez, E., Jr, Cunha, T., Menshenina, J., Barcellos, D., Chan, L. Y., Risbridger, G., Baskin, L., & Cunha, G. (2012). Morphology of the external genitalia of the adult male and female mice as an endpoint of sex differentiation. *Molecular and Cellular Endocrinology*, 354(1–2), 94–102. <https://doi.org/10.1016/j.mce.2011.08.009>
- Wellik, D. M., & Capecchi, M. R. (2003). Hox10 and Hox11 genes are required to globally pattern the mammalian skeleton. *Science*, 301(5631), 363–367. <https://doi.org/10.1126/science.1085672>
- Wijesooriya, K., Jadaan, S. A., Perera, K. L., Kaur, T., & Ziemann, M. (2022). Urgent need for consistent standards in functional enrichment analysis. *PLoS Computational Biology*, 18(3), e1009935. <https://doi.org/10.1371/journal.pcbi.1009935>
- Williams, C. G., Lee, H. J., Asatsuma, T., Vento-Tormo, R., & Haque, A. (2022). An introduction to spatial transcriptomics for biomedical research. *Genome Medicine*, 14(1), 68. <https://doi.org/10.1186/s13073-022-01075-1>

- Wilson, V., & Conlon, F. L. (2002). The T-box family. *Genome Biology*, 3(6), REVIEWS3008. <https://doi.org/10.1186/gb-2002-3-6-reviews3008>
- Xie, L., Hoffmann, A. D., Burnicka-Turek, O., Friedland-Little, J. M., Zhang, K., & Moskowitz, I. P. (2012). Tbx5-hedgehog molecular networks are essential in the second heart field for atrial septation. *Developmental Cell*, 23(2), 280–291. <https://doi.org/10.1016/j.devcel.2012.06.006>
- Xu, B., Hrycaj, S. M., McIntyre, D. C., Baker, N. C., Takeuchi, J. K., Jeannotte, L., Gaber, Z. B., Novitch, B. G., & Wellik, D. M. (2013). Hox5 interacts with Plzf to restrict Shh expression in the developing forelimb. *Proceedings of the National Academy of Sciences of the United States of America*, 110(48), 19438–19443. <https://doi.org/10.1073/pnas.1315075110>
- Xu, B., & Wellik, D. M. (2011). Axial Hox9 activity establishes the posterior field in the developing forelimb. *Proceedings of the National Academy of Sciences of the United States of America*, 108(12), 4888–4891. <https://doi.org/10.1073/pnas.1018161108>
- Xu, H., Xiang, M., Qin, Y., Cheng, H., Chen, D., Fu, Q., Zhang, K. K., & Xie, L. (2019). Tbx5 inhibits hedgehog signaling in determination of digit identity. *Human Molecular Genetics*. <https://doi.org/10.1093/hmg/ddz185>
- Xu, X., Weinstein, M., Li, C., Naski, M., Cohen, R. I., Ornitz, D. M., Leder, P., & Deng, C. (1998). Fibroblast growth factor receptor 2 (FGFR2)-mediated reciprocal regulation loop between FGF8 and FGF10 is essential for limb induction. *Development*, 125(4), 753–765. <https://doi.org/10.1242/dev.125.4.753>
- Yamaguchi, T. P., Bradley, A., McMahon, A. P., & Jones, S. (1999). A Wnt5a pathway underlies outgrowth of multiple structures in the vertebrate embryo. *Development*, 126(6), 1211–1223. <https://www.ncbi.nlm.nih.gov/pubmed/10021340>
- Yang, J. H., Menshenina, J., Cunha, G. R., Place, N., & Baskin, L. S. (2010). Morphology of mouse external genitalia: implications for a role of estrogen in sexual dimorphism of the mouse genital tubercle. *The Journal of Urology*, 184(4 Suppl), 1604–1609. <https://doi.org/10.1016/j.juro.2010.03.079>
- Yue, F., Cheng, Y., Breschi, A., Vierstra, J., Wu, W., Ryba, T., Sandstrom, R., Ma, Z., Davis, C., Pope, B. D., Shen, Y., Pervouchine, D. D., Djebali, S., Thurman, R. E., Kaul, R., Rynes, E., Kirilusha, A., Marinov, G. K., Williams, B. A., ... Mouse ENCODE Consortium. (2014). A comparative encyclopedia of DNA elements in the mouse genome. *Nature*, 515(7527), 355–364. <https://doi.org/10.1038/nature13992>

- Zaragoza, M. V., Lewis, L. E., Sun, G., Wang, E., Li, L., Said-Salman, I., Feucht, L., & Huang, T. (2004). Identification of the TBX5 transactivating domain and the nuclear localization signal. *Gene*, *330*, 9–18. <https://doi.org/10.1016/j.gene.2004.01.017>
- Zhang, C.-H., Gao, Y., Hung, H.-H., Zhuo, Z., Grodzinsky, A. J., & Lassar, A. B. (2022). Creb5 coordinates synovial joint formation with the genesis of articular cartilage. *Nature Communications*, *13*(1), 7295. <https://doi.org/10.1038/s41467-022-35010-0>
- Zhang, R., Knapp, M., Suzuki, K., Kajioka, D., Schmidt, J. M., Winkler, J., Yilmaz, Ö., Pleschka, M., Cao, J., Kockum, C. C., Barker, G., Holmdahl, G., Beaman, G., Keene, D., Woolf, A. S., Cervellione, R. M., Cheng, W., Wilkins, S., Gearhart, J. P., ... Reutter, H. (2017). ISL1 is a major susceptibility gene for classic bladder exstrophy and a regulator of urinary tract development. *Scientific Reports*, *7*, 42170. <https://doi.org/10.1038/srep42170>
- Zhang, Z., Sui, P., Dong, A., Hassell, J., Cserjesi, P., Chen, Y.-T., Behringer, R. R., & Sun, X. (2010). Preaxial polydactyly: interactions among ETV, TWIST1 and HAND2 control anterior-posterior patterning of the limb. *Development*, *137*(20), 3417–3426. <https://doi.org/10.1242/dev.051789>
- Zheng, Z., Armfield, B. A., & Cohn, M. J. (2015). Timing of androgen receptor disruption and estrogen exposure underlies a spectrum of congenital penile anomalies. *Proceedings of the National Academy of Sciences of the United States of America*, *112*(52), E7194-203. <https://doi.org/10.1073/pnas.1515981112>
- Zhu, C. C., Yamada, G., Nakamura, S., Terashi, T., Schweickert, A., & Blum, M. (1998). Malformation of trachea and pelvic region in goosecoid mutant mice. *Developmental Dynamics: An Official Publication of the American Association of Anatomists*, *211*(4), 374–381. [https://doi.org/10.1002/\(SICI\)1097-0177\(199804\)211:4<374::AID-AJA8>3.0.CO;2-E](https://doi.org/10.1002/(SICI)1097-0177(199804)211:4<374::AID-AJA8>3.0.CO;2-E)
- Zhu, J., Patel, R., Trofka, A., Harfe, B. D., & Mackem, S. (2022). Sonic hedgehog is not a limb morphogen but acts as a trigger to specify all digits in mice. *Developmental Cell*. <https://doi.org/10.1016/j.devcel.2022.07.016>
- Zhulyn, O., Nieuwenhuis, E., Liu, Y. C., Angers, S., & Hui, C.-C. (2015). Ptch2 shares overlapping functions with Ptch1 in Smo regulation and limb development. *Developmental Biology*, *397*(2), 191–202. <https://doi.org/10.1016/j.ydbio.2014.10.023>